Article:

Pang, J., Colombera, L., Mountney, N.P. orcid.org/0000-0002-8356-9889 et al. (3 more authors) (2024) Mapping palaeoshorelines of river-dominated deltas in lacustrine ramp settings: Application of sedimentological analyses to the Triassic Yanchang Formation (Ordos Basin, China). Marine and Petroleum Geology, 164. 106797. ISSN 0264-8172

https://doi.org/10.1016/j.marpetgeo.2024.106797

Mapping palaeoshorelines of river-dominated deltas in lacustrine ramp settings: application of sedimentological analyses to the Triassic Yanchang Formation (Ordos Basin, China)

Jungang Pang[a,b,d], Luca Colombera[c], Nigel P. Mountney[d], Ji'an Guo[e], Kewen Yang[f], Wenhou Li[g]

a College of Earth Science and Engineering, Xi'an Shiyou University, Xi'an 710065, China

b Shaanxi Key Laboratory of Petroleum Accumulation Geology, Xi'an Shiyou University, Xi'an 710065, China

c Dipartimento di Scienze della Terra e dell'Ambiente, Università di Pavia, Via Ferrata 1, 27100 Pavia, Italy

d School of Earth and Environment, University of Leeds, Leeds, LS2 9JT, UK

e No.2 Comprehensive Geophysical Prospecting Brigade, Shaanxi Geological Mining CO. Ltd., Xi'an, 710016, China

f Changqing Oil Field Branch Company of China Petroleum, Xi'an, 710021, China

g Geological Department, State Key Laboratory of Continental Dynamics, Northwest University, Xi'an ,710069, China

Abstract

In the preserved successions of clastic lacustrine systems receiving substantial sediment input from fluvial sources, the boundary between delta-plain and delta-front facies belts marks the position of ancient lacustrine shorelines. Placing and predicting the position of this boundary in nearshore

lacustrine deposits of the Triassic Yanchang Formation (Ordos Basin, China) is of considerable applied significance, since sandstone deposits of this succession host numerous geological resources, yet delta-top and delta-front deposits differ fundamentally in terms of sandstone fraction, sandbody geometries, and petrophysical properties. However, established sedimentological criteria for shoreline identification relevant to marine environments are only partially applicable to this lacustrine setting. For example, in lacustrine systems, (i) water salinity can be considerably lower, (ii) tidal processes are negligible, (iii) wave activity is often limited and of local significance (e.g., distal and lateral delta-front fringes; transgressive periods of delta-lobe reworking), (iv) seasonal fluctuations in water chemistry and biogenic productivity may be common, and (v) the rate, frequency and magnitude of oscillations in base level differ from marine counterparts. Collectively, these factors hinder the differentiation of delta-plain and delta-front deposits in the Yanchang Formation. Yet the establishment of effective criteria with which to make such distinction is important for palaeogeographic restorations, and for resource exploration and exploitation.

On the basis of detailed sedimentological descriptions of well cores and outcrop exposures of the Yanchang Formation in the southeastern Ordos Basin, sedimentary facies accumulated as part of different sub-environments and facies belts are studied. Delta-plain deposits can be readily differentiated from those of delta-front origin on the basis of criteria relating to sediment texture, sedimentary structures, palaeontological content, well-log profiles, and vertical facies successions. These criteria are summarized and applied to better characterize the deltaic setting and to reconstruct the evolution of lacustrine shorelines during accumulation of the Yanchang Formation, particularly for the northeastern area of the basin.

A key outcome of this study is the development of a broadly applicable model for the recognition of sub-environments in river-dominated lacustrine deltaic successions. A generalized workflow is established to demonstrate how techniques in sedimentary facies analysis can be employed to reconstruct siliciclastic lacustrine delta shorelines, and thereby predict reservoir characteristics.

Keywords: lithofacies; shoreline; delta; lake; delta-front; delta-top; fluvial; lacustrine; facies model.

1. Introduction

Clastic successions of shallow-water deltas in lake basins have been the subject of considerable research in recent years (e.g., Shanley et al., 1994; Bohacs et al., 2000, 2003; Keighley et al.,2002, 2003; Overeem et al., 2003; Pusca, 2004; Taylor and Ritts, 2004; Bhattacharya et al., 2010; Zou et al., 2010; Shaw et al., 2013; Feng, et al., 2013, 2016; Gall et al., 2017; Fongngern et al., 2018; Gong et al., 2019; Keighley et al., 2019; Birgenheier et al., 2020; Jorissen et al., 2020; Wang et al., 2020; Zhang et al., 2020; Olariu et al., 2021). In clastic lacustrine reservoirs, sandstones of delta-plain origin are associated with a range of subaerial sub-environments, including distributary channels, floodplains and swamps (Plummer and Gostin, 1981; McCabe, 1984; Wu et al., 2004; Li et al., 2009; Olariu et al., 2021). By contrast, sandstones of delta-front origin, are represented by different types of subaqueous sub-environments, including mouth bars, delta-front sheets, and in some cases subaqueous distributary-channel fills (Mei and Lin, 1991; Neill and Allison, 2005; Yang et al., 2009; Zou et al., 2010; Martini and Sandrelli, 2015; Fu et al., 2019).

These two classes of deposits differ fundamentally in terms of lithofacies, facies associations, sandstone proportion and thickness, especially for river-dominated deltaic successions associated with ramp-like margins of lake basins (Overeem et al., 2003; Li et al., 2009; Zou et al., 2010; Zhao et al., 2015; Olariu et al., 2021), such as the Triassic Yangchang Formation of the Ordos Basin, China. Moreover, these deposits exhibit contrasting values of porosity and permeability where they act as petroleum reservoirs (Yang et al., 2009; Qu et al., 2019). Compared to delta-plain sandstones, sandbodies of delta-front origin are commonly characterized by higher primary porosity and permeability due to the preferential winnowing of fine-grained sediment fractions by lake currents and local wave activity, typically acting at delta-front fringes during transgressive periods thus leaving compositionally and texturally mature sands (Li et al., 2009; Jiang and Liu, 2010; Fu et al., 2019). Moreover, enhanced secondary porosity can commonly develop in delta-front sandstones due to partial grain dissolution associated with the migration of fluids into these deposits from nearby hydrocarbon-generating source rocks (Taylor and Ritts, 2004; Neill and Allison, 2005; Zavala et al., 2006; Wei et al., 2007; Jiang and Liu, 2010; Liu et al., 2015).

The delta plain is the dominantly subaerial physiographic element of a delta, whereas the delta front is its proximal subaqueous portion. The boundary between these two distinct sub-environments corresponds to the lacustrine shoreline, which shifts in position as a function of the gradient of the lake bed close to the shore, seasonal to longer-term variations in lake level, and changes in rates of sediment delivery. This may be expressed, for example, in shifts in the position of coal seams, which are relatively common in delta-top deposits, and of oil-stained shales, which instead are more common in delta-slope successions. The lacustrine shoreline and its associated facies belts are oriented approximately along strike relative to the regional palaeo-slope and average sediment-flux direction (Fig. 1) (Coleman and Prior, 1982; Postma, 1990; Olariu and Bhattacharya, 2006; Jiang, 2010; Taral and Chakraborty, 2018; Keighley et al., 2019).

The Triassic Yanchang Formation of the Ordos Basin was accumulated in a tectonic setting where the basin topography sloped gently towards a series of depocentres, each separated by relative topographic highs (Hutchinson, 1957; Carroll and Bohacs, 1999; Zhao et al., 2009). In this physiographic context, coarser-grained siliciclastic deposits were primarily deposited at the lake margins, whereas finer-grained sediments were dominantly accumulated in the central parts of the basin. The preserved facies belts exhibit considerable and significant lateral extent; they shifted rapidly and over considerable distances (tens of kilometres) in response to lake expansion and contraction over a time-span of millions of years (Renaut and Gierlowski-Kordesch, 2010). These lake-level fluctuations occurred primarily in response to both climatic changes and changes in the pattern and rate of subsidence across the basin (Dong et al., 2011; Xie and Heller, 2013; Zhao et al., 2015). They are in part now recorded in highly variable vertical facies sequences characterized by the alternation of terrestrial and subaqueous strata of delta-plain or delta-front origin (Yang et al., 2009; Zhao et al., 2009; Jiang, 2010; Liu et al., 2014). The reconstruction of histories of delta shoreline migration is therefore paramount for understanding the styles of infill and stratal architecture of lacustrine successions like the Yanchang Formation, especially in relation to hydrocarbon exploration and production (Wei et al., 2007; Li et al., 2009; Beate et al., 2010; Fu et al., 2019).Based on well-log, seismic and core data, a lacustrine paleoshoreline reconstruction for the Yanchang Formation in a sequence stratigraphic framework was attempted by Fu et al. (2019) for depositional sequences SQ1 to SQ6. In this paper, the temporal evolution of lake palaeoshorelines has been further elucidated based on a detailed characterization of architectural elements of the Yanchang Formation in outcrops and subsurface data, by employing facies criteria for the differentiation of delta-plain and delta-front deposits.

There exist distinct differences between lakes and seas (Bohacs et al., 2000; Bhattacharya, 2006;

Anthony, 2015; Wei et al., 2007; Keighley et al., 2019; Olariu et al., 2021). For example, in most lakes, tidal processes are negligible. Wave reworking is limited and of local significance; only limited longshore sediment transport occurs. Water salinity can be considerably lower in freshwater lakes. The rate, frequency and magnitude of oscillations in lake level differ from their counterparts in the marine environment. In marine river-dominated deltas, delta-plain facies belts may be influenced by eminently marine processes, such as tides (Tye and Coleman, 1989; Wu et al., 2004; Yang et al., 2009). These differences may leave a discernible record in the stratigraphy of lacustrine and marine systems. For example, the Yanchang lake basin was associated with ramp-like basin margins, characterized by absent or very limited tides, and local wave influence (e.g., at delta-front fringes, during transgressive periods) (Mei and Lin, 1991; Wu at al., 2004; Zou et al., 2010). The river inflow was probably dominated by inertial forces as density underflows. In the preserved successions of Yanchang river-dominated lake deltas, the offlap break recognized in clinoforms on this ramp margin likely indicates the position of the shoreline, marking the gradient break between coastal-plain and delta-front domains; delta fronts were dominated by distributary channels fills over mouth bars and lacked a well-developed clinoform profile (Coleman and Prior, 1982; Nemec et al., 1988; Postma, 1990; Mei and Lin, 1991; Overeem et al., 2003; Liu et al., 2014; Olariu et al., 2021). However, in highly constructive elongate marine deltaic settings, delta-front deposits are mostly characterized by sheet-like geometries arising from the coalescence of mouth bars, because the density of the sediment-laden river discharge is typically less than that of normal seawater, such that the river effluent overrides marine water and spreads laterally, forming a buoyant plume (hypopcynal flow). Corresponding sedimentary strata are dominated by coarsening- and thickening-upward successions, and exhibit distinct delta-slope clinoforms, as well as large-scale soft-sediment deformation features associated with rapid deposition and destabilization of river-mouth and slope deposits (Fisk, et al., 1954; Olariu and Bhattacharya, 2006; Anthony, 2015; Rossi and Steel, 2016). Therefore, established sedimentological criteria for shoreline identification relevant to marine environments are only partially applicable to lacustrine settings.

The Yanchang Formation is presented here as an example to demonstrate the application of sedimentological criteria for lake-shoreline reconstructions, in view of its economic interest and of the large dataset available (cf. Fu et al., 2019). The Ordos Basin hosts huge petroleum reserves, accounting for nearly 33% of the total oil and gas output of China, a large part of which is found in Late Triassic lacustrine successions (Yang et al., 2010; Zou et al., 2010; Qiu et al., 2014). These successions can be characterized comprehensively thanks to outcrop exposures in the marginal areas of the basin, and a large database of well logs and cores from within the central part of the basin. For the Yanchang Formation, different interpretations have been proposed with regards to the spatio-temporal evolution of the lacustrine shorelines in response to variations in the extent of the lake through time; such varied interpretations have resulted in contrasting views regarding the genetic mechanisms and environmental models invoked to explain sandstone-body characteristics and distributions through the stratigraphy and at different locations (Wu et al., 2004; Li et al., 2009; Yang et al., 2009; Qiu et al., 2014; Fu et al., 2019). In this study, we demonstrate how these controversies can be resolved through the application of facies-based recognition criteria for reconstructing the evolution of the lacustrine palaeoshorelines recorded in these Triassic strata of the Ordos Basin, which remain a key target for petroleum exploration (Yang et al., 2005; Yang et al., 2009; Deng et al., 2011).

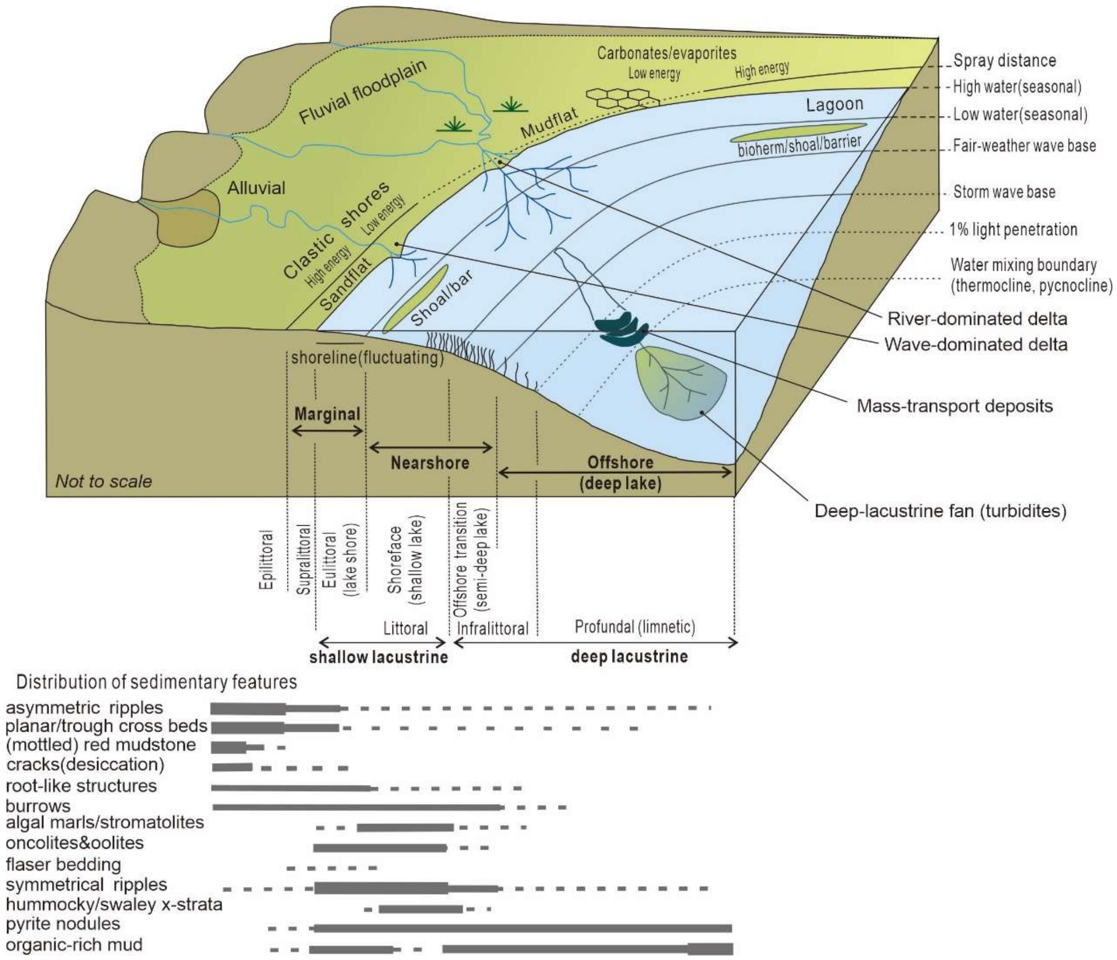

Fig. 1. Classification of lacustrine sub-environments based on bathymetry, reporting the frequency of occurrence of different sedimentary features. Modified after Keighley et al. (2019).

The aim of this paper is to undertake a sedimentological characterization of part of the Triassic hydrocarbon-bearing lacustrine succession of the Ordos Basin to unravel its record of the spatio-temporal evolution of lake palaeoshorelines. This is achieved through the following specific objectives: (1) establishing a classification scheme of lithofacies and lithofacies associations for the Yanchang Formation; (2) analyzing and identifying delta-plain versus delta-front facies belts, vertically and laterally, based on lithofacies types, facies associations, and other observations that are diagnostic of depositional sub-environments; (3) constructing a depositional model to describe the spatio-temporal distribution of delta-plain and delta-front facies belts; (4) mapping palaeoshorelines of part of the Late Triassic lake of the Ordos Basin.

2. Geological setting

The Ordos Basin is the second largest sedimentary basin in China. It is a petroliferous basin developed on archean granulites and lower Proterozoic greenschists of the North China block (Zhu and Xu, 1990), and infilled with Proterozoic to Cenozoic sedimentary successions that bear a record of multiple tectonic events of mid-late Proterozoic, early Paleozoic, late Paleozoic, Mesozoic, and Cenozoic ages. The Ordos Basin is situated in the western part of the Sino-Korean Block, and is bordered by the Yinshan, Luliang, Qinling, Liupanshan and Helan mountain ranges; it is subdivided into six tectonic belts based on tectonic history and present-day morphology (Zou et al., 2010; Xie et al., 2013) (Fig. 2A). The sediment fill of the basin has a total thickness exceeding 8 km in its southwestern part (Zhu and Xu, 1990; Darby and Ritts, 2002). A regional seismic survey shows that the basin fill dips gently (<2°) to the west, except where the basin margin is locally determined by normal faults that were active in the Neoproterozoic (He, 2002; Xie and Heller 2013). Unlike the basin margins, the interior of the Ordos Basin has experienced a generally stable tectonic history, particularly in the Yishan Slope area (Fig. 2A) (Xie, 2016).

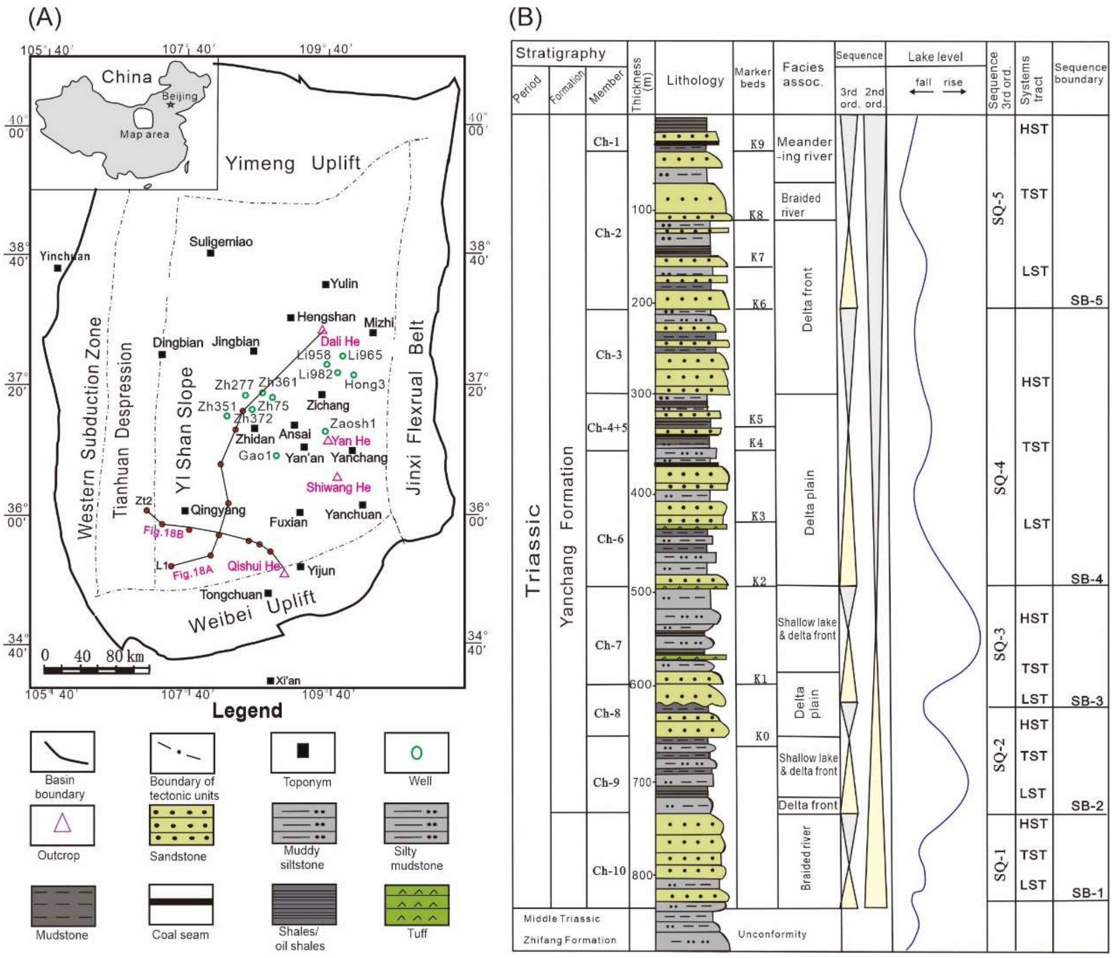

Fig. 2. Location of the study area and stratigraphic column of the Upper Triassic Yanchang Formation in the Ordos Basin (China). (A) Location of the study area. (B) Stratigraphic column illustrating lithostratigraphic and sequence stratigraphic classifications.

Much of the central part of the Ordos Basin was occupied by a lacustrine sedimentary system during the Late Triassic. It experienced conditions of rapid subsidence in its southern part, in response to tectonic loading associated with the rapid uplift of the Qinling range (Yang et al., 2004; Li et al., 2007; Zou et al., 2010; Deng et al., 2011; Bao et al., 2014; Xie et al., 2016). The Yanchang Formation is the most important oil-bearing interval of the basin. This formation is composed mainly of fine sandstone, siltstone, mudstone and tuffaceous intervals, with a total preserved thickness of 1000 to

1300 m (Yang et al., 2005). The Yanchang Formation mostly represents the accumulated deposits of alluvial-fan, fluvial, deltaic and lacustrine systems (Li et al., 2009; Zou et al., 2010). Its contact with the underlying Middle Triassic Zhifang Formation is unconformable in the marginal parts of the basin, due to spatially variable and irregular uplift during the first phase of the Indosinian Orogeny (Yang et al., 2005; Dong et al., 2011). The contact with the overlying Early Jurassic Yan'an-Fuxian Formation is unconformable; the uppermost part of the Yanchang Formation was variably eroded by the third phase of the Indosinian Orogeny (Liu et al., 1998).

There exist both lithostratigraphic and sequence stratigraphic schemes for the Yanchang Formation (Fig. 2B). Lithostratigraphic divisions are largely based on marker beds (termed as K0 to K9 from bottom to top) (i.e., Pang et al., 2010; Zou et al., 2010; Zhao, 2015) that can be correlated between closely spaced wells and/or outcrops, with consideration of the thickness of the units and variations thereof across the Yanchang lake basin. These marker beds (K0 to K9) are laterally extensive, variably correspond to fine-grained marker lithology (shales and oil shales, coal streak or beds, tuffs, mudstones), and have a distinct response on wireline log that makes them useful for subsurface correlation. The Yanchang Formation can thus be subdivided into members Ch-10 to Ch-1, from bottom to top, and further subdivided into several sub-members (Mei and Lin, 1991; Pang et al., 2010; Zhao, 2015).

With regards to the sequence stratigraphy of the Yanchang Formation, the basin-wide sequence boundaries at the top and bottom of the Yanchang Formation are considered as bounding a second-order sequence whose development was mainly controlled by tectonic activity (Dong et al., 2011; Bao et al., 2014). Lacustrine shales, including oil shales, in Ch-7 record the position of Maximum Flooding Surfaces (MFS). Five third-order sequences of region-wide extent (SQ-1, SQ-2, SQ-3, SQ-4 and SQ-5) are identified in the Yanchang Formation (Zou et al., 2010). The total length of time of deposition of the Yanchang Fm is 28.5 Myr; hence, the time-averaged span recorded by each sequence is inferred as being ca. 5.6 Myr. The sequence boundaries within the Yanchang Formation signify the transition from highstand normal regression to falling-stage forced regression; this is marked by the occurrence of prominent, laterally amalgamated sandstone units formed at a time of low accommodation, and typically characterized by some of the coarsest channel deposits. Systems tracts (LST, TST and HST) can be identified in the sequences from subsurface and, to a lesser extent, outcrop data (Zou et al., 2010; Zhao et al., 2015). Formation of the five third-order sequences recorded in the Yanchang Formation was likely driven by multiple external controls: tectonics and climate change determining variations in lake level and the rate at which the lake became infilled (Zou et al., 2010; Dong et al., 2011; Zhao et al., 2015; Xie, 2016). Maximum Flooding Surfaces (MFSs) are located mainly in basin-wide, shallow- to deep-lacustrine dark mudstones (shales), commonly occurring at basinal condensed sections recognizable due to high gamma-ray values, low-velocity, high organic-matter content; these characters reflect how uranium is concentrated in organic rich low-density sediments. These surfaces are recognized in shallow-lacustrine dark mudstone in the middle of Ch-10, shallow-lacustrine dark mudstone in upper Ch-9 (K0), shallow- to deep-lacustrine dark mudstone and shale in mid Ch-7 (K1), shallow-lacustrine dark mudstone in mid Ch-4+5 (K5), and shallow-lacustrine dark mudstone at the bottom of Ch-1 (K9) (Pang et al., 2010; Zou et al., 2010; Zhao et al., 2015) (Fig. 2B).

The Yanchang Formation records the evolution of a large lake basin, from a phase of initial subsidence (Ch-10), through rapid lake development (Ch-9-Ch-8), maximum lake deepening (Ch-7), gradual lake shrinkage (Ch-6-Ch-4+5) and final lake disappearance (Ch-3-Ch-1) by ultimately becoming infilled. These phases were primarily controlled by both tectonic drivers and climate-related hydrological variability (Li et al., 2009; Deng et al., 2013). A black-oil shale, deposited during a phase of maximum lake expansion during Ch-7 times, acts as the main hydrocarbon source rock of Yanchang Formation reservoirs (Li et al., 2009; Deng et al., 2013). Deltaic sediments are primarily preserved and are targets for petroleum exploration in members Ch-3, Ch-4+5, Ch-6 and Ch-8; these intervals are the main focus of this paper.

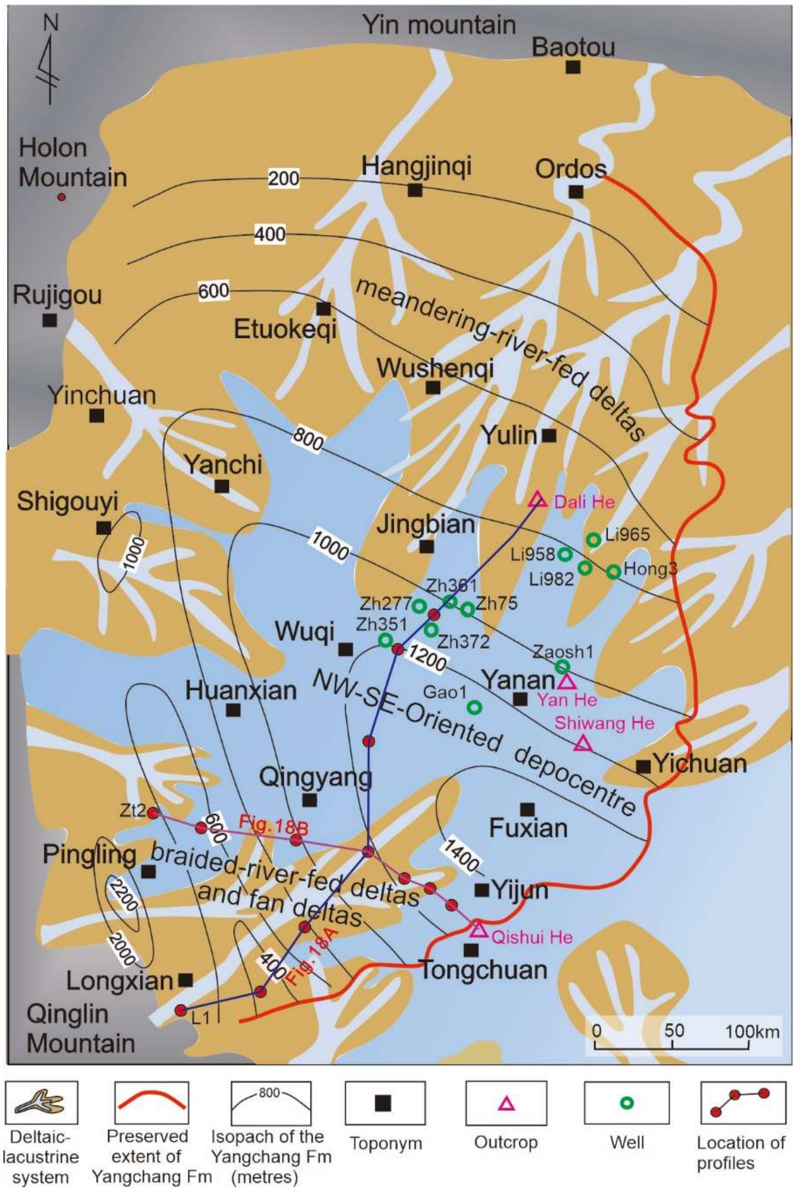

Fig. 3. Palaeogeography and isopach map of the Yanchang Formation, Ordos Basin (modified after

Zhao et al. 2015). Only the locations of outcrops and wells considered for this study are shown.

During the late Triassic Yanchang period, the Ordos Basin was occupied by an extensive, hydrologically open lake with an outlet to the southeast; at this time, a NW-SE-oriented depocentre existed in the areas of Yichuan-Wuqi-Yijun (Fig. 3). The evolutionary history of the lacustrine environments of the Yanchang Formation was partly dictated by the basin physiography: the southwestern lake boundary was associated with a steep topographic slope, whereas a gentle slope existed in the northeast (He, 2002; Bao et al., 2014). During this time, lake-level fluctuations of a several metres to a few tens of metres and of relatively high frequency took place. These were likely the effect of a climatic control on lake hydrology and, over longer timescales (10^0 to 10^1 Myr), of episodic tectonic activity. For instance, the record of maximum lake expansion tied to a MFS in Ch-7 of the Yanchang Formation is commonly interpreted as due to rapid subsidence of the southern Ordos Basin in response to a documented episode of tectonic activity of the Qinling Range (Deng et al., 2011; Xie and Heller, 2013). These changes resulted in the development of a series of major transgressive and regressive cycles varying over a wide range of scale in time and space (Yang et al., 2007; Li et al., 2009; Xie and Heller, 2013). Along the more gently sloping northeastern margin of the basin, meandering rivers are inferred to have fed deltas; by contrast, along the steeper southwestern margin, deltas and fan deltas were in most part fed by braided rivers (Mei and Lin, 1991; Yang et al., 2007; Li et al., 2009).

In previous work, it has been recognized that, within members Ch-8, Ch-6, Ch-4+5 and Ch-3, the main hydrocarbon-reservoir units of paralic origin are deltaic. The Yanchang setting of the Ordos Basin is commonly cited as an example of preserved shallow-water siliciclastic deltaic system (Wu et al., 2004; Zou et al., 2010; Deng et al., 2011; Liu et al., 2015; Zhao et al., 2015). The total area covered by delta-plain and delta-front facies belts was ca. 22,000 km^2 in Ch-6 times (Zou et al., 2010). Although the deltaic deposits of these units have already been documented by previous studies, a detailed reconstruction of lake-shoreline locations based on facies criteria through the times of the Yanchang Formation has yet to be proposed (Mei and Lin, 1991; Wu et al., 2004; Li et al., 2009; Yang et al., 2010; Zou et al., 2010; Zhao et al., 2015).

3. Methods and data

This study is primarily based on sedimentological analyses of 40 drill cores, with a total core length of ca. 820 m, and three detailed outcrop profiles documented at Yan He (Yanan), Shiwang He (Yichuan) and Qishui He (Tongchuan) and Dali He (Zizhou) (Fig. 2A). These data are supplemented with well-log data (SP – spontaneous potential, GR – gamma ray, AC – acoustic, 2.5RT – resistivity) from 2,350 wells, 520 of which were drilled in the northeastern area of Zhidan. The outcrops provide excellent vertical coverage but have limited lateral exposure. Vertical sedimentary logs have therefore been logged from several individual outcrop localities, each of which provides continuous exposure within the four main outcrops. In total, sections in both outcrop and core with a cumulative length of 1,000 m have been logged at 1:10 scale. A total of 2,600 photographs have been taken from these exposures and from well cores (Fig. 2A). Lithofacies and lithofacies associations have been described, classified and interpreted in both core and outcrop, based on sedimentological analyses. Sandstone proportions for individual members are separately calculated for 2,350 wells. A large dataset (1,630 wells) records information on lithology, colour, sedimentary structures. Wireline logs are used to identify the architectural elements, and to place the boundaries of deltaic facies belts in individual wells, on correlation profiles, and on maps for individual members of the Yanchang Formation.

4. Lithofacies association of deltaic systems of the Yanchang Formation

4.1 Lithofacies

Using a facies classification that largely follows the scheme by Miall (1978; 1985; cf. Eyles et al., 1983; Zhao et al., 2015), 13 lithofacies types are defined; these represent the main lithologies of fine- to medium-grained sandstone, siltstone and claystone of members Ch-3, Ch-4+5, Ch-6, Ch-7 and Ch-8 of the Yanchang Formation. Details of these facies types are reported in Table 1.

Based on their systematic co-occurrence in stratal packages, these facies are assigned to three generalized depositional facies belts: delta plain, delta front and prodelta. At a more detailed level, lithofacies are assigned to 11 specific facies associations representing different types of prodelta, delta-front or delta-top sub-environments. These facies associations are presented and are documented in more detail in Table 2, whereas their characteristics in outcrop and in well data are illustrated in Figs. 4-16.

In delta-top strata, subaerial distributary channel (DC), floodplain (FP), crevasse splay (CS), levee (LV), and swamp (SM) architectural elements are identified. In delta-slope strata, terminal distributary channel (also DC – see below), interdistributary bay (IDB), proximal mouth-bar (MB), distal mouth-bar (DMB) and delta-front sheet (DFS) elements are recognized.

Mouth-bar elements represent individual accretionary barform units developing at river mouths within the broader delta-front facies belt. We refer to delta-front distributary channel fills as “terminal distributary channels”, and to delta-plain distributary channel fills as “subaerial distributary channels”. The code “DC” has been used to denote both element types because of strong similarity in lithofacies association (e.g., common presence of lithofacies Sm, St, Sp, Sl) in both delta-front and delta-top settings, and because a clear-cut distinction of subaqueous and subaerial channel fills is not applicable when offshore channel propagation associated with delta progradation makes certain subaqueous features become subaerial through time.

Table 1. Summary of the characteristic features of the lithofacies encountered in the Yanchang Formation. Facies codes adapted from Miall (1985; cf. Eyles et al., 1983; Colombera et al., 2012, 2013; Zhao et al., 2015).

Code	Grainsize	Sedimentary structure	Interpretation
Sm	Fine- to medium-grained sandstone	Massive, structureless to weakly stratified, often with basal erosional surfaces	Rapid deposition of sand in suspension, mainly as basal scour fill, which prevents the development of structures or grading, and which may have resulted from different processes, including river flood flows (Frazier and Osanik, 1961; Miall, 1985), turbidity flows, and debris flows, often accompanied by the development of water-escape features

			(Talling et al., 2012).
St	Fine- to medium-grained sandstone	Medium (5~10cm)- to large-scale trough cross-bedded; common mud- and subordinate quartz clasts at base; rarely deformed	Lower flow regime bedforms with sinuous crests; thinner cross-sets (<0.5 m) were generated by migration of 3D dunes; thicker sets (>0.5m) may have been generated by migration of 3D unit bars (McKee and Weir, 1953; Allen, 1963; Ono et al., 2020).
Sp	Fine- to medium-grained sandstone	Medium (5~10cm)- to large-scale planar cross-bedded	Lower flow regime bedforms with straight crests; thinner cross-sets (<0.5 m) were generated by migration of 2D dunes; thicker sets (>0.5m) may have been generated by migration of 2D unit bars (McKee and Weir, 1953; Ingram, 1954; Allen, 1963; Smith, 1972; Ono et al., 2020).
Sl	Fine- to medium-grained sandstone	Low-angle (<10°) cross-stratification; parting lineation	Migration of low-relief dunes or transcritical bedforms, or deposition of upper flow regime plane beds on low-relief topography (Pettijohn and Potter, 1964; Allen, 1963, 1964; Paola et al.,1989; Massari et al., 1996; Baas et al.,

			2016).
Sd	Fine-grained sandstone	Convolute beddings, flames structures, load structures, ball-and-pillow structures	Post depositional soft-sediment deformation due to loading and fluid escape (Mills, 1983; Van Loon and Brodzikowski, 1987; Bhattacharya, 2010; Collinson and Mountney, 2019).
Shl	Very fine-grained sandstone	Planar horizontal lamination	Deposition of bedload from unidirectionally tractive currents in the field of stability of upper flow regime plane beds (Fielding, 2010; Bhattacharya et al., 2010).
Sr	Very fine- to fine-grained sandstone to siltstone	Asymmetrical ripple cross-lamination	Migration of 2D and 3D current ripples (Williams and Kemp, 1971; Reineck and Singh, 1986; Alexander et al., 2001).
Sw	Very fine- to fine-grained sandstone to siltstone	Symmetrical ripple cross-lamination	Deposition by migrating wave ripples formed by dominantly oscillatory flows (Williams and Kemp, 1971; Alexander et al., 2001).
Fh	Siltstone and silty claystone	Horizontally laminated, with root	Deposition under probable subaerial conditions as indicated by the upper parts of root marks in

		marks	waning-stage flood deposits; post-depositional root features may have affected originally subaqueous deposits (Williams, 1971; Miall, 1985; Boulesteix et al., 2020).
Fwlf	Interbedded siltstone and claystone	Wavy, lenticular or flaser lamination and cross-lamination	Fluctuating environmental energy causing alternation of traction and fall out (Reineck and Wunderlich, 1968; Terwindt and Breusers, 1972; Nutz et al., 2015).
Fm	Siltstone and claystone	Massive, locally with soft-sediment deformation and/or bioturbation	Product of suspension fallout in subaerial or subaqueous settings; the lack of preserved sedimentary structures may have been caused by soft sediment deformation or bioturbation (Williams, 1971; Miall, 1985; Boulesteix et al., 2020; Olariu et al., 2021).
Fl	Laminated mudstone	Horizontal laminations are common, mud cracks, raindrop imprints and root marks; bioturbation is rare to common	Deposition took place through settling in standing water, but subsequent subaerial exposure is recorded by bioturbatation associated with mud cracks and raindrop imprints, or by post-depositioanl plant-root marks which may have partly overprinted the originally subaqueous deposits (Pettijohn

			1949, 1964; Boulesteix et al., 2020; Olariu et al., 2021).
C	Thin coal beds or organic mudstone	Laminated where clayey, or in the form of coal seams	Accumulation of organic material in peat swamps (Styan and Bustin, 1983; McCabe, 1984).

Table 2. Facies associations recognized in lacustrine successions of the Yanchang Formation, Ordos Basin (codes modified after Zhao et al., 2015).

Facies belts	Facies association – (code)	Lithofacies	Description	Interpretation	Core vs outcrop
Delta plain	Subaerial distributary channel (DC)	Sm, St, Sp, Sl	Units of this facies association are typically 5 to 15 m thick and are mainly composed of fine- to medium-grained, mostly grey and grey-white, light yellow or red, feldspathic sandstones, with poorly sorted, sub-rounded to angular grains (Fig. 4A, F). The sandstones dominantly exhibit large-scale trough or tabular cross-bedding, planar horizontal lamination, and low-angle cross-stratification (Fig. 5A, B, C, D, E, F, G, H; Fig. 6A, B, C,	The erosional surface and associated lag deposits and the large-scale cross-bedding collectively indicate a current with erosive power, transitioning rapidly to depositional conditions (Cartigny et al., 2014; Lang et al., 2020). The attitude of the beds, together with palaeoflow oriented obliquely with respect to their dip direction, and the observed spatial association with proximal overbank deposits, are indicative of bank-	outcrop

			F, G, H; Fig.7A, C, E, F, G; Fig. 12C, D). Distributary channel deposits demonstrate lenticular units that are between 1.5 and 20 m thick, whose basal erosional surfaces are lined by discontinuous lags of mud clasts that are between 1 and 5 cm in diametre and have associated carbonized plant fragments that are up to 5-cm in diameter. Individual units generally show fining-upward trends, with gradational transitions from fine- to medium-grained sandstones with large-scale trough and tabular cross-bedding to finer sandstones and siltstones with small-scale cross-lamination. Sand bodies typically have channelized geometries that appear symmetric or nearly symmetric, with concave base and flat top in strike-	attached bars migrating obliquely to the main flow (Miall, 1985). The geometries of the sand bodies indicate that deposition occurred in a channel form (Galloway and Hobday, 1996; Fielding, 2006; Collinson and Mountney, 2019), where lateral migration of sandy bars gave rise to the sets of large-scale inclined beds. Their internal architecture dominantly records lateral or downstream accretion associated with fluvial barform growth, and only subordinate vertical streambed aggradation, sand was transported on the bar surface mainly as dunes or upper-plane laminae (Reineck and Singh, 1986; Alexander et al., 2001; Cartigny et al., 2014). The evidence of subaerial exposure leads to	

			oriented sections. These are preserved as several juxtaposed sand bodies, generally 30 to 50 m wide, locally separated by thin mudstone beds. Palaeocurrent directions, measured from cross-stratified sands and basal scours, are oblique to the dip of beds. Cross-bedded units bear evidence of subaerial exposure (e.g., root traces) in their uppermost parts, and are locally capped by mud lenses; spatially associated with proximal overbank deposits; bioturbation is rare; the top is gradational to LV.	interpretation of these units as subaerial distributary channels located in a delta-plain setting (Mohrig et al., 2000; Van der Kolk et al., 2015; Taral and Chakraborty, 2018). The range in grainsize, poor sorting, sedimentary structures, sedimentary-body geometry, accretion style, presence of multiple erosional surfaces, fining-upward trend, and presence of still largely articulated plant fragments are also indicative of subaerial distributary-channel deposits, accumulated in a terrestrial setting interpreted as a delta-plain environment (e.g., Frazier and Osanik, 1961; Allen, 1965; Li et al., 2009; Bhattacharya, 2010; Rossi and Steel, 2016).	

	Floodplain (FP)	Fh, Fm, Shl (rare)	Units of this facies association are mainly composed of thin- and medium-bedded grey and grey-green, variegated and purplish red mudstone, argillaceous siltstone and siltstone (Fig. 4B, F; Fig. 6B, G; Fig. 7A, B, C), which are extensively bioturbated; horizontal bedding is dominant; well-preserved raindrop imprints and desiccation cracks in mudstone are common; large plant fragments (in particular silicified *Neocalamites*) and rootlets are common.	These fine-grained deposits with extensive bioturbation mainly settled out of suspension from floodwaters (Galloway and Hobday, 1996). Raindrop marks, desiccation cracks and plant-root traces are all indicative of an environment subject to intermittent or protracted subaerial exposure (e.g., Plummer and Gostin, 1981; Allen, 1986; Collinson and Mountney, 2019). Regular horizontal bedding and silicified plants remains are indicative of deposition in a quiet-water environment with oxygen-deficient conditions (Olariu et al., 2006; Van der Kolk et al., 2015). The abundance of plant fragments and rootlets are suggestive of local, intermittent or protracted waterlogged conditions that	both

				may have favored the preservation of plant remains (Blatt et al., 1980; Bhattacharya, 2010; Yang, 2010). These observations and the association of these sediments with DC deposits suggest deposition on the floodplain of a delta plain (cf., Miall, 1985; Rossi and Steel, 2016).	
	Swamp (SM)	C, Fh, Fm	Units of this facies association are mainly composed of thin- and medium-bedded, grey and green-grey carbonaceous mudstone and argillaceous siltstone, and occasional thin-bedded siltstones (Fig. 4C, F). These deposits display abundant plant roots and plant fragments, and contain abundant coal seams or layers/streaks, and brown palaeosols in places (Fig. 5J;	These generally fine-grained deposits indicate a quiet-water environment dominated by suspension settling from floodwaters (Galloway and Hobday, 1996; Collinson and Mountney, 2019); the abundant coal seams or layers indicate the accumulation of organic material in a peat swamp (Blatt et al., 1980; McCabe, 1984); the brown palaeosols in this unit indicate	both

			Fig. 6I), the coal layers are commonly more than 2 m in thickness in the northern Ordos Basin (members Ch-4+5 to Ch-2 of Wells Z361, Z178, Z75, 3010 and Z 216).	intermittent exposure (Bhattacharya, 2010; Collinson and Mountney, 2019). This facies association is therefore interpreted as the preserved product of a peat-forming environment in a subaerial delta-plain or protracted waterlogged conditions enabled accumulation of abundant plant debris (Coleman and Gagliano, 1965; Styan and Bustin, 1983; McCabe, 1984; Yang, 2010; Fu et al., 2018).	
	Crevasse splay (CS)	Fm, Sr	Units of this lithofacies association occur in the form of lenticular lobes and sheet-like bodies, individual unit is typically between 0.3 and 2 m thick, with lateral extent of at least tens of metres, and containing deposits that are coarser than associated levee deposits (Fig. 4D, F; Fig.	This facies association is interpreted as crevasse-splay deposits, originated where flood-driven breakouts occurred in the levees of deltaic subaeral distributary channels, leading to overspills into the relatively more quiet floodplain sub-environment (Smith et al., 1989;	outcrop

			6A, B, G; Fig. 7A, B, C, D). Deposits can be intimately associated with fine-grained levee deposits (LV). Based on cross-bedding orientations, the general palaeocurrent direction was approximately perpendicular or at high angle to the gross palaeocurrent trends of DC (Fig. 7A). A coarsening-upward trend is generally seen in each unit, in the form of a gradual transition from muddy siltstone with small-scale ripple cross-lamination and planar horizontal lamination, to silt- and rarely fine- sandstone with small-scale current ripple and flaser bedding; soft-sediment deformation is common. These units are seen tapering laterally where they grade into fine-grained deposits of likely floodplain origin.	Galloway and Hobday, 1996); The coarsening-upward trend indicates a progressive increase in environmental energy and landform progradation, where deposition from traction and suspension occurs by currents carrying both bedload and suspended sediments as they debouch suddenly onto the floodplains (Blatt et al., 1980; Mohrig et al, 2000). Rapid accumulation could have driven sediment deformation in response to liquefaction (Allen, 1963; Williams et al., 1971; Collinson and Mountney, 2019). The general palaeocurrent trend indicates the overspills may have been funneled via distinct channels cutting across the levees (Smith et al., 1989).	

	Levee (LV)	Fh, Sr	Units of this facies association mainly comprise of beds of clayey siltstones and siltstones, with climbing-ripple cross-lamination and planar parallel lamination (Fig. 4E, F). Desiccation cracks or raindrop imprints, rootlets and limonite and siderite concretions are common. These deposits take the form of units with gross tabular or wedge-like shape that border and taper away from the margins or on the top of distributary channel fills (DC) (Fig. 5H, I; Fig. 6A, B, D, E, G, H). These deposits occur interbedded with those of interpreted crevasse-splay origin (CS).	This lithofacies association is interpreted as levee deposits, accumulated on portions of floodplains bordering distributary channels; deposition resulted from waning flows overtopping channel banks (Allen, 1963; Friend et al., 1965; Van der Kolk et al., 2015). Desiccation cracks or raindrop imprints both indicate the deposits were intermittently exposed (Blatt et al., 1980; Collinson and Mountney, 2019). The presence of limonite and siderite concretions may indicate variations in redox conditions, probably due to repeated wetting and drying cycles, possibly linked with alternating subaqueous and subaerial conditions (Galloway and Hobday, 1996; Jiang 2010). Rootlets are	outcrop

				suggestive of a sub-environment that supported plant growth (Galloway and Hobday, 1996). The interbedding of deposits of crevasse-splay origin (CS) containing most of the sand bordering the formative channels further supports the interpreted origin of these units as levee deposits (Blatt et al., 1980; Fielding, 2006; Fidolini and Ghinassi, 2016).	
Delta -front	Terminal distributary channels (DC)	Sm, St, Sp, Sl	This facies association is comprised of thick-bedded grey fine- and medium-grained sandstones (with moderately sorted, rounded to sub-rounded grains) interlayered with thin-bedded grey to deep-grey layers of argillaceous siltstone (Fig. 8A, F). These units commonly take the form of multi-storey vertically stacked sandbodies	This facies association is interpreted as the preserved expression of terminal distributary channels. These may have developed partly under subaqueous conditions, as the offshore extension of subaerial distributary channels on delta fronts (Pettijohn et al., 1964; Van der Kolk et al., 2015; Baas et al., 2016; Ono, et al., 2020). The	outcrop

			showing channelized shapes with a thickness of 15-60 m, and usually display a gross fining-upward trend (Fig. 9A, B, C, H). Internally, discrete channelized units display a style of accretion that is aggradational, concentric and lateral. Basal scour surfaces with moderate relief, lined by lag deposits of mud clast and rounded quartz grains, are commonly seen. Trough and tabular cross-bedding and planar horizontal lamination are common; ripple cross-lamination can be found occasionally in the upper portion of the sandstone units. Palaeocurrent directions inferred from sedimentary structures (i.e., trough- and tabular- cross- bedding, ripple cross-lamination, parting lineation) tend to be orientated at high angle with the	internal architecture and geometry of these bodies both indicate that this facies association was produced by deposition in a confined distributary channel (Fielding, 2006; Gibling, 2006; Fu et al., 2015; Keighley et al., 2019). The style of concentric accretion is more evident in channel deposits of presumed subaqueous origin (Allen, 1965; Gibling, 2006; Collinson and Mountney, 2019). These channels may have been incised by the erosive capacity of jet flows connected with river effluents and feeding the most proximal mouth-bars (Wright, 1997). Subaqueous lacustrine conditions are partially inferred based on the presence of sedimentary structures associated with wave processes (e.g.	

			inferred orientation of the palaeoshoreline (Fig. 9A, H) (see below). These units overlie mouth bar sandstones and are overlain by interdistributary-bay or shallow-lake mudstones, to which they transition gradually. They are also seen to transition laterally to shallow-lake deposits. Bioturbation is rare, and no significant evidence of subaerial exposure is reported.	symmetric wave ripples), the occurrence of freshwater fossils (especially phyllobranchiae, lamellibranchiae), the common occurrence of *Skolithos* trace-fossil assemblages, and high bioturbation in the interlayered fine-grained beds (Mei and Lin 1991; Olariu et al. 2005; Olariu and Bhattacharya, 2006; Van der Kolk et al., 2015; Fu et al., 2018). The interlayering of grey to dark-grey thin-layers, and terminal distributary channel itself with light-grey colour, the absence of sedimentary structures and features suggestive of subaerial exposure (i.e., mud crack, raindrop imprint, rootlets and lignite), and the close relationship with mouth-bar, interdistributary-bay or shallow-lake deposits, indicate	

				that the unit was dominantly deposited under subaqueous conditions (Mei and Lin 1991; Yang at al., 2009; Jiang, 2010; Liu et al., 2014; Anthony, 2015; Martini and Sandrelli, 2015; Keighley et al., 2019). The limited degree of bioturbation suggests high sedimentation rates (Pettijohn et al., 1964; Van der Kolk et al., 2015).	
	Inter-distributary bay (IDB)	Fh, Fm, Fl,	This facies association is mainly comprised of grey, grey-green, and dark-grey medium- and thick-bedded mudstones, argillaceous siltstones and siltstones, with horizontal lamination and small-scale ripples (Fig. 8E, F; Fig. 9A, E, F, G; Fig. 10A; Fig. 11A, B, F, G; Fig. 12A, B). Flaser- and lenticular-bedded siltstones occur	This facies association is interpreted as the product of accumulation in a relatively tranquil and reducing subaqueous sub-environment, often in proximity of distributary channels (Phillips, 2003; Bhattacharya, 2010; Burton et al., 2014). Heterolithic structures, calcite nodules and limonite concretions in black	outcrop

			occasionally. Calcareous nodules are common, whereas limonite concretions and iron impregnation (most examples are less than 1 cm in diameter) are locally seen hosted in black carbonaceous mudstones with abundant fossils (ostracoda, phyllobranchiae, lamellibranchiae, fossil fish scales; these include *Saurichthys, Perleidus, Boreosomus, Triassodus, Coelacanthiformes; Phylopoda*) and comminuted plant fragments. This facies association also displays a highly diverse trace-fossil assemblage, with *Skolithos* and *Diplocraterion* ichnogenera. Generally, these deposits take the form of tabular or wedge-shaped bodies, which are commonly associated with DC in a delta-front setting.	carbonaceous mudstones have been described from semi-protected and protected oxygen-deficient interdistributary bays (Phillips, 2003; Wu et al., 2004; Bhattacharya, 2010). The fossil content, indicates dominant fresh-water conditions in a shallow-lacustrine environment (Hutchinson, 1957; Seilacher, 1967; Buatois and Mangano, 1993; Bhattacharya, 2010; Yang et al., 2016). Vertical and subvertical burrows are indicative of sporadically agitated conditions in a shallow-water setting (Blatt et al., 1980; Van der Kolk et al., 2015).	

	Proximal mouth- bar (MB)	Sd, Sr/ Sw, Fh, Sp/St, Fwlf	This facies association is made of grey and grey-green, medium- and thick-bedded argillaceous siltstones and fine sandstones, whose thickness typically ranges between 1 and 3 m, and in which sand grains are well rounded and well sorted (Fig. 8B, F; Fig. 9A, D; Fig. 10; Fig. 12A, B). Commonly observed structures include trough cross-bedding, tabular cross-bedding, lenticular bedding, ripple cross-lamination, convoluted bedding, ball-and-pillow as well as load structures including flames. Ripple marks occur rarely on bedding planes. This facies association also displays a high various trace-fossil assemblage, i.e. *Psilonichnus* and *Macanopsis* ichnogenera; *Psilonichnus* is characterized by both x-	This facies association is interpreted as proximal mouth-bar deposits. Sandbodies with similar geometries, facies trends and relationships with other facies associations have previously been interpreted as partially preserved mouth bars in lacustrine strata, including those of the Yanchang Formation (Mei and Lin, 1991; Wu et al., 2004; Fielding, 2005; Schomacker, 2010; Liu et al., 2014). Their shape, vertical succession and association with soft-sediment deformation are all typical characteristics of mouth bars, where syn-sedimentary deformation and slope instability are due to loading and rapid deposition on delta slopes (Davies, 1965; Van Loon and Brodzikowski, 1987; Yang et al., 2009;	both

			shaped and y-shaped burrows whereas *Macanopsis* is characterised by vertical shafts. These strata are arranged according to a gross coarsening-upward succession (Fig. 10). The shape of these sandstone bodies is lenticular, with a flat base and a convex top. These units tend to overlie the interpreted distal mouth-bar or interdistributary-bay deposits, and they are in turn overlain by distributary-channel fills.	Fielding, 2010; Tanner and Lucas, 2010; Gao et al., 2019). The preserved sedimentary structures indicate that bedform migration dominantly took place under unidirectional and subordinately oscillatory currents, and under hydrodynamic conditions of lower flow-regime (Pettijohn, 1949, Pettijohn and Potter, 1964; Allen, 1963, 1964; Fielding, 2006; Baas et al., 2016). *Psilonichnus* and *Macanopsis* ichnogenera are developed in softground substrates and are indicative of agitated conditions in shallow-water settings (Schomacker et al., 2010; Fu et al., 2018). Wave reworking resulted in relatively higher sorting and increased particle roundness (Galloway and Hobday	

				1996; Fielding et al., 2005; Collinson and Mountney, 2019).	
	Distal mouth-bar (DMB)	Sd, Sr/Sw, Fh, Fwlf	This facies association comprises of interbedded grey muddy sandstones, siltstones and fine-grained sandstones, typically ranging in thickness between 0.5 and 2.5 m (Fig. 8C, F; Fig. 11A, B, C, D, E). Sand grains are well rounded and well sorted. Syn-depositional deformation, ripple cross-lamination and planar horizontal lamination are the dominant structures. Comminuted plant debris and carbonaceous fragments are common along bedding surfaces. Bioturbation is commonly intense, with abundant burrows. These bodies are characterized by convex-up accretion geometries in	This facies association is interpreted as the product of deposition in the distal portion of proximal channel mouths offshore the delta-front (Fielding, 2005). Syn-depositional deformation structures indicate sediment loading and rapid deposition (Mills, 1983; Fielding, 2010; Nutz et al., 2015). The common occurrence of plant and carbonaceous fragments may reflect deposition in locations that are relatively proximal to up-dip deltaic distributaries (Van Loon and Brodzikowski, 1987; Tanner and Lucas, 2010). Bioturbation and abundant burrows are both indicators	outcrop

			cross section (Fig.12A). These deposits tend to be arranged in a coarsening-upward succession, and commonly occurring below proximal mouth-bar units or interlayered with interdistributary-bay deposits. (Fig. 11A, B; Fig.12A, B).	of agitated flow conditions (Fidolini and Ghinassi, 2016). The convex-up external shape and the presence of coarsening-upward successions, accompanied by high textural maturity, are typical characteristics of distal mouth-bar deposits (Schomacker et al., 2010; Alexander et al., 2018; Keighley et al., 2019; Olariu et al., 2021). All these characters and the relationship of these bodies with proximal mouth- bar elements, indicate that the sediment was accumulated after bypassing, or after being re-entrained from, distributary-fed mouth bars (cf. Fielding, 2010; Liu et al., 2014; Gao et al., 2019).	

	Delta-front sheets (DFS)	Sl, Sr/Sw, Fh, Fwlf, Sd (rare)	This facies association is dominantly comprised of multiple layers of grey siltstones and sandstones with well-sorted and well-rounded grains. Single beds are usually up to 0.5 m in thickness and are commonly interlayered with grey thick-bedded laminated mudstones of interpreted interdistributary-bay or shallow-lake origin. These units exhibit wavy bedding, lenticular bedding, planar parallel lamination, asymmetrical and symmetrical ripple cross-laminations, low-angle cross-stratification, load structures (especially that deform original wave-ripple strata), burrows and various ichnofossils (i.e., *Arenicolites ichnosp., Ancorichnus coronus., Skolithos ichnosp.*). They are extensively	This facies association is interpreted as the deposits of delta-front sheets, made of sediment that possibly originated by the reworking of proximal mouth-bar deposits, by longshore currents and waves; they are inferred to occur distally away from proximal channel mouths along strike, associated with coarser mouth bar deposits (cf. Galloway and Hobday, 1996; Anthony, 2015; Rossi and Steel, 2016). Collectively, the common sedimentary structures indicate deposition by unidirectional alongshore currents and subordinate oscillatory wave motion, which likely caused the notable textural maturity of the sand (Fielding, 2006, 2010). Burrows, various ichnofossils and abundant	both

			bioturbated. These deposits form sheet-like and laterally extensive sandstone bodies with flat base and top, upward-coarsening trends or the lack of any distinct vertical variation of grain size are common. These deposits are commonly topologically associated with DC and MB (Fig. 8D, F; Fig. 11F, G, H, I)	bioturbation more generally are likely due to delta-lobe abandonment or lake transgression (Seilacher, 1967; Blatt et al., 1980; Fu et al., 2018). Load structures, which appear to be more common in strata that originally displayed wave ripples, reflect the effect of load at interfaces with grain-size contrasts (Mills, 1983; Neill and Allison, 2005). This facies association, in view of its characters and its associated interlayering with grey thick-bedded fine-grained deposits, is tentatively interpreted as the principal sedimentary record of periods of localized delta destruction following lobe abandonment (Reineck and Singh,1986; Tye and Coleman, 1989; Anthony, 2015).	

Pro delta	Prodelta (PD)	Fm, Fh, Fwlf	This facies association is mainly composed of black to grey, laminated mudstones (Fig. 8F), occasionally interlayered with thin-bedded siltstones to fine-grained sandstones, which mostly contain cross-laminations associated with starved symmetric and asymmetric ripples. Thin bedsets of rippled siltstone to fine-grained sandstone exhibit coarsening- followed by fining-upward trends (Fig. 13). Horizontal lamination and massive structure are common. Fossils of fish (notably, *Triassodus*) and bivalves (notably, Unio *Shaanxiconcha*) are very common. The top is gradational into more sand-prone distal delta-front heterolithic facies; the base is gradational to deep-lacustrine laminated and massive	This facies association is the product of sedimentation under low-energy conditions, and is interpreted as the record of a prodelta environment located offshore of the delta front (Mei and Lin, Li et al., 2009; Liu et al., 2014; Van der Kolk et al., 2015). The thin bedsets of rippled siltstone to fine-grained sandstone are interpreted as the product of waxing-waning in relation to floods (cf. river-fed hyperpycnal flows) traversing an otherwise quiet environment (Zavala et al., 2006; Bhattacharya, 2010; Olariu et al., 2010; Rossi and Steel, 2016; Yang et al., 2017). The commonly identified fish and bivalve fossils are indicators of a fresh-water lacustrine	outcrop

			black mudstones. In gamma-ray logs, deposits of this association display low-amplitude and approximately flat log signature, with occasional low-amplitude spikes associated with layers of silt and fine sandstone.	environment (Seilacher, 1967; Blatt et al., 1980; Buatois and Mangano,1993; Yang et al., 2016).	

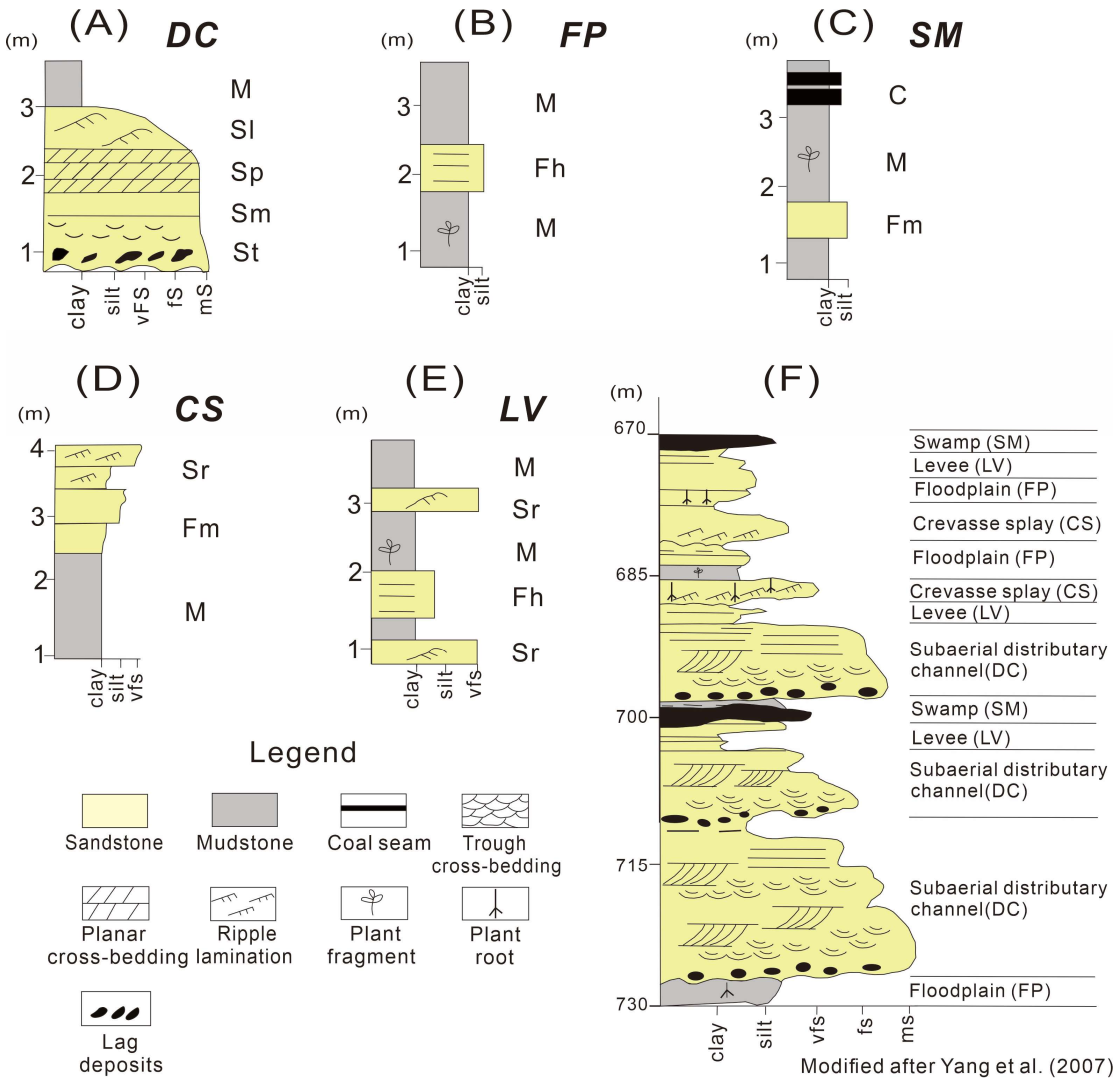

Fig. 4. Lithofacies associations of delta-plain deposits. (A) Subaerial distributary channel (DC). (B) Floodplain (FP). (C) Swamp (SM). (D) Crevasse splay (CS). (E) Levee (LV). (F) Delta-plain deposits of Ch-3 as observed on a section of well Zaoshen 1. See Fig. 2A for well location and Table 1 for facies codes (M denotes generic mudstones).

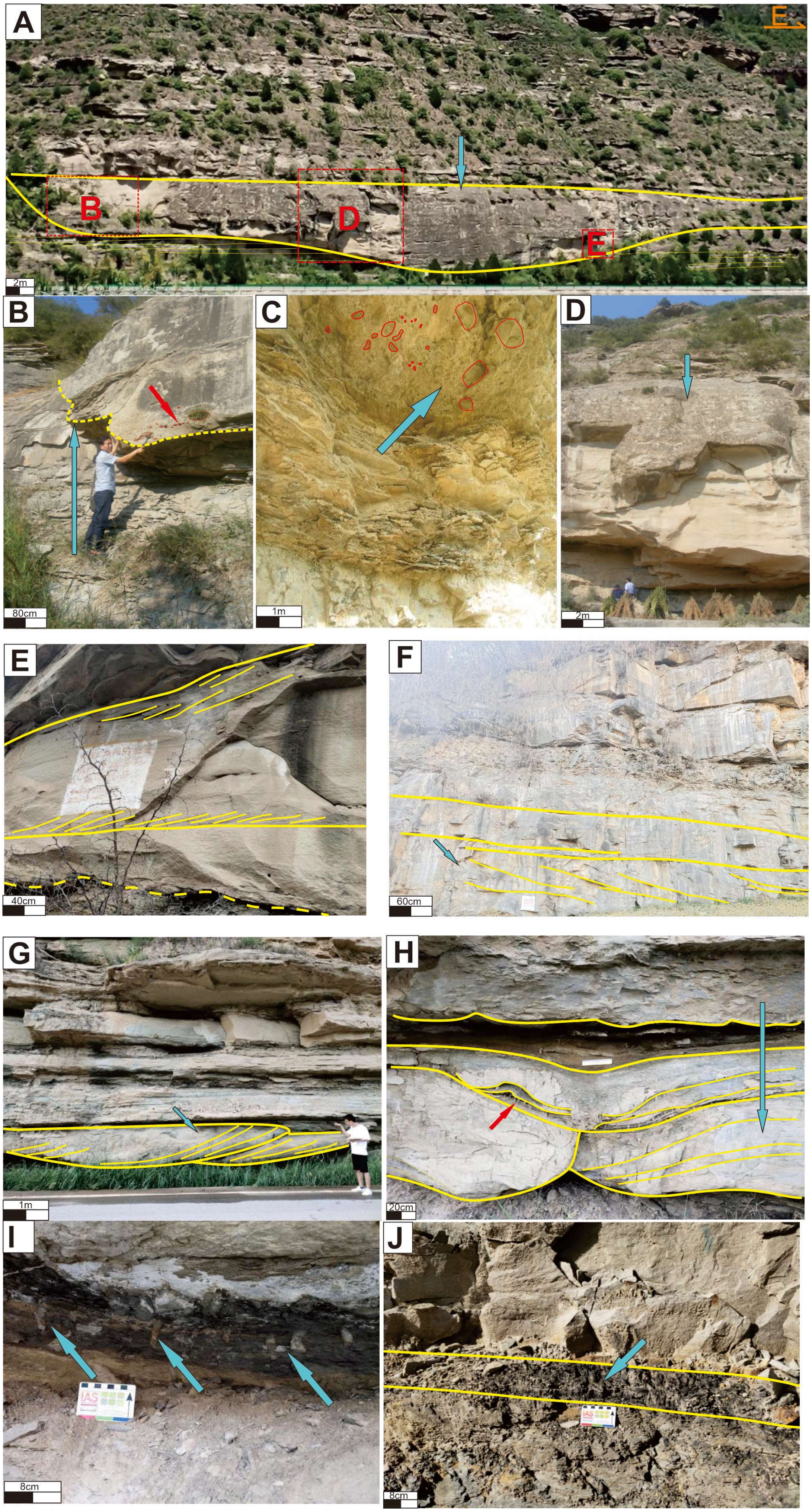

A
E
B
D
E
2m
B
80cm
C
1m
D
2m
E
40cm
F
60cm
G
1m
H
20cm
I
8cm
J
8cm

Fig. 5. Facies associations and architectural characteristics of the delta-plain deposits, Ch-6, Yan He outcrop. (A) Large delta-plain subaerial channel body (DC) of nearly symmetric lenticular shape in strike sections. (B) Basal erosion (indicated by blue arrow) and mud-clast accumulations (indicated by red arrow) delineates evident lenticular-shaped units with concave-base and flat-top in body shown in (A). (C) Grey-green mud clasts on the basal surface of a distributary-channel fill (DC). (D) Aggradation of the infill of the channel body (DC), shown in (A). (E) Erosional base and massive structure and large-scale planar cross-bedding in the subaerial distributary channel deposits (DC) shown in (A). (F) Large-scale epsilon-type cross-bedding in subaerial distributary channel deposits (DC), Ch-8, Qishui He outcrop. (G) Laterally juxtaposed cross-stratified units in distributary channel deposits (DC). (H) Large-scale trough (dm-thick) cross-stratification (blue arrow), possibly produced by unit bars in a subaerial distributary channel (DC), and silicified Neocalamites growing perpendicular to the bedding (red arrow) in a mud-prone bed (LV). (I) Silicified plant stems of Neocalamites in levee deposits (LV). (J) Mudstones and coal layers in swamp (SM). See Fig. 2A for outcrop locations. See Table 2 for abbreviations.

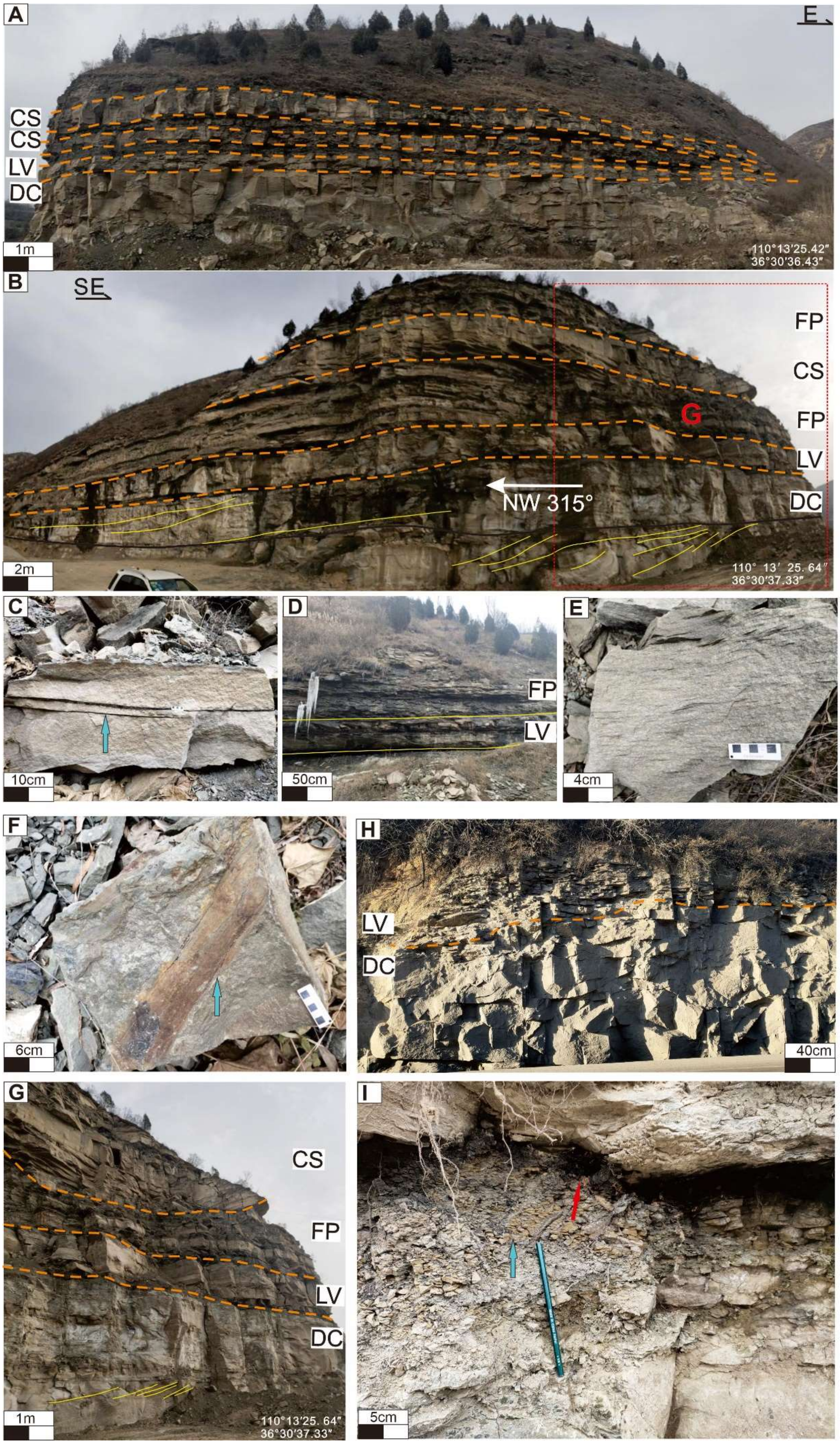
A
E
CS
CS
LV
DC
1m
110°13'25.42"
36°30'36.43"
B
SE
FP
CS
G
FP
LV
NW 315°
DC
2m
110° 13' 25. 64"
36°30'37.33"
C
10cm
D
FP
LV
50cm
E
4cm
F
6cm
H
LV
DC
40cm
G
CS
FP
LV
DC
1m
110°13'25. 64"
36°30'37.33"
I
5cm

Fig. 6. Facies associations and architectural characteristics of the delta-plain deposits, Ch-8, A-F, G from Yan He outcrop. (A) Delta-plain channel body (DC) overlain by thin-bedded levee siltstone (LV) and an overbank succession containing two crevasse-splay elements that pinch out laterally (CS). (B) Delta-plain channel body with large-scale cross-bedding (DC) overlain by thin-bedded levee siltstone (LV), passing into a suite of interlayered overbank mudstones and thin-bedded siltstones (FP) with crevasse-splay siltstones showing a coarsening-upward trend (CS). (C) Coal streaks interlayered within fine-grained sandstone (DC). (D) Levee siltstone with small-scale cross-bedding (LV), overlain by interlayered mudstones and muddy siltstones (FP). (E) Small-scale cross-bedding in siltstones of levee deposits (LV). (F) Plant stem with diameter of about 5 cm, in grey sandstone (DC). (G) Facies associations and architectural characteristics of the delta-plain deposits, shown in (B). (H) Vertical relationships between a grey channel sandstone body with cross-bedding (DC) and interbedded siltstones and mudstones of levee origin (LV), Ch-8, Qishuihe outcrop. (I) Brown palaeosols (blue arrow) and black coal streak (red arrow) in the fine-grained deposits of facies association SM. Ch-8, Shiwang He outcrop. See Fig. 2A for outcrop locations. See Table 2 for abbreviations.

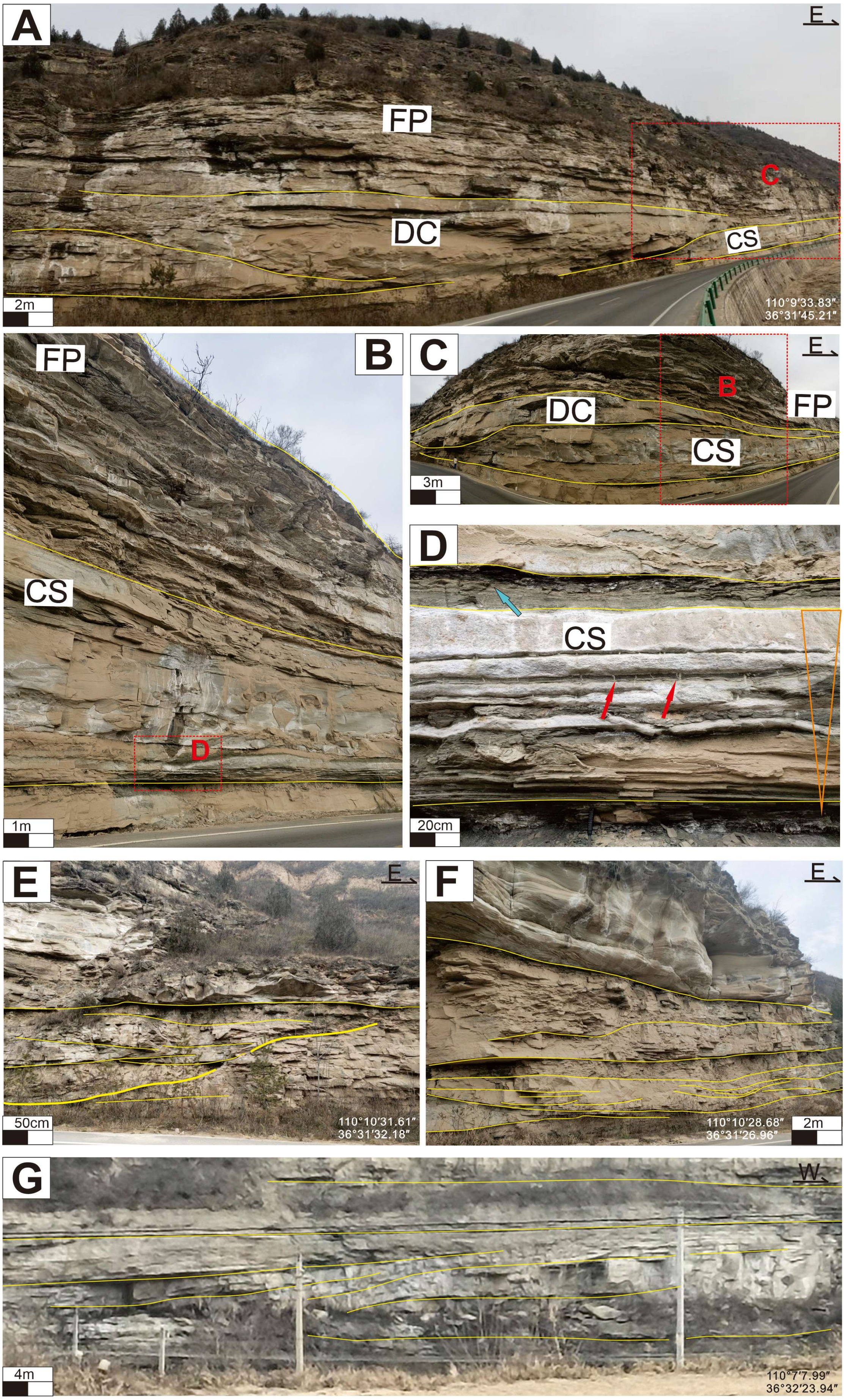
A
E
FP
C
DC
CS
2m
110°9'33.83"
36°31'45.21"
B
FP
CS
D
1m
C
E
DC
B
FP
CS
3m
D
CS
20cm
E
E
50cm
110°10'31.61"
36°31'32.18"
F
E
110°10'28.68"
36°31'26.96"
2m
G
W
4m
110°7'7.99"
36°32'23.94"

Fig. 7. Facies associations and architectural characteristics of the delta-plain deposits, Ch-6, Yan He outcrop. (A) Subaerial distributary-channel fill with nearly symmetric lenticular shape (DC), bordering laterally with interlayered sandstone, mudstone and coal strata (CS), which are in turn overlain by interlayered overbank mudstones and siltstones (FP); the inferred palaeocurrent direction of DC is towards the viewer, whereas lateral-accretion deposits indicate sideway bank migration; the palaeocurrent direction of CS is from left to right (from west to east). (B) Vertical succession of crevasse splay (CS) and floodplain (FP) deposits; see (A) and (C) for location. (C) Subaerial distributary channel (DC), crevasse-splay (CS) and floodplain (FP) elements; see (A). (D) Coarsening-upward trend of a crevasse-splay element (CS), containing a carbonaceous layer (blue arrow) and rootlets testifying to growth perpendicular to bedding (red arrow). (E) Accretion geometries in subaerial distributary channel deposits (DC). (F) Style of accretion of subaerial distributary-channel deposits (DC) characterized by stacked sandstone bodies and lenticular mudstone presumably representing an abandoned-channel fill. (G) Lateral-accretion geometries in a subaerial distributary- channels fill (DC). See Fig. 2A for well location and Table 1 for facies codes (M denotes generic mudstones).

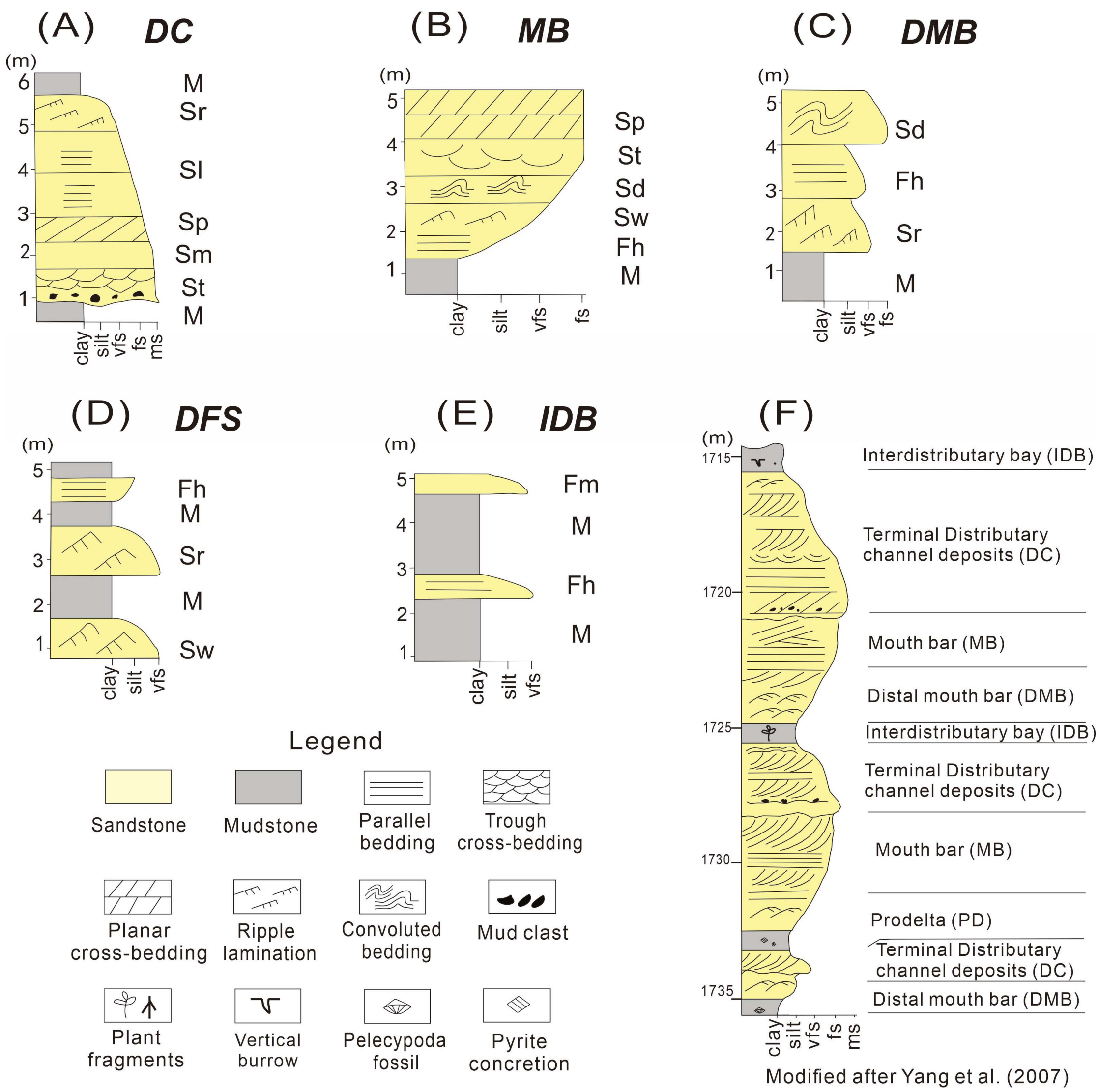

Fig. 8. Lithofacies associations of delta-front deposits. (A) Terminal distributary channel (DC). (B) Mouth bar (MB). (C) Distal mouth-bar (DMB). (D) Delta-front sandsheets (DFS). (E) Interdistributary bay/shallow-lacustrine mudstone (IDB). (F) Delta-front deposits of member Ch-6 as observed on a section of well Gao 1. See Fig. 2A for well locations and Table 1 for facies codes (M denotes generic mudstones).

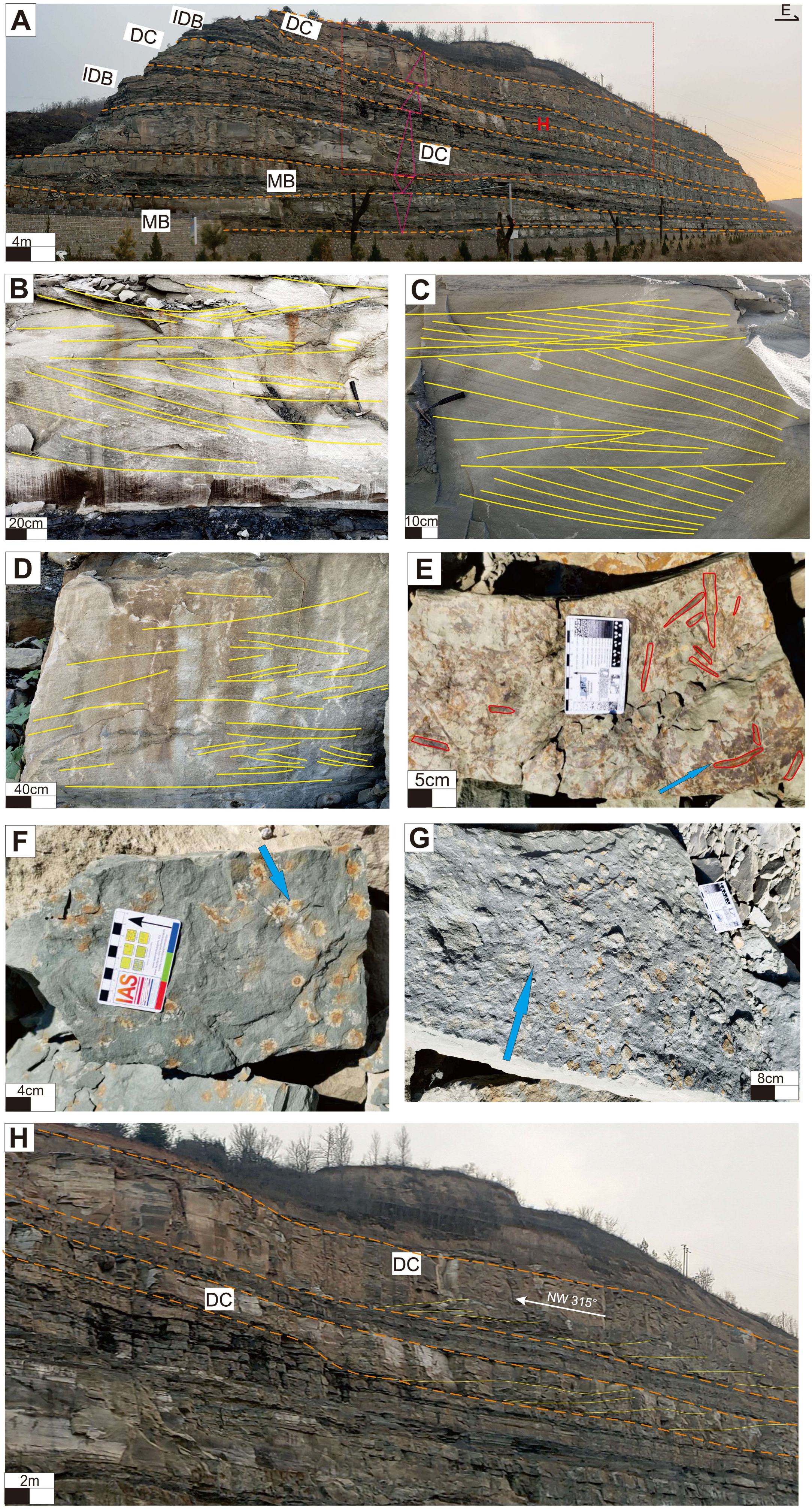
A
IDB
DC
IDB
DC
E
H
DC
MB
MB
4m
B
20cm
C
10cm
D
40cm
E
5cm
F
4cm
G
8cm
H
DC
DC
NW 315°
2m

Fig. 9. Facies associations and architectural characteristics of medial delta-front deposits, Ch-3, Yan He outcrop. See Fig. 2A for outcrop locations. (A) Vertical facies sequence of delta-front deposits, mainly of DC and MB types, interlayered with interdistributary bay fines (IDB). (B) Trough cross-bedding of terminal distributary channel (DC). (C) Planar cross-bedding of terminal distributary channel (DC). (D) Trough cross-bedding and coarsening-upward succession of proximal mouth-bar deposit (MB). (E) Plant debris in IDB deposits. (F) Siderite concretions and iron impregnation of interdistributary-bar (IDB); most examples are less than 1 cm in diameter; present in sandstone beds of IDB. (G) Vertical and sub-vertical burrows on a bedding surface in IDB deposits. (H) Lateral-accretion deposits in terminal distributary channels fills (DC) in delta front, palaeocurrent direction of DC is from north to south (pointed to the reviewer) based on channel-shape and the associated lamina accretion direction; details of deposits shown in (A). See Fig. 2A for outcrop locations. See Table 2 for abbreviations.

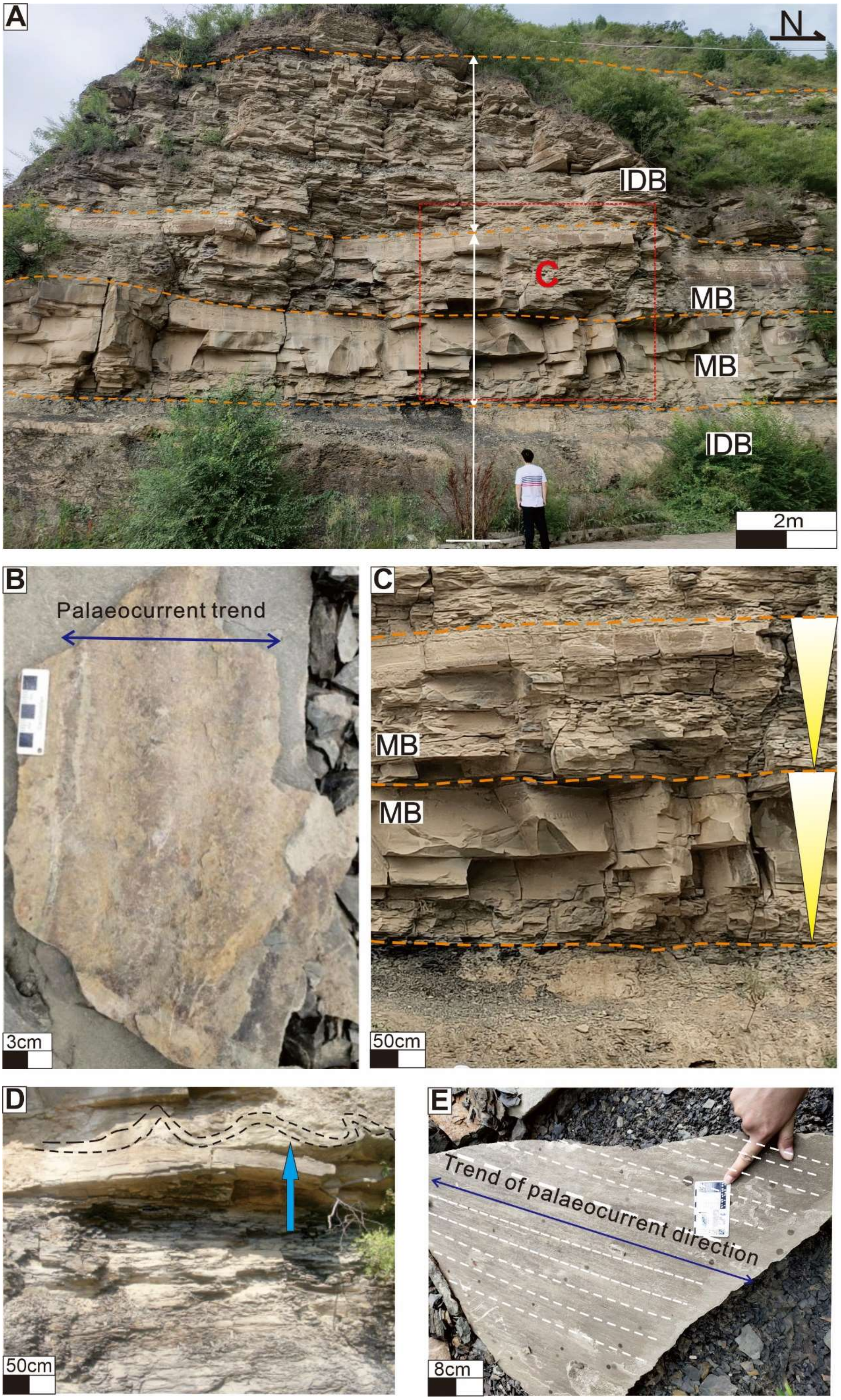
A
N
IDB
C
MB
MB
IDB
2m
B
Palaeocurrent trend
3cm
C
MB
MB
50cm
D
50cm
E
Trend of palaeocurrent direction
8cm

Fig. 10. Facies associations and architectural characteristics of proximal mouth-bar (MB) deposits interbedded with interdistributary-bay (IDB) strata of interval Ch-7, Yan He outcrop. (A) Architectural characteristics of two stacked proximal mouth-bar (MB) units interbedded with thin-bedded laminated mudstone and silty mudstone of IDB origin. (B) Wave ripples in proximal mouth bar (MB) deposits. (C) Two in gross coarsening-upward and thickening succession of proximal mouth bar (MB) deposit, and composed of argillaceous siltstone, siltstone to fine-grained sandstone; details of deposits shown in (A). (D) Convolute bedding in MB deposits. (E) Parting lineation (i.e., primary current lineation) in MB deposits. See Fig. 2A for outcrop locations. See Table 2 for abbreviations.

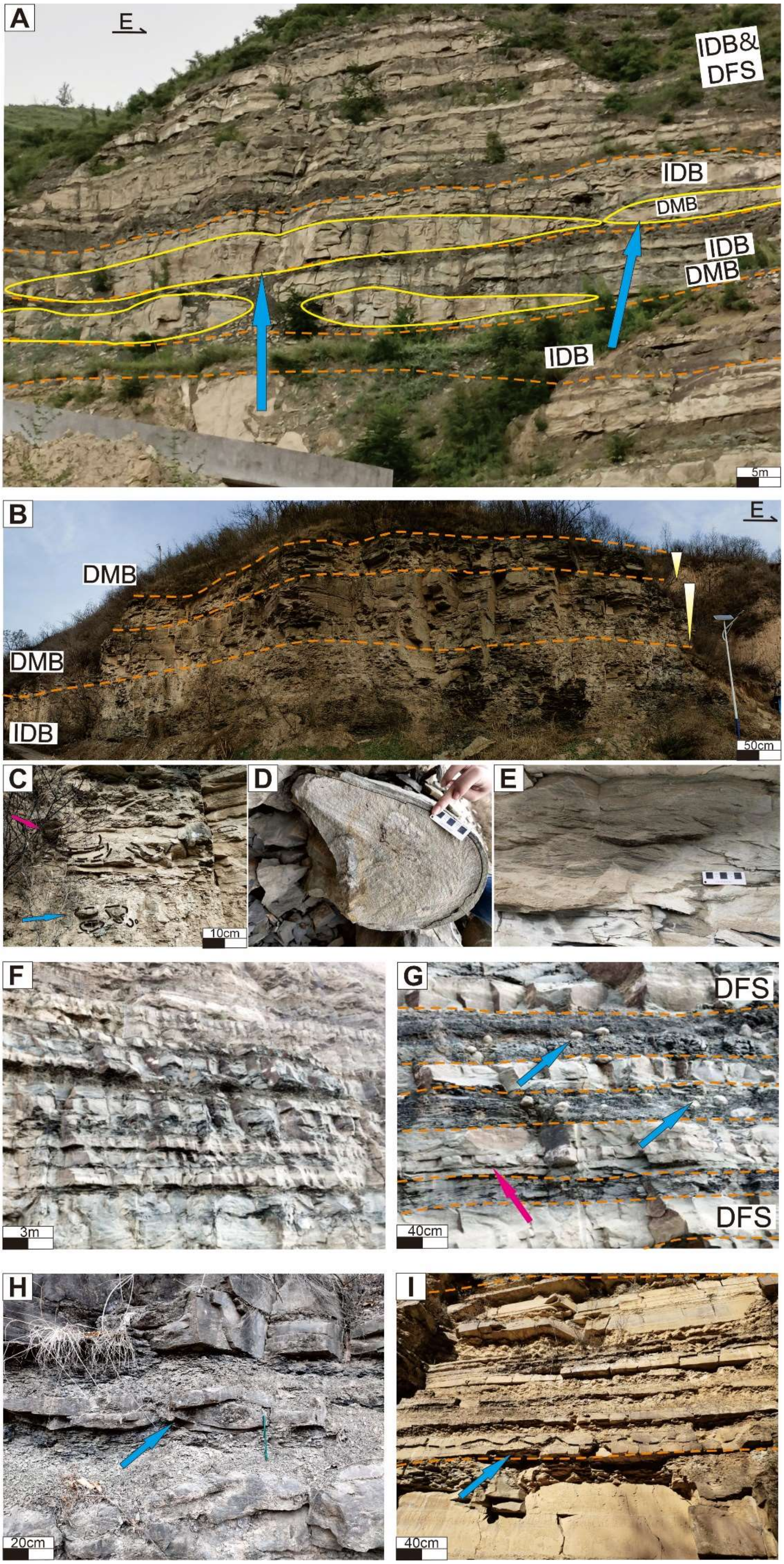
A
E
IDB&
DFS
IDB
DMB
IDB
DMB
IDB
5m
B
E
DMB
DMB
IDB
50cm
C
10cm
D
E
F
3m
G
DFS
DFS
40cm
H
20cm
I
40cm

Fig. 11. Architectural characteristics of distal delta-front deposits. (A) Lenticular sand body with sharp flat basal surface and convex-up top, displaying a gross coarsening-upward trend of distal mouth-bar (DMB) deposits interlayered in thin-bedded dark-grey mudstone and siltstone of IDB; Ch-8, Yan He outcrop; palaeocurrent direction likely towards the viewer on the basis of accretion geometries. (B) Architectural characteristics of two superimposed distal mouth-bar (DMB) units, arranged in gross a coarsening-upward trend, and overlying thin-bedded laminated dark mudstone and shales of IDB; Ch-9, Shiwang He outcrop. (C) Ball-and-pillow structures in mudstones (blue arrow), and convolute bedding in grey siltstones (red arrow) of DMB; detailed view of outcrop in (B). (D) Ball-and pillow structures in DMB strata; detail of (B). (E) Ripple cross-lamination in siltstones of DMB; Ch-9, Shiwang He outcrop. (F) Bedded fine-grained sandstone of DFS interlayered with dark mudstone and shales of IDB origin, in interpreted distal delta-front strata; Ch-8, Yan He outcrop. (G) Globular masses of calcite (blue arrow) concentrated along bedding surfaces in IDB dark mudstones and shales with coarsening-upward trends (fuchsia arrows) of delta-front sheet (DFS) deposits; details of deposits in (F). (H) Symmetrical ripple cross-lamination in thin-bedded sandstone of delta-front sheets (DFS); Ch-6, Shiwang He outcrop. (I) Load structures in thin-bedded sandstones of delta-front sheets (DFS) interlayered with mudstones of IDB; Ch-7, Qishui He outcrop. See Fig. 2A for outcrop locations and Table 2 for abbreviations.

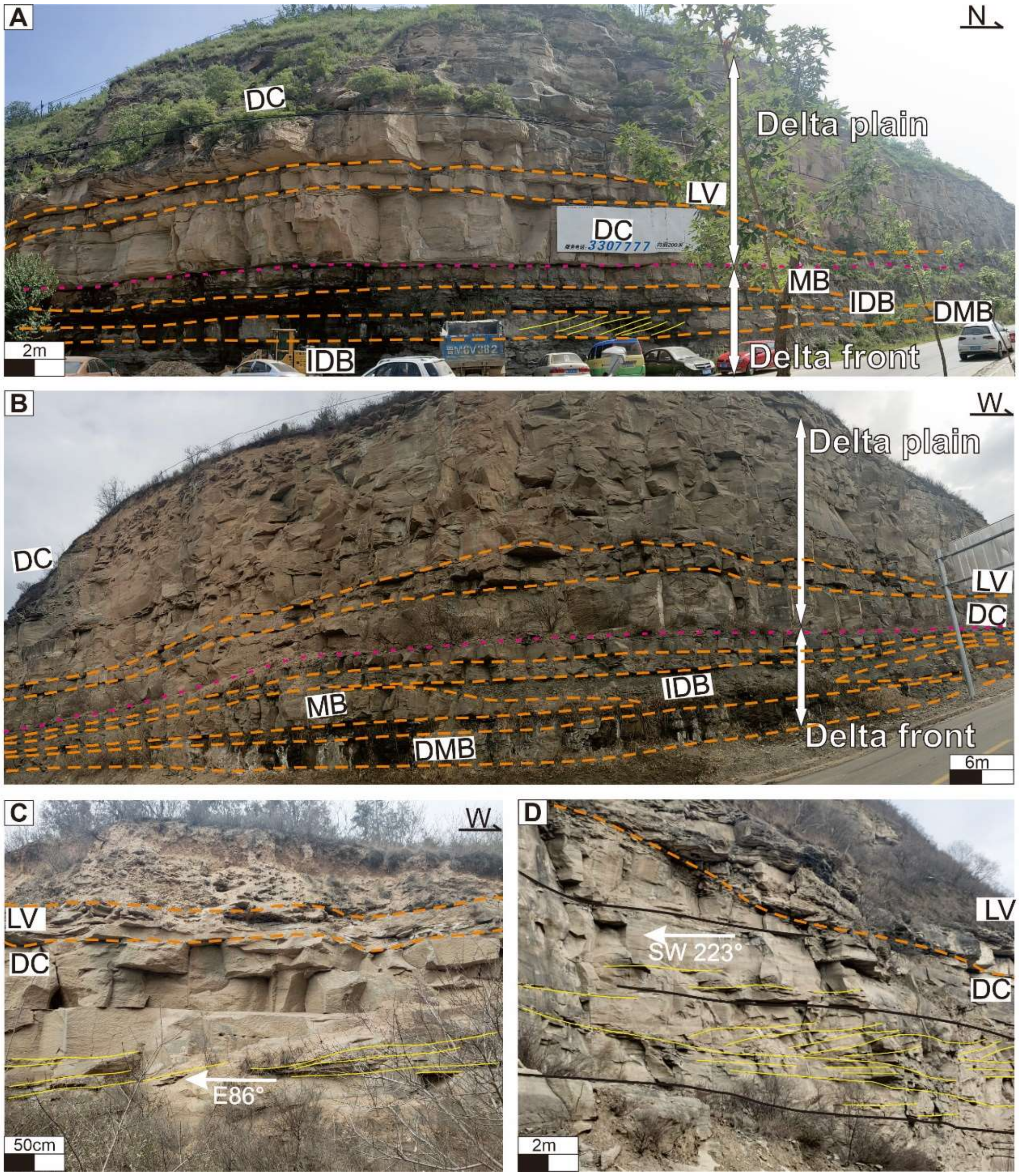

Fig. 12. Architectural characteristics of delta-front and delta-plain deposits; Ch-8, Shiwang He outcrop. (A) Architectural characteristics of deposits transitioning vertically from delta-front to delta-plain facies associations, corresponding to the transition from interbedded dark-grey shales (IDB) with thin-bedded MB (occurring as coarsening-upward trend) and DMB (distinct downstream-accretion geometries) (mouth-bar) sandstones, overlain by thick-bedded fine-grained subaerial distributary channel (DC) sandstones, interlayered with thin-bedded siltstone and mudstone of levee (LV) origin; Ch-8, Shiwang He outcrop. (B) Dip view of architectural

characteristics in (A), showing the distinct sharp flat basal surface and convex-up top of mouth bar deposits (MB), and their intimate relationship with distal mouth-bar (DMB) strata; palaeocurrent direction of MB is likely away from the viewer (north to south) based on observed architectures. (C) Vertical transition from sandstone with large-scale cross- bedding (DC) to siltstone and mudstone with planar parallel bedding (LV); channel deposits exhibit lateral-accretion surfaces; detail of (A). (D) Multi-storey subaerial channel (DC) sandstone with evidence of barform accretion. See Fig. 2A for outcrop locations and Table 2 for abbreviations.

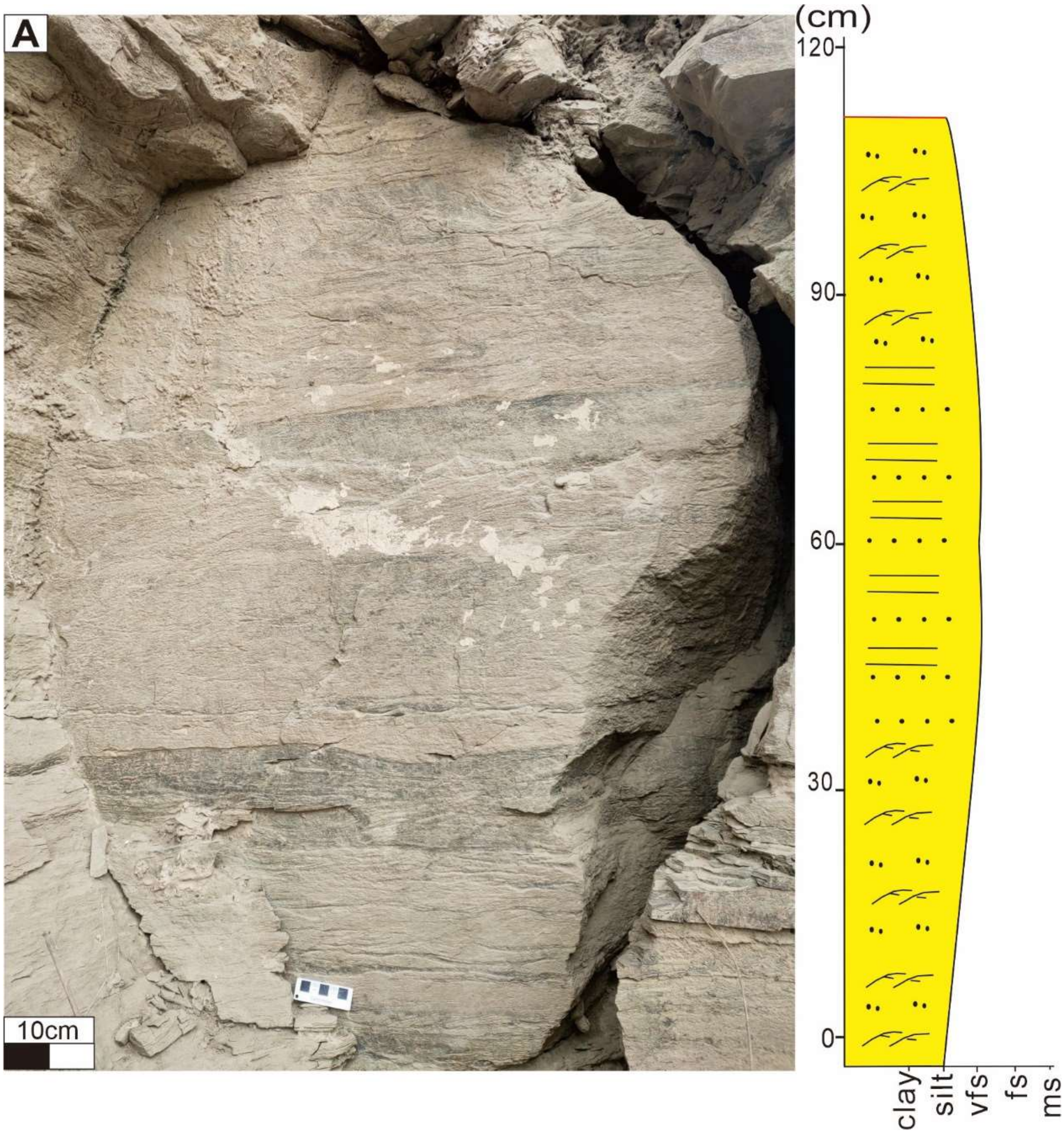

Fig. 13. Succession of rippled siltstone to fine-grained sandstone displaying coarsening- followed by fining-upward trend in interpreted hyperpycnites from prodelta deposits; Ch-9, Shiwang He outcrop. See Fig. 2A for outcrop location.

5. On the differentiation of delta-plain and delta-front deposits

In subsurface datasets of lacustrine successions, differentiation between delta-plain and delta-front strata can be challenging in cases where there exists similarity in bedding style and lithology and close vertical and lateral juxtaposition of their constitutive architectural elements. For example, deposits of coastal distributary channels and those of terminal, perhaps also subaqueous, distributary channels display similar facies organization, primarily related to tractional flows (Fig. 4A, F, Fig. 8A, F; Fig. 14A, B, C; Fig. 16)., and both tend to exhibit SP logs with box or bell shape (Fig. 16; Fig.18). The deposits of crevasse splays and mouth bars show similar coarsening-upward successions and funnel-shaped SP logs (Fig. 16; Fig.18).

Differentiation between delta-top and delta-front deposits can be particularly difficult where frequent lake-shoreline shifts are recorded. This is the case in members Ch-3, Ch-4+5, Ch-6, Ch-7 and Ch-8 of the Yanchang Formation, where rapid lake-shore dislocations are preserved as highly variable vertical facies successions of delta-plain and delta-front strata (Fig.12; Fig.18), and where well-developed deltaic edifices cannot be recognized in the stratigraphy(Zou et al., 2010; Liu et al., 2014). Sedimentological criteria are therefore needed in order to establish a workflow for recognizing the record of palaeoshorelines in well datasets and mapping the position of these palaeoshorelines in planview through the studied stratigraphy.

By combining the study of well cores and logs with sedimentological analyses of outcrop exposures, some of the key differences between delta-plain and delta-front deposits of the Triassic Yanchang Formation in the Ordos Basin have been recognized. These have value as criteria for discriminating the two sets of deposits in subsurface datasets, and have been summarized systematically in terms of characteristics of lithological texture, sedimentary structures, palaeontological content, well-log expression, and vertical facies sequence. These differences are summarized below.

(1) Lithology

In most delta-plain deposits, vertical plant rootlets or stems containing organic matter are common (Fig.5H, I; Fig.15G); root traces mostly taper and branch downward. Palaeosols are occasionally observed (Fig. 6I), which were presumably formed in typically waterlogged anoxic lowland areas that were intermittently subaerially exposed (Mei and Lin 1991; Yang et al., 2009). Coal layers (up to >1 m thick) or coaly streaks are locally observed (Fig. 4C, F; Fig.5J). Mud-prone deposits forming lithosomes with concave bases are locally seen, which likely record the infill of abandoned channels (Miall, 1985; Yang et al., 2009; Jiang, 2010). In delta-front settings, dark-grey mudstones and shales are seen in places, but coals are absent (Mei and Lin 1991; Wu et al., 2004).

(2) Sedimentary structures

In delta-plain settings, raindrop imprints and desiccation cracks that testify to subaerial conditions are common (Blatt et al., 1980; Yang et al., 2009; Jiang, 2010). Limonite concretions with wide variations in diameter occur in sandstone beds; this authigenic limonite is associated with an environment that is subject to intermittent or protracted subaerial exposure and relatively oxidizing conditions (Chen et al., 2007; Yang et al., 2007; Collinson and Mountney, 2019). In contrast, in delta-front settings, synsedimentary deformation structures associated with sediment liquefaction and water-escape driven by rapid deposition and gravitative slumping are common (Fig. 10D; Fig. 11C, D; Fig. 14D, E, F, G) (Wright., 1971; Yang et al., 2009; Jiang, 2010; Ventra et al., 2015; Gao et al., 2019). Locally, evidence of wave reworking is seen (Fig. 10B; Fig. 11H, I) (cf. Keighley et al., 2019). Spherical masses of calcite and pyrite concretions are common authigenic minerals, typically associated with quiet-water and oxygen-deficient conditions, and usually occurring in dark shales (Galloway and Hobday,1996; Yang et al., 2007). Siderite concretions and iron impregnation are occasionally found (Fig. 9F), which likely indicate weakly reducing conditions (Galloway and

Hobday, 1996).

(3) Palaeo-fauna and palaeo-flora

In delta-plain deposits, it is common to observe large plant fragments and stems, as silicified *eocalamite* that grew perpendicular to the bedding, carbonaceous fragments, vertical growth of plant rootlets, and lignite (Fig. 5I, J; Fig. 6I; Fig. 7D; Fig. 15A, B, G, H) (Reineck and Singh, 1986; Yang et al., 2009). In delta-front units, fresh-water fossils are abundant, and include ostracoda, phyllobranchiae, lamellibranchiae, and comminuted plant debris (Fig. 15D, E, F) (Yang et al., 2007; Fu et al., 2018). Vertical and sub-vertical burrows are more common, taking the form of dwelling or escape burrows (Fig. 9G); *Skolithos* is common; the *Psilonichnus* ichnofacies is recognized (Fig. 15I); all of these features are indicative of a shallow-lacustrine setting with sporadically agitated waters (Yang et al., 2009; Renaut and Gierlowski-Kordesch, 2010; Fu et al., 2018).

(4) Well-log signatures

In delta-plain settings, the SP logs of distributary-channel deposits commonly display tree-like, toothed bell- or box-shaped profiles, high-amplitude, and sharp tops and bottoms (Fig. 16A; Fig. 18). Thick log signatures may reflect amalgamation of channel bodies with thin or absent mudstone interlayers (Reineck and Singh, 1986; Mei and Lin, 1991; Wu et al., 2004; Yang et al., 2009; Burton et al., 2014). The SP logs of both floodplain and swamp deposits approximate the low amplitude of the mudstone baseline and have flat profiles (Fig. 16A; Fig. 18). The AC log of swamp deposits displays a leptokurtic profile with high amplitude due to the higher organic content. The SP log of levee deposits has a flat low-amplitude profile, but with higher amplitude on average than that of floodplain units due to coarser grain sizes. The SP log of crevasse-splay units is typically funnel-shaped and low to medium amplitude (Yang et al., 2009; Burton et al., 2014) (Fig. 16A; Fig. 18). By contrast, in delta-front successions, the SP logs of distributary channel deposits are commonly bell-shaped and display medium- to high-amplitude, with sharp base and gradual transitional top (Fig. 16B; Fig. 18) (Reineck and Singh, 1986; Mei and Lin, 1991; Wu et al., 2004). The SP log of interdistributary-bay deposits approximates the low-amplitude mudstone baseline and is flat, whereas the GR log has a tooth-like profile with high values (Fig. 16B; Fig. 18). Progradation of mouth bar deposits is expressed as SP and GR logs with funnel shapes, sharp tops and gradual medium- to high-amplitude variations (Fig. 16B; Fig. 18) (Reineck and Singh, 1986; Mei and Lin, 1991; Wu et al., 2004; Burton et al., 2014). Distal mouth-bar deposits of SP and GR exhibit funnel shapes with lower amplitude than that of proximal mouth-bars (Reineck and Singh, 1986; Mei and Lin, 1991; Yang et al., 2009; Burton et al., 2014) (Fig. 16B; Fig. 18)..

(5) Vertical facies successions

Here, a distinction is drawn between lacustrine delta-plain and delta-front deposits, with the ultimate goal of identifying a record of palaeoshoreline position in the Yanchang successions. Sediments from laterally contiguous sub-environments in lacustrine delta-plain settings alternate vertically, largely in response to distributary-channel avulsion (Yang et al., 2009; Fu et al., 2015). Coarse channel-lag deposits are commonly overlain by sand-prone fining-upward distributary channel deposits, which themselves tend to be in turn overlain by fine-grained deposits primarily composed of silty, muddy and lignite deposits of channel margin and floodbasin origins; the way these units are interbedded may not display any obvious ordering (Fig. 6; Fig. 12C, D). Coal layers that accumulated in backswamp areas can be a common feature (Fig. 4C, F; Fig. 16A). Instead, the basinward progradation of subaqueous environments of river-dominated lacustrine deltas results in gross coarsening-upward successions (Yang et al., 2009; Li et al., 2009; Burton et al., 2014; Liu et al., 2014), reflecting vertical transition from fine-grained prodelta deposits, through distal mouth-bar, sometimes delta-front sheet, interdistributary-bay and mouth bar deposits, and culminating in distributary-channel fills (Fig. 8F; Fig. 9A, H; Fig. 12A, B; 16B). The vertical stacking of single delta lobes results in the alternation of coarsening-upward successions of delta-lobe aprons, primarily because of autogenic dynamics of delta-lobe progradation, switching and abandonment. Shales can be an integral part of subaqueous deltaic deposits (Zou et al., 2010; Liu et al., 2015; Collinson and Mountney, 2019).

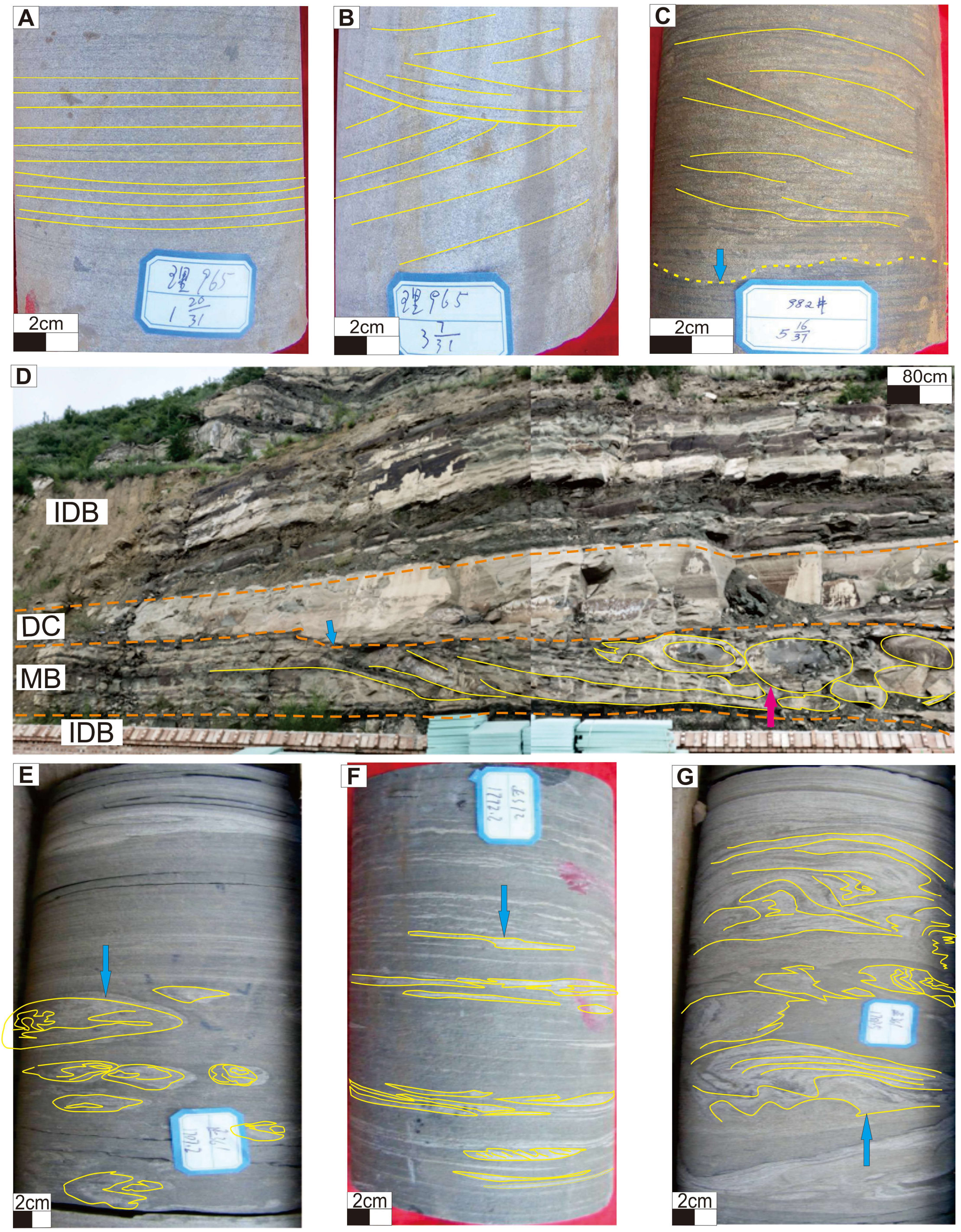

Fig. 14. Sedimentary structures of the deltaic deposits. (A) Planar horizontal lamination of DC in delta-plain deposits; well Li 965, 534.05 m, Ch-4+5. (B) Trough cross-bedding of DC in delta-plain deposits; well Li 965, 584.09 m, Ch-61. (C) Trough cross-bedding and basal erosion (indicated by blue arrow) of DC in delta-plain deposits; well Li 982, 555.42 m, Ch-62. (D) Medial delta-front channel body of terminal distributary channel (DC) with basal erosion (indicated by blue arrow)

and mouth bar (MB) with ball-and-pillow structures (between 40 and 85 cm in diameter) (indicated by red arrow) developed on a likely palaeoslope; Yan He outcrop, Ch-8. (E) Ball-and-pillow structures of DMB in delta-front deposits; sand pillows are between 1 and 5 cm in diameter; well Zh361, 1707.2 m, Ch-6. (F) Lenticular lamination of DFS in delta-front deposits; well Zh372, 1772.2 m, Ch-6. (G) Soft-sediment deformation of DMB in delta-front deposits; well Zh 361, 1707.5 m, Ch-6. See Fig. 2A for well and outcrop locations and Table 2 for abbreviations.

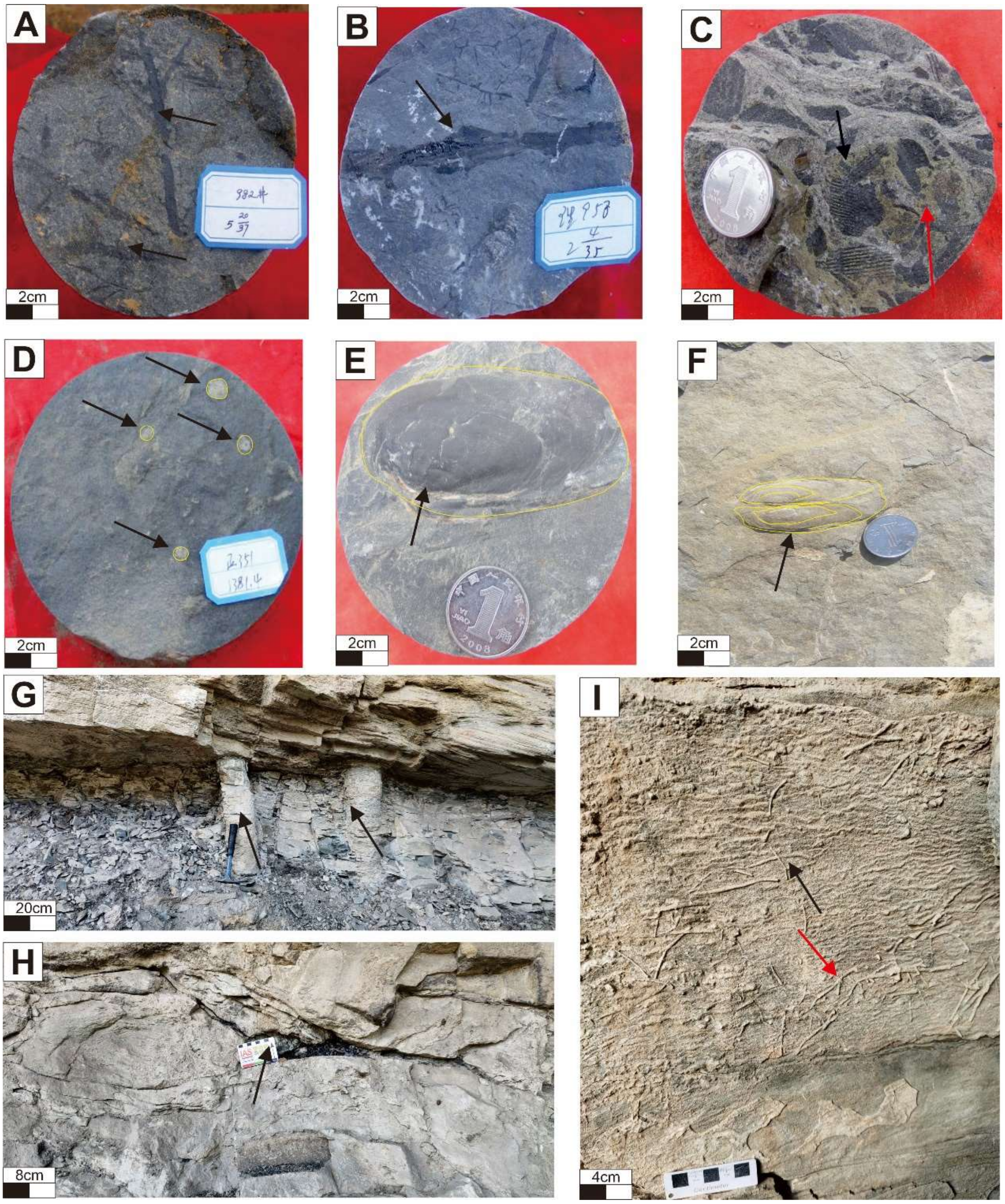

Fig. 15. Palaeontological and ichnological content of deltaic deposits of the Yanchang Formation. (A) Plant stems of FP in delta-plain deposits; well Li 982, 556.43 m, Ch-6. (B) Plant stems of FP in delta-plain deposits; well Li 958, 594.4m, Ch-4+5. (C) Plant stems (indicated by black arrow) and pyrite concretions (indicated by red arrow) of IDB in delta-front deposits; well Hong 3, 446.52 m, Ch-7. (D) Vertical burrow of IDB in delta-front deposits; well Zh 351, 1381.4 m, Ch-3. (E) Pelecypod shell (Unio.) of IDB in delta-front deposits; well Hong 3, 443.7 m, Ch-7. (F) Pelecypod

shell (Unio.) of IDB in delta-front deposits; Yan He outcrop, Ch-7. (G) Large plant stems (silicified *Neocalamites* growing perpendicular to bedding) of FP in delta-plain deposits; Qishui He outcrop, Ch-8. (H) Carbonaceous fragments of DC in delta-plain deposits; Qishui He outcrop, Ch-8. (I) Psilonichnus ichnofacies (i.e., ichnogenera *Psilonichnus* and *Macanopsis*) characterized by X-shaped (black arrow) and Y-shaped burrows (red arrow) in siltstone of MB in delta-front deposits; Shiwang He outcrop, Ch-7. See Fig. 2A for well and outcrop locations and Table 2 for abbreviations.

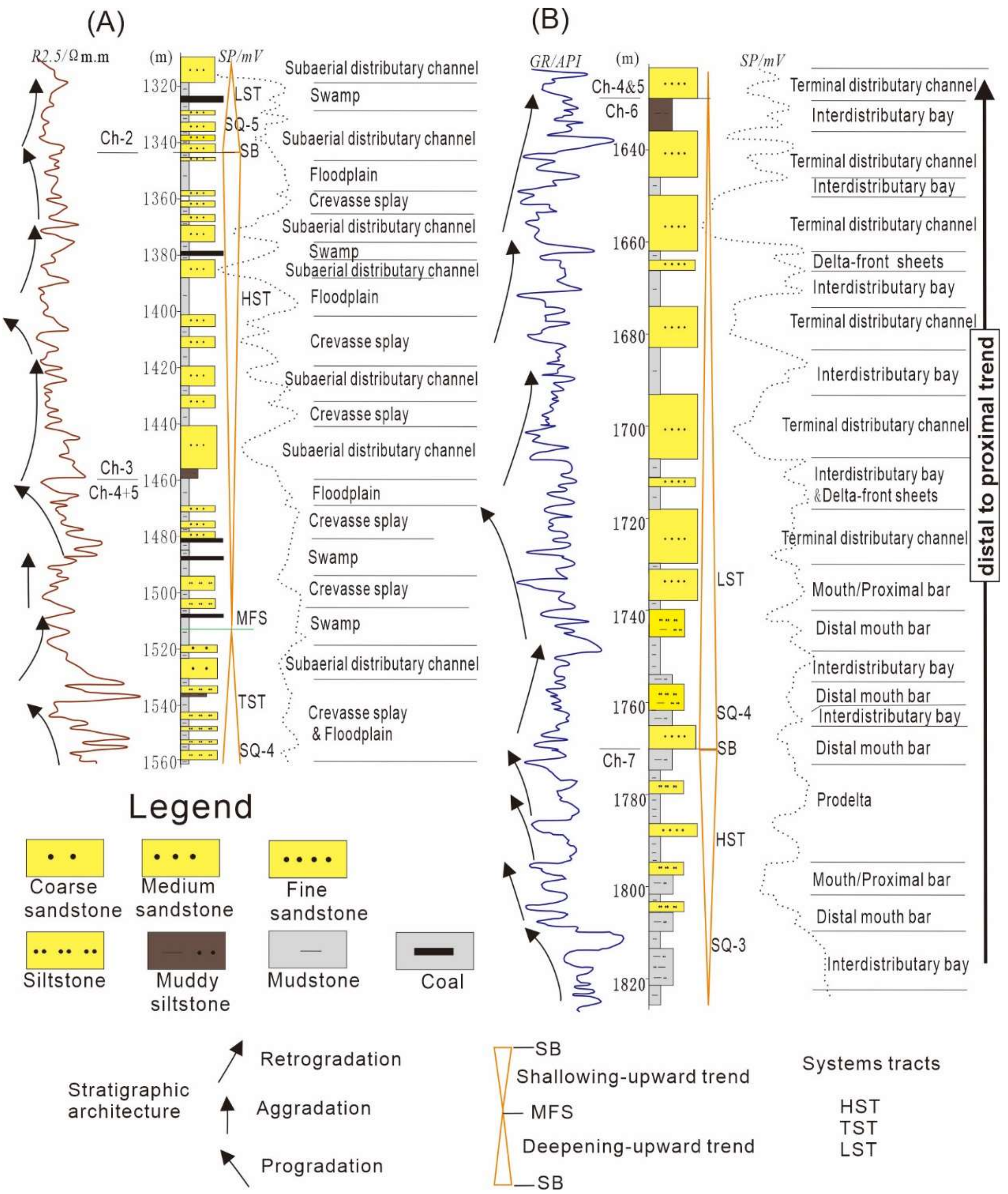

Fig. 16. Lithological and well-log signature and sequence stratigraphy of delta deposits. (A) Delta plain; well Zh 75, members Ch-2, Ch-3, Ch4+5. (B) Delta front and prodelta; well Zh 277, member Ch-6. See Fig. 2A for well locations.

6. Depositional model of lacustrine deltas of the Yanchang Formation

Based on results of both this work and earlier sedimentological studies (Mei and Lin, 1991; Shanley et al., 1994; Lemons and Chan, 1999; Bohacs et al., 2000, 2003; Keighley et al., 2002, 2003; Overeem et al., 2003; Pusca, 2004; Wu et al., 2004; Li et al., 2009; Yang, 2010; Zou et al., 2010; Feng, et al., 2013, 2016; Liu et al., 2015; Zhao et al., 2015; Aschoff et al., 2016; Gall et al., 2017; Fongngern et al., 2018; Gong et al., 2019; Wang et al., 2020; Birgenheier et al., 2020; Jorissen et al., 2020; Zhang et al., 2020; Budai et al., 2021; Olariu et al., 2021), a summary depositional model is proposed that synthesizes the main sedimentological features of shallow-water river-dominated ramp-margin deltas preserved in the Yanchang Formation, with a special focus on characteristics of their delta-plain and delta-front facies belts (Fig. 17). The salient features of the model are summarized in the following points.

(1) Sandbody extension and orientation.

The Yanchang geological history was characterized by lake-level fluctuations of a few metres or tens of metres, potentially developing in response to high-frequency climatic oscillations, acting in parallel with longer-term changes (over millions to tens of millions of years) in subsidence rates across the basin. These lake-level fluctuations appear to have forced shorelines to migrate over kilometres or tens of kilometres, in particular on the gentler northeastern slope (Dong et al., 2011;

Zhang et al., 2020). These shoreline shifts caused nearshore sandbodies to be distributed over a wide domain, in which subaerial or terminal distributary-channel fills oriented at high angle with the palaeoshoreline are the dominant types (85~95%); mouth-bar sandbodies that are roughly elongated along strike represent a subordinate fraction (15~5%) of the stratigraphy (Wei et al., 2007; Li et al., 2009; Zou et al., 2010; Deng et al., 2011).

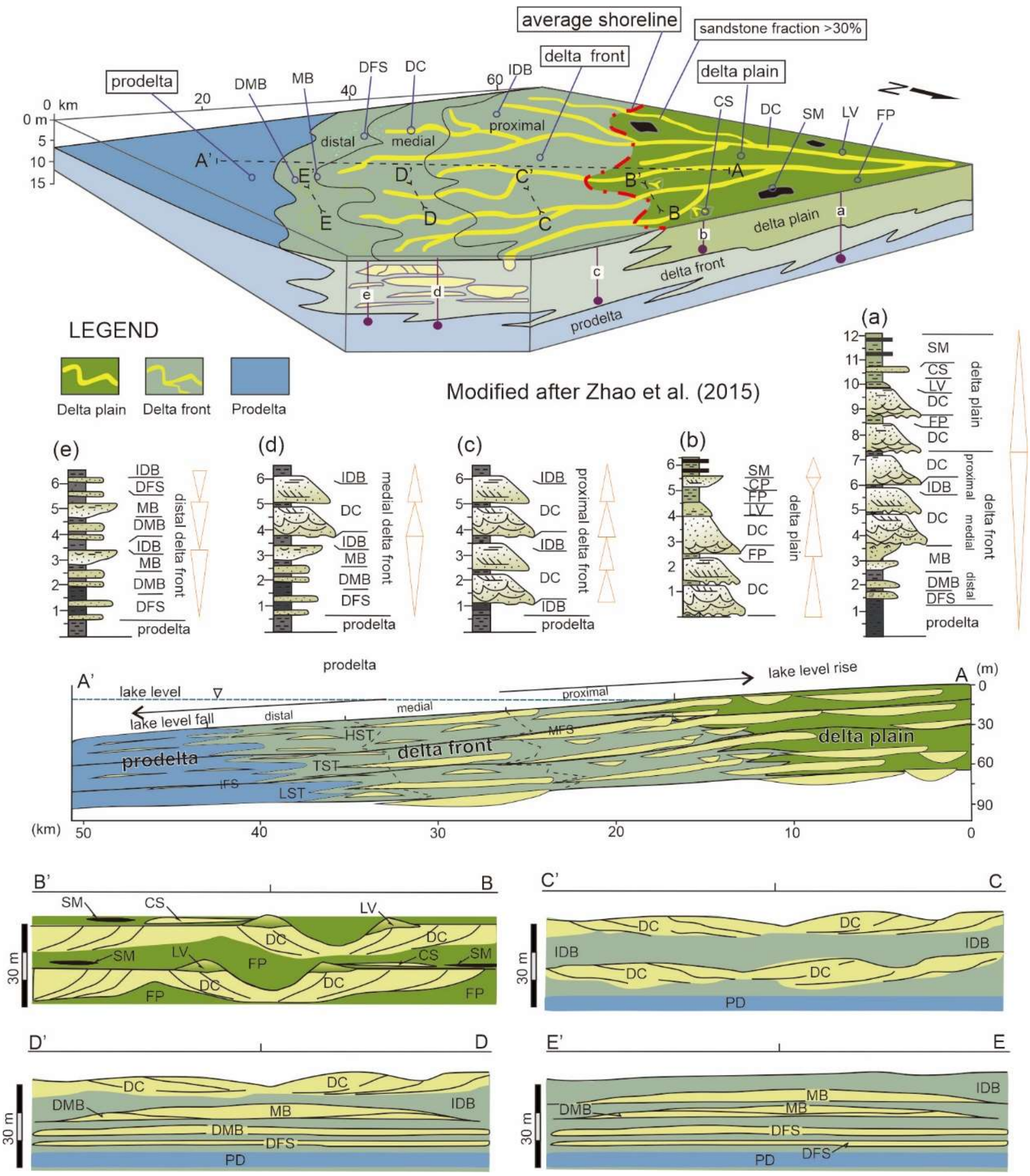

Fig. 17. Depositional model of shallow-water deltaic facies in the Yanchang Formation.

Representative vertical sections are shown: (a) coarsening -upward succession recording a vertical transition from prodelta, to delta-front, to delta-plain; modified in part after Zhao et al. (2015); (b) delta-plain succession; (c) proximal delta-front succession; (d) medial delta-front succession; (e) distal delta-front succession. DC: Subaerial (or terminal) distributary Channel; FP: Floodplain; CS: Crevasse Splay; LV: Levee; SM: Swamp; IDB: Interdistributary Bay; MB: Proximal Mouth-Bar; DMB: Distal Mouth-Bar; DFS: Delta-front sheets; PD: Prodelta. LST, lowstand systems tract; TST, transgressive systems tract; HST, highstand systems tract, IFS, initial flooding surface, MFS, maximum flooding surface; Positions of representative vertical sections a-e and two-dimensional architectural sections A-A' to E-E' are shown in the block diagram.

(2) Geometry of river-dominated deltas.

In the Yanchang lacustrine setting, siliciclastic material supplied from the neighbouring mountain ranges was delivered to the Ordos Basin by rivers, which formed river-dominated deltas with lobate geometry, but which were typically elongated basinward because of the limited reworking by wave process, which may have been restricted to the fringes of delta front and to transgressive periods, primarily due to attenuation and dissipation of the limited wave energy by the gently sloping ramp basin margin (Keighley et al., 2003; Overeem et al., 2003; Olariu et al., 2006 ,2021; Zou at al., 2010; Anthony, 2015). The dispersion in orientation of delta-top channels, arising from stream bifurcation and avulsion, increased progressively as the delta prograded basinward, as seen in modern shoal-water river-dominated lake deltas (Keighley et al., 2003; Overeem et al., 2003; Zou at al., 2010; Shaw et al., 2013; Olariu et al., 2021). In this type of deltaic environments the deposits of multiple laterally mobile distributary channels may dominate over those of mouth bars, as compared to the stratigraphy of digitate deltas (i.e., Mississippi delta) for which channels tend to be more stable (Wu et al., 2004; Olariu and Bhattacharya, 2006; Zou et al., 2010; Ahmed et al., 2014; Anthony, 2015).

(3) Internal architecture of progradational deltas.

In the studied Yanchang lacustrine deltaic deposits, progradational trends are expressed by vertical successions of facies associations, which however are not matched by a clear physiographic differentiation of the deltaic succession into topset, foreset and bottomset geometries. Evident clinoform geometries are absent, likely because of the limited bathymetry (and hence accommodation space) and the relatively high sediment supply that characterized the ramp-like margins of the lake basin in which these deltas built out. The geological surfaces that represent the gradient of topographic surfaces of deposition exhibit downdip slopes that are generally less than 1°. Furthermore, the offlap break that would be expressed in clinoform geometries on this ramp margin is likely to be at the shoreline, where coastal-plain gradients that reflect river processes pass into slightly steeper delta-front gradients. The presence of mouth bar deposits overlain by terminal distributary channels fills may serve as an indicator of proximity to an offlap break; the stacking pattern of a vertical succession of parasequences of the Yanchang setting (i.e., progradational, aggradational and retrogradational stacking patterns) indicates the migration of facies belts, i.e., lakeward or landward shifts of the offlap break (Coleman and Prior, 1982; Nemec et al., 1988; Postma, 1990; Mei and Lin, 1991; Overeem et al., 2003; Liu et al., 2014; Rubi et al., 2018; Budai et al., 2021; Olariu et al., 2021). Accordingly, in reflection-seismic datasets (Liu et al., 2014), progradational successions are associated with parallel continuous, intermittent reflectors or shingled clinoforms (if resolved), and stratal geometries indicative of progradation are rarely seen.

Also, these progradational trends are not typically expressed by funnel-shaped well-log profiles, and may even be manifested as box- or bell-shaped wireline-log patterns, since the main sandstone units in delta-front settings are represented by terminal distributary-channel bodies, as discussed below (Mei and Lin, 1991; Li et al., 2009; Yang, 2010; Zou et al., 2010; Shaw et al., 2013; Liu et al., 2014).

(4) Terminal distributary-channel bodies as principal delta-front sandbodies.

The types of sediments deposited at river mouths of marginal-lacustrine settings depend on the relative dominance of (1) outflow inertia, (2) turbulent bed friction lakeward of the river mouth, and (3) outflow buoyancy (Wright, 1997; Fidolini and Ghinassi, 2016). In the Yanchang lacustrine system, where wind fetch was likely limited (Zou et al., 2010) and effluent outflows characterized by sediment concentrations that likely made their density higher than that of the standing water body (Zavala et al., 2006; Yang et al., 2017), sediment may have been delivered at river mouths and beyond more rapidly than the rate at which it could be reworked by shoreline processes. River outflows dominated by inertial forces could have extended long distances offshore of the river mouth, promoting the development of terminal distributary channels as the dominant features of delta-fronts (Mei and Lin, 1991; Wu et al., 2004; Li et al., 2009; Yang et al., 2009; Zou et al., 2010; Olariu et al., 2012; Fidolini and Ghinassi, 2016). Terminal distributary-channel fills associated with levees are seen in modern deltas and Holocene deltaic successions, such as the Volga delta and the Ganjiang River delta; in these examples, proximal delta-slope areas exhibit a network of distributary channels acting as conduits for currents derived from failure of river-mouth sediments, which can be transported offshore for long distances (1～10 kilometres) (Mathews and Shepard, 1962; Tye et al., 1989; Hart et al., 1992; Kostaschuk et al., 1992; Overeem et al., 2003; Zou et al., 2010; Olariu et al., 2021). The lakeward extension of these channels determines the shoestring geometry of their preserved sandbodies. Primarily due to progradation, switching and abandonment of delta-lobes controlled by autogenic dynamics, the vertical stacking of single lobes likely resulted in the alternation of coarsening-upward successions and in the lateral amalgamation of delta-lobe aprons containing multiple distributary-channel fills (Zou et al., 2010; Liu et al., 2015). Distributary channels of the Yanchang lacustrine system probably occurred in both subaerial and subaqueous environments of the shallow-water deltas, as partially reflected by the presence of channel deposits encased in both lacustrine and floodplain deposits (Fig. 4; Fig. 5; Fig. 6; Fig. 7; Fig. 8; Fig. 9; Fig. 12; Fig. 16; Fig. 18). Distinguishing the products of subaqueous and subaerial channels near the river mouths is rendered difficult by the fact that offshore channel propagation associated with delta progradation makes certain subaqueous features become subaerial through time (Shaw et al., 2013; Martini and Sandrelli, 2015); this may have been the case for the Yanchang lacustrine environments, characterized by low gradients and high rates of lake-level change, which likely resulted in high rates of deltaic shoreline migration (Renaut and Gierlowski-Kordesch, 2010; Zou et al., 2010; Olariu et al., 2021). This contrasts with dynamics seen in other river-dominated delta slopes, such as those of the Wabash delta, where distributary channels tend to develop and be infilled under fully subaqueous conditions (Ahmed et al., 2014).

Sandstones of terminal distributary channel origin in delta-front facies belts form the dominant proximal delta-front facies association of the Yanchang lacustrine system; these deposits also form up to 50% of the medial delta-fronts. By contrast, these sandstones are rare in distal delta-front settings, where associated units of (distal) mouth-bar origin are less than 2 metres in thickness and commonly have a sandstone fraction <30% (Mei and Lin 1991; Wu et al., 2004).

(5) Limited preservation of proximal mouth-bar sandstones in delta-fronts.

The influence of wave reworking processes on mouth-bar sand bodies is inferred to have been relatively limited in the fluvial-dominated deltaic setting of the Yanchang depositional systems (Wright, 1977; Wu et al., 2004; Li et al., 2009; Zou et al., 2010). Instead, it is thought that a major control on the preservation of proximal mouth-bar units was played by the occurrence and mobility of distributary channels, whose morphodyamics could have caused the entrainment and basinward transport of delta-front deposits. This mechanism of sediment dispersal may have been particularly important because of the limited palaeobathymetry (accommodation space), gentle offshore gradient, and high rates of fluvial sediment supply of the system. These conditions may have enhanced the formation and offshore propagation of river-dominated sub-environments (i.e., distributary-channel deposits). Furthermore, as the mouths of terminal distributary channels advanced, mouth bars became partially incised, in particular where compactional subsidence was low, as generally expected for the Yanchang shoal-water lake basin. Distributary incision of mouth bars may have locally caused complete erosion of proximal mouth-bar facies, thereby determining their small proportions in proximal delta-fronts (Mei and Lin, 1991; Overeem et al., 2003; Schomacker et al., 2010; Li et al., 2009; Olariu et al., 2021). This is in agreement with physical simulations that attempt to model depositional conditions for the Ch-6 of the Ordos Basin, and which demonstrate that the ultimate preservation potential of mouth-bar deposits is relatively limited (Zhang et al., 2000). This view provides explanation for the relative increase in the abundance of thin-bedded mouth-bar deposits in the distal delta-front regions, relative to the more proximal facies belt. Proximal delta-front settings are instead characterized by the dominance of laterally and vertically amalgamated terminal distributary-channel sandbodies with higher preservation potential, whereas intervals that accumulated in the medial delta-front exhibit vertical sequences of facies associations that record the transition between the two architectural styles (Fig. 16B). In general, delta-front facies belts display a basinward decrease in sandstone fraction and thickness (Mei and Lin, 1991; Wu et al., 2004; Bhattacharya, 2010).

(6) Subaerial distributary-channel fills as dominant sandbodies of subaerial delta-tops.

The subaerial delta-tops were dominated by channel and overbank fluvial processes, which operated in a variety of depositional sub-environments (i.e., subaerial distributary channels, floodplain, levees, crevasse splays and swamps). The numerous subaerial distributary channel fills are preserved as linear shoestring-shaped sandbodies embedded in floodplain deposits that make up the largest fraction of preserved delta-plain stratigraphy (20-55%). The recognition of levee deposits bordering the distributary-channel fills may relate to progressive channel aggradation, which could have driven channel superelevation above the floodplain, a condition that facilitates channel avulsion (Allen, 1963; Selley, 1965; Bryant et al., 1995; Mohrig et al., 2000). Typically, the relative palaeocurrent directions of CS elements are approximately perpendicular or at high angle to the gross palaeocurrent trends of the genetically related DC elements (Fig. 7). It is inferred that the combination of repeated avulsions with the development of distributary networks may have resulted in the formation of an intricate interconnected web of elongated sandbodies, which are in physical connection where avulsion nodes and channel bifurcations were originally established (Brizga and Finlayson, 1990; Jones and Schumm, 1999; Mohrig et al., 2000; Ke et al., 2019).

7. Mapping of Yanchang lake palaeoshorelines: approach, results and applications

7.1 Reconstructions of palaeoshoreline positions

A record of the position of palaeoshorelines in lacustrine successions can be deciphered by integrating sedimentological, geophysical and geochemical datasets (Bohacs et al., 2000; Wei et al., 2007; Yang et al., 2009; Jiang and Liu, 2010; Liu et al., 2014; Keighley et al., 2019). In this work, the mapping of palaeoshorelines through the studied stratigraphy is undertaken exclusively on the basis of facies criteria, with consideration of the depositional model for the Yanchang lacustrine deltas.

The following principles and steps define the workflow adopted for delineating the average position of the lacustrine shoreline for each studied member of the Yanchang Formation. Firstly, the identification and classification of facies associations is performed on sedimentological logs of cores, on well logs, and in outcrop. Secondly, these classes of deposits are correlated laterally across multiple wells and outcrop exposures (Fig.18). Thirdly, these correlation panels are projected in plan-view, to enable visualization of both vertical and lateral changes (Jiang, 2010). This is applied to maps on which the location of each well and outcrop section is indicated, and on which variations in sandstone fractions can be drawn. Areas in which the studied member has a sandstone ratio >30% commonly reflect a high density of terminal and/or subaerial amalgamated distributary-channel fills and mouth bars; an overall decrease in sandstone fraction is observed from delta-plain to distal delta-front settings. Finally, to reconstruct a time-averaged position of the palaeoshoreline for each member, the relative proportion of delta-plain and delta-front deposits at any one place in the members was considered. As a practical rule, the shoreline is placed relatively more basinward when the unit as a whole contains a relatively larger proportion of delta-plain deposits, and vice versa (Fig.18).

This simplified approach to the consideration of lacustrine shorelines enables a practical, evidence-based approach for mapping overall trends while handling a large volume of well data.

The approach and related facies criteria can be generalized to other lake basins, in particular those with ramp margins and river-dominated deltas discharging into depocentres dominated by finer-grained sediments, by considering some aspects of stratigraphic architecture. For example, the preserved lacustrine facies belts recorded in highly variable vertical facies sequences are characterized by the alternation of delta-plain and delta-front deposits and a lack of recognizable deltaic edifices (distinct delta-slope clinoforms). Deltaic sand aprons comprise of linear shoestring distributary channel-fill sandbodies, which may be amalgamated, and which tend to be encased in fine-grained deposits of both lacustrine and floodplain origin. The offlap break that may be recognized in the gentle clinoforms on this ramp margin is likely to embody the position of the palaeoshoreline, marking the gradient break between coastal-plain and delta-front domains. Mouth-bar deposits overlain by distributary-channel fills may serve as an indicator of proximity to the offlap break when observed. The variably progradational, aggradational and retrogradational parasequence stacking patterns indicate the migration of facies belts associated with the lakeward or landward shift of the offlap break and the palaeoshoreline.

7.2 Reconstructed positions of lake palaeoshorelines

Applying the approach outlined above, the position of the lake palaeoshoreline and the lake extent have been reconstructed for members of the Yanchang Formation, and this was done in particular detail for the Zhidan area. The results of this work unravel the temporal evolution of lake palaeoshorelines of the Ordos Basin over the length of time embodied by the nine stratigraphic intervals Ch-10 to Ch-1 (oldest to youngest). Since the total length of time of deposition of the Yanchang Formation is 28.5 My (238 to 198 Ma; Yang et al. 2017), the average time length of deposition for each member is ca. 3 My.

A NW-SE-oriented depocentre existed from Ch-10 to Ch-3 times, which was centred on the area near Zhidan during Member Ch-9, and which then migrated westward. Maximum lake expansion occurred during accumulation of Member Ch-7. During Ch-2 times, the depocentre assumed a W-E-orientation, which was maintained until the times of Member Ch-1, when deep-lacustrine environments only existed in the northeastern area of Zichang (Fig. 18; Fig. 19) (Wu et al., 2004; Wang et al., 2006; Li et al., 2009; Yang et al., 2009; Zhao et al., 2009).

During Ch-10 times, the Yanchang lake formed in the basin. The planform morphology of the lake indicated by the reconstructed average shoreline position was narrow in the northwest and wide in the southeast; the shoreline was located along the areas of Zhengning—west of Huachi—north of Anbian—Yan'an—Fuxian.

During Ch-9 times, the initial and primary lake expansion occurred, and the lake shoreline was located along the areas of Zhenyuan—well Feng 3—Anbian — Zichang—well Wang 10. The lake basin gradually enlarged from the early to the late Ch-9 stage, through a distinct transgressive period. A deltaic-lacustrine sedimentary succession accumulated during the early periods of Ch-9 times, as LST of SQ2 (cf. Deng et al, 2011). The upper part of Ch-9, as TST of SQ2, records a semi-deep lake area covering an area ca. 4×10^4 km^2; the corresponding stratigraphy acts as an important source-rock interval called the "Lijiapan Shale" (or K1 marker bed) (Pang et al., 2010; Zou et al., 2010).

During Ch-8 times the lake expansion continued: the lake covered a wider area and expanded to the west and southwest. In the northeast, the shoreline trended around the areas of well Feng 5—Anbian—Zichang. In the southwest, instead, the shoreline was located outside the study area, and as such the entire southwestern sector was submerged by the lake. Ch-8 overall records a rapid fall-and-rise cycle over Ch-8_2 to Ch-8_1 times (Yang et al., 2010); Ch-8_2 records marked delta progradation as the HST of SQ2, whilst Ch-8_1 records deltaic retrogradation and aggradation in the LST of SQ3.

During Ch-7 times, a climax of lake expansion was reached, when the extent of Yanchang lacustrine system was at its largest. The lake was approximately circular in planform, and its shoreline in the northeast reached the areas of Zichang—Jingbian; the whole southwestern area was still occupied by the lake. Deep and semi-deep lacustrine deposits accumulated over an area of ca.10×10^{4} km^2 (Deng et al, 2011); these take the form of interbedded siltstones and mudstones and turbidite fine-grained sandstones. The Ch-7 member incorporates the TST and HST of SQ3, as well as a Maximum Flooding Surfaces (MFS) of the Yanchang Formation second-order sequence (Li et al., 2009; Pang et al., 2010).

During Ch-6 times, the lake decreased in extent, and in the northeast the shoreline trended along the areas of Yan'an—Anbian—well Feng5, whereas the entire areas of the southwest were still submerged below the lake level. Ch-6 records fluvio-deltaic progradation during the early LST of SQ4 (Deng et al, 2011; Zou et al., 2010). A series of distinct progradational units of fluvial and deltaic lobe-aprons are recognized from subsurface data along the northeast margin of the basin (Zou et al., 2010; Deng et al, 2011; Zhao et al., 2015).

During Ch-4+5 times, the lake area shrank further, and the shoreline shifted in an approximately concentrical manner. The northeast shoreline trended along the areas of well Feng5—Anbian—Yan'an—Fuxian, whereas the western shoreline was located along the areas of Zhenyuan—Changwu. Regionally, Ch-4+5 comprises of thicker and extensive mudstone units and coal layers recording an episode of lake expansion during the late TST and early HST of SQ4 (Pang et al., 2010).

During Ch-3 times, the lake gradually contracted further as it began to be progressively infilled, approaching its complete shrinkage and disappearance, at times of relatively reduced subsidence rates in relation to the progressive reduction in strike-slip fault activity since Ch-10 times (Li et al., 2009; Deng et al., 2013). The shoreline migrated further basinward; thus, in the northeast it trended along the areas of Yan'an—Zhidan—Well Xin64—well Feng3, whilst in the southwest it was located along the areas of Huanxian—Qingyang. During Ch-3 times, the progradation of fluvial and deltaic systems was associated with a progressive fall of the lake level and associated reduction in accommodation space in lake-margin environments, which occurred in the late HST of SQ4 (cf. Yang et al., 2010; Deng et al, 2011).

During Ch-2 times, durtherr lake contraction occurred, only a small remnant of the former shallow lake survived, and the intense uplift and denudation of the Ordos Block accelerated the process of lake infill (Li et al., 2009; Deng et al., 2013). In the southwest, the shoreline trended along the areas of Wuqi—Zhidan—Yongning—Zhiluo—Fuxian. This evolution is linked to abundant sediment supply, and low accommodation space in the LST and TST of SQ5 (cf. Zou et al, 2010).

During Ch-1 times, the southern margin of the basin was upheaved due to uplift of the Qinling range, the depocentre and locus of fastest subsidence both migrated to the northeast area of Zichang, around which the shoreline trended concentrically; deep-water turbidites accumulated around the areas of Zichang—Hengshan (Wang et al., 2006; Li et al., 2009; Zhao et al., 2009; Deng et al., 2013). During this terminal phase of the Yanchang lacustrine basin, in spite of the overall trend of lake shrinkage, the delta-plains still experienced waterlogged conditions. In the lower part of Ch-1, corresponding to the late LST and early HST of SQ5, shallow- and deep- lake deposits of local occurrence form an important source-rock interval in the northeast areas (K9 marker bed) (Pang et al, 2010). Deltas and deep-lacustrine turbidite are mainly developed in the upper part of Ch-1, in which a distinct progradational trend is recorded. Under these conditions, local peat accumulation gave rise to thin-bedded coal seams or layers, represented by the Wayaobu coal series in the Zichang area, whose stratigraphic distribution may in part reflect autogenic delta-lobe switching. However, it is inferred that water-table fluctuations were primarily allogenic and induced by relative lake-level changes occurring due to climatic and tectonic controls. During the warm climate of the studied period, lake transgression coupled with limited sediment input produced expanses of wetlands and large vegetated swamps (Bohacs et al., 2000, 2003; Wang et al., 2006; Li et al., 2009).

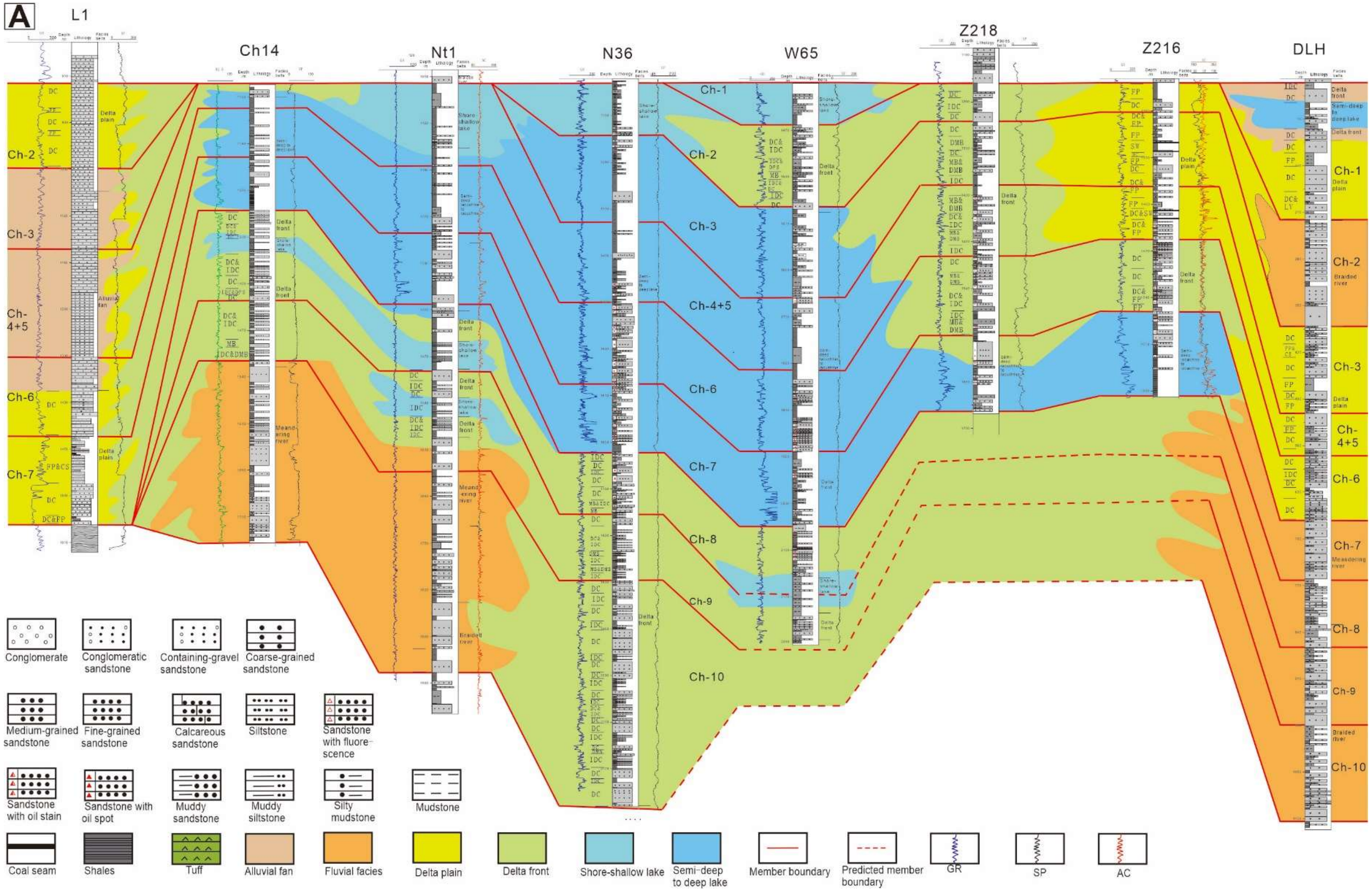
A
L1
Ch14
Nt1
N36
W65
Z218
Z216
DLH
Ch-1
Ch-2
Ch-3
Ch-4+5
Ch-6
Ch-7
Ch-8
Ch-9
Ch-10
Conglomerate
Conglomeratic sandstone
Containing-gravel sandstone
Coarse-grained sandstone
Medium-grained sandstone
Fine-grained sandstone
Calcareous sandstone
Siltstone
Sandstone with fluorescence
Sandstone with oil stain
Sandstone with oil spot
Muddy sandstone
Muddy siltstone
Silty mudstone
Mudstone
Coal seam
Shales
Tuff
Alluvial fan
Fluvial facies
Delta plain
Delta front
Shore-shallow lake
Semi-deep to deep lake
Member boundary
Predicted member boundary
GR
SP
AC

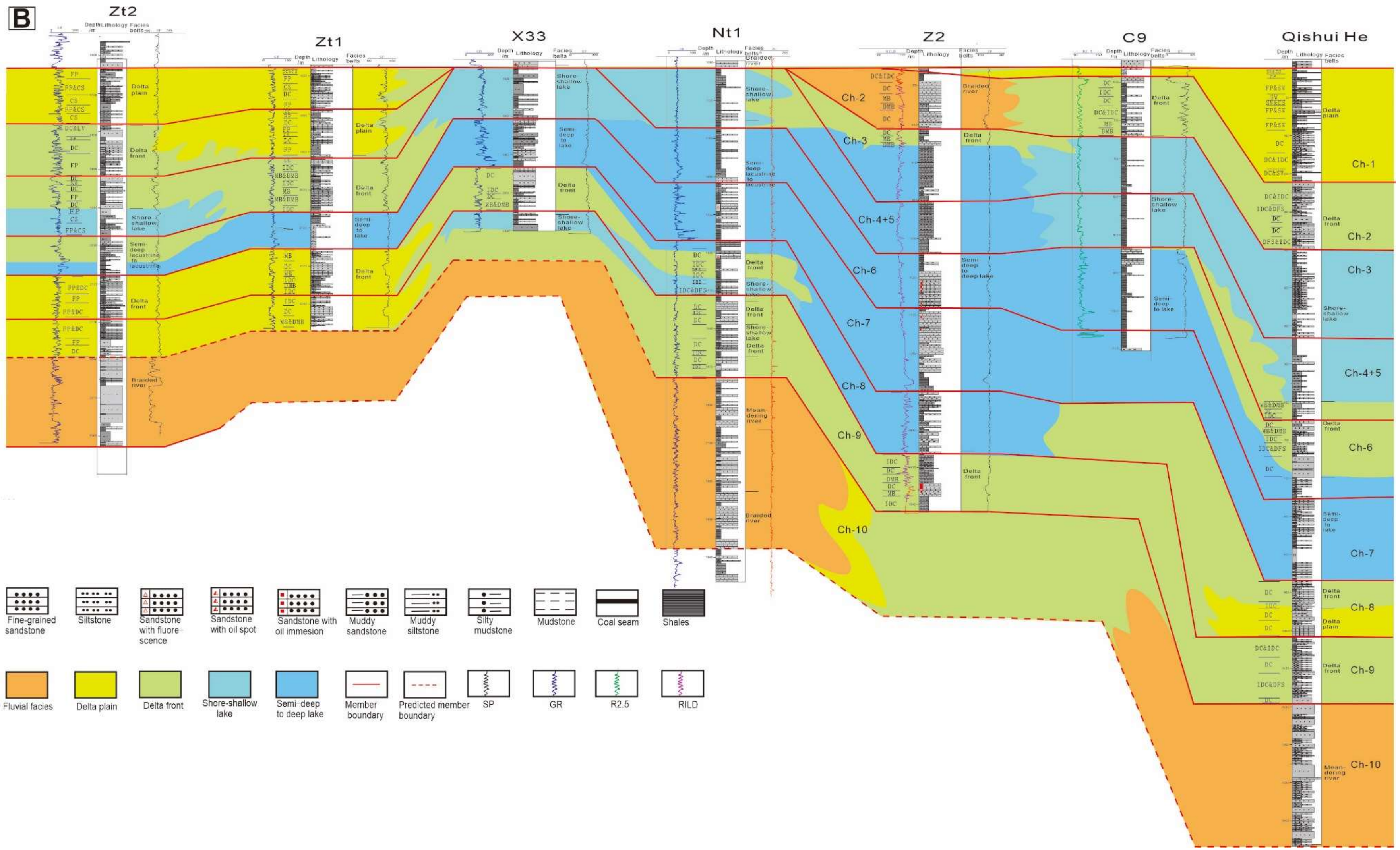
B
Zt2
Zt1
X33
Nt1
Z2
C9
Qishui He
Ch-1
Ch-2
Ch-3
Ch-4+5
Ch-6
Ch-7
Ch-8
Ch-9
Ch-10
Fine-grained sandstone
Siltstone
Sandstone with fluorescence
Sandstone with oil spot
Sandstone with oil immesion
Muddy sandstone
Muddy siltstone
Silty mudstone
Mudstone
Coal seam
Shales
Fluvial facies
Delta plain
Delta front
Shore-shallow lake
Semi-deep to deep lake
Member boundary
Predicted member boundary
SP
GR
R2.5
RILD

Fig. 18. Cross-sections illustrating tentative correlations, facies-belt boundaries, and well-log signatures of architectural elements. (A) Profile between Well L1 to outcrop Dalihe River, oriented along depositional dip. (B) Profile between Well Zht2 to outcrop Qishuihe River, oriented along depositional strike. See Table 2 for abbreviations.

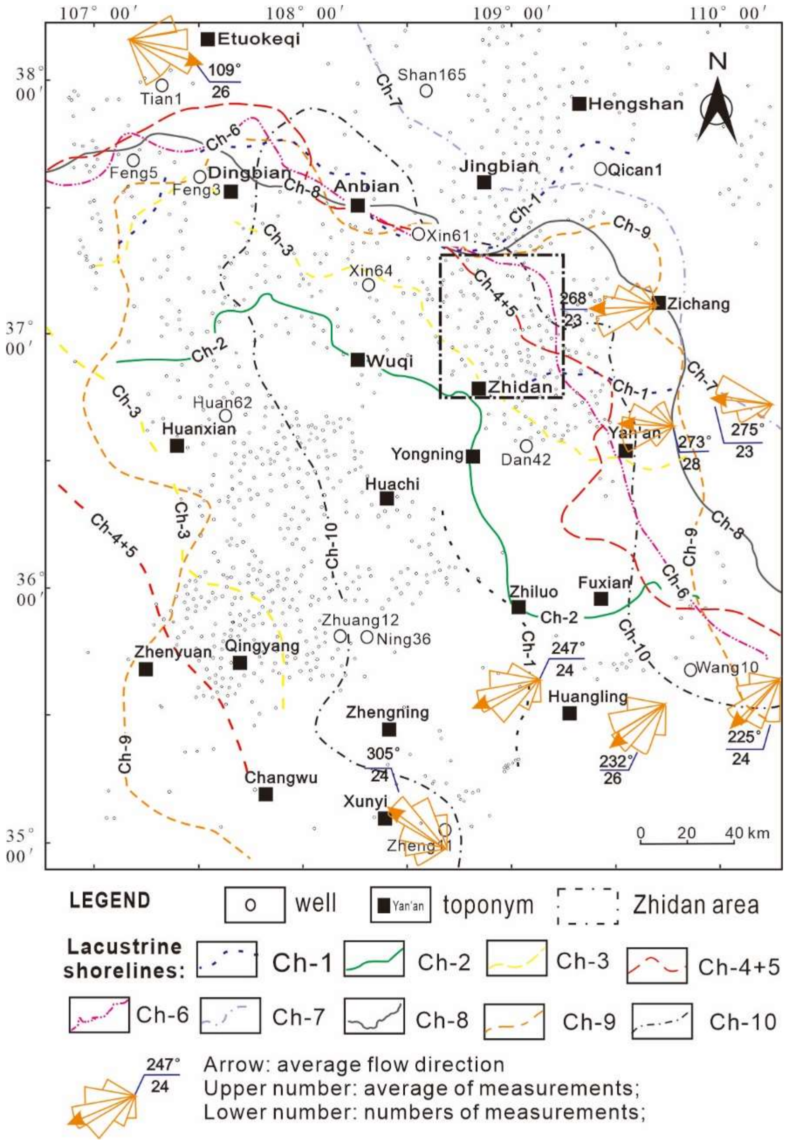

Fig. 19. Position and evolution of lacustrine shorelines of the Yanchang Formation in the studied sector of the Ordos Basin, as time-averaged for each studied member. Rose diagrams of palaeocurrents of the lower and middle section of Yanchang Formation are modified from Xie (2016) and are based on palaeoflow indicators from distributary-channel deposits. The dashed box indicates the location of the Zhidan area shown in Fig.20.

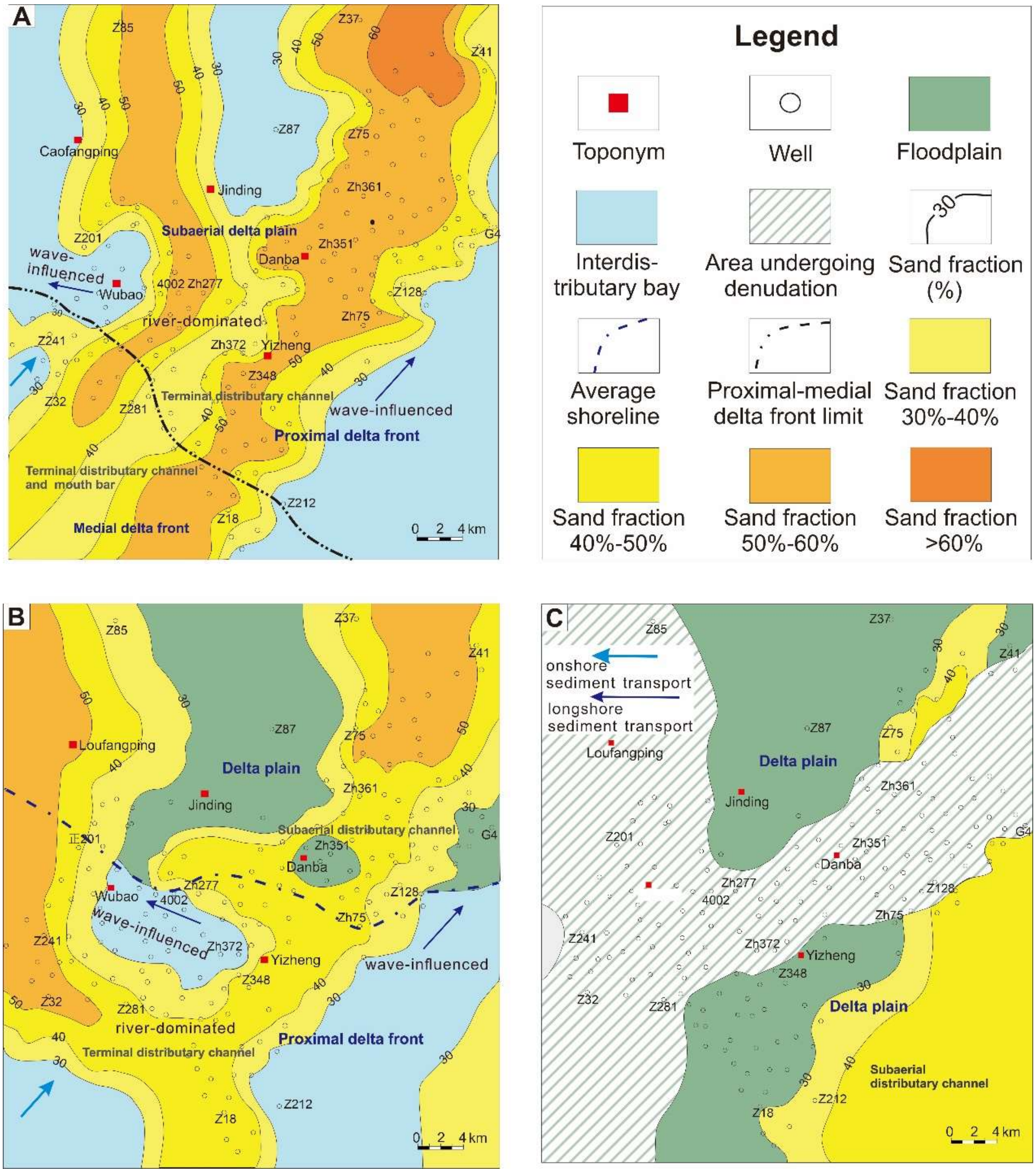

Fig. 20. The distribution and evolution of sedimentary facies associations of the Yanchang Formation in the Zhidan area, northeast Ordos Basin. (A) Ch-6. (B) Ch-4+5. (C) Ch-1. The location of this area is shown in Fig. 19.

The area of Zhidan in the Ordos Basin has been studied in detail to characterize the evolution of the Yanchang deltaic settings in relation to lacustrine shoreline shifts, particularly for members embodying important palaeoshoreline migration in response to oscillations of the lake level.

During Ch-10, Ch-9 and Ch-8 times, the study area was dominated by delta-front and shallow lacustrine sedimentation. A northward transition from deep-lake to shallow-lake environments is documented for the Ch-7 member. During Ch-6 times, the study area was primarily occupied by a delta-front setting (Fig. 20A). During Ch-4+5 times, the delta plain transitioned to the south into a proximal delta-front environment, and the palaeoshoreline trended along the areas of wells Z201—4002—Z128 (Fig. 20B). This overall distribution of the depositional environments persisted during times Ch-3 and Ch-2, but it relates to a progressive increase in sandstone fraction (with ranges varying from 30%-50% to 40%-60%). During Ch-1 times, the study area was dominated by the delta-front facies belt, but strata in the central portion of study area are locally not preserved due to subsequent uplift and erosion by Jurassic palaeochannels (Fig. 20C).

The sedimentological evidence that allowed the planform mapping of the facies associations (Fig. 20) points to the preservation of lake-margin environments that were dominated by alluvial coastal plains, with only subordinate wave-influenced environments. The limited and only local (e.g., at delta-front fringes) importance of wave processes as drivers of sediment redistribution and of growth in coastal topographic relief may have favoured the lateral mobility of channels by avulsion (cf. Swenson, 2005; Syvitski and Saito, 2007; Rossi and Steel, 2016; Bhattacharya et al., 2019). Temporal variations in sediment entry points and in the loci of deposition within the delta may have therefore been important: this factor may have contributed to the complex spatial distribution of sand-prone sedimentary units.

7.3 Broader significance for petroleum exploration in lacustrine basins

The migration of lacustrine shorelines preserved as the boundary of delta-front and delta-plain facies belts is related to the stacking pattern of deltaic sand bodies; the identification of the preserved record of lacustrine shorelines is therefore critical for supporting petroleum exploration in the Yanchang deltaic setting. Discovered petroleum reserves, which are mostly contained in stratigraphic traps, are primarily focused on targets located basinward of the palaeoshorelines, and secondarily on landward targets. Delta-front and delta-top sandstones were produced in sub-environments that are intimately associated with organic-rich lacustrine shales that acted as potential source rocks, which accumulated in prodelta and possibly even in interdistributary or shallow-lake settings (Yang et al., 2005; Qu et al., 2020). The reconstructed palaeoshorelines of the Yanchang lake reveal frequent fluctuations of lake level that have resulted in a complex vertical and lateral juxtaposition of sandstones and mudstones, in response to multiple progradational and retrogradational cycles that may have given rise to source-reservoir-cap rock assemblages, thereby facilitating stratigraphic trapping (Wei et al., 2007; Li et al., 2009; Zou et al., 2010; Fu et al., 2019). Exploration data confirm (Yang et al., 2007; Deng et al., 2011; Zhao et al., 2016; Qu et al., 2020) that viable source and seal rocks were developed in Ch-9, Ch-7 and Ch-4+5, and Ch-1 in relation to lake transgressive periods, when deltaic retrogradation produced sandbodies with relatively limited lateral extent and continuity. Marked progradations of deltaic systems occurred during stages of lake contraction during Ch-10, Ch-8, Ch-6, Ch-3, and Ch-2 times. The resulting sand bodies are coarser and amalgamated, forming potentially attractive reservoirs. The facies criteria outlined in this work can be applied for this purpose. More generally, the same approach outlined in this work for the delineation of facies belts and palaeoshorelines can be applied to the characterization of deltaic subsurface successions associated with shallow-water deltas lacking a clear physiographic differentiation of topset, foreset and bottomset geometries.

The depositional model constructed for the studied interval of the Yanchang Formation envisages the presence of deltaic sand aprons made of subaerial or terminal amalgamated channel fills that are elongated seaward; these sand aprons are distributed over a wide domain in response to m-scale lake-level fluctuations that drove shoreline migration over kilometres or tens of kilometres. This highlights the potential for extending exploration basinward, which however should be undertaken with consideration of the local orientation of the palaeoshoreline across the interval being explored.

8. Conclusions

An integrated study of subsurface and outcrop datasets (four outcrops, 2,350 well logs, 820 m of cores) of the sedimentology and stratigraphy of the Triassic Yanchang Formation of the Ordos Basin has been undertaken to reconstruct the evolution of lacustrine palaeoshorelines and associated sub-environments through each studied member. A particular focus has been placed on the differentiation between delta-plain and delta-front deposits of shallow-water river-dominated ramp lacustrine deltas. Recognition criteria for discriminating delta-plain and delta-front facies belts, based on sediment texture, sedimentary structures, palaeofauna and flora, well-log profiles, and vertical facies successions of their sub-environments, have been summarized and applied to reconstruct the temporal evolution of the Yanchang lake. A gross depositional model for the Yanchang Formation has also been proposed that synthesizes characteristics of reservoir architecture that can be expected based on inferences of the position of a reservoir interval relative to its correlative time-averaged palaeoshoreline. These results can inform petroleum exploration in this productive unit of the Ordos Basin. Results are also applicable more generally to gain improved understanding of controls on the sedimentology, stratigraphy and paleogeography of river-fed siliciclastic ramp-margin lake shoreline systems.

Acknowledgements/Funds

This work was supported by the Major National Science and Technology Projects (Grant No. 2016ZX05050006) and Scientific Research and Innovation Group of Xi'an Shiyou University (Grant No. 2013KYCXTD03). LC and NPM thank AkerBP, Areva (now Orano), BHPBilliton, Cairn India (Vedanta), CNOOC, ConocoPhillips, Chevron, Equinor, Murphy Oil, Occidental, Petrotechnical Data Systems, Saudi Aramco, Shell, Tullow Oil, Woodside and YPF for their financial support of the Fluvial, Eolian & Shallow-Marine Research Group at the University of Leeds. We thank the anonymous reviewers of this article and Associate Editor Roberto Tinterri for their constructive criticism, which has improved the paper.

References

Ahmed, S., Bhattacharya, J. P., Garza, D. E., Li, Y., 2014. Facies architecture and stratigraphic evolution of a river- dominated delta front, Turonian Ferron sandstone, Utah, USA. J. Sediment. Res. 84: 97–121.

Alexander, J., Bridge, J. S., Cheel, R. J., Leclair, S. F., 2001. Bedforms and associated sedimentary structures formed under water flows over aggrading sand beds. Sedimentology 48, 133–152.

Alexander, R. S., Antonio B. R., John, B. A., 2018. Bayhead deltas and shorelines: Insights from modern and ancient examples. Sedimentary Geology. doi:10.1016/j.sedgeo.2018.07.004

Allen, J. R. L. 1963. The classification of cross-stratified units, with notes on their origin. Sedimentology 2, 93–114.

Allen, J. R. L. 1964. Primary current lineation in the Lower Old Red Sandstone (Devonian) Anglo-Welsh basin. Sedimentology 3, 89–108.

Allen, J. R. L., 1965. Fining upward cycles in alluvial succession. Lpool. Manchr. Geol. J., 4, 229–46.

Allen, J. R. L. 1986. On the curl of desiccation polygons. Sediment. Geol. 46, 23–32.

Anthony, 2015. Wave influence in the construction, shaping and destruction of river delta: A review, Marine geology 361, 53–78.

Aschoff, J. L., Olariu, C., Steel, R. J., 2016. Recognition and significance of bayhead delta deposits in the rock record: A comparison of modern and ancient systems."Accepted Article"; doi: 10.1111/sed.12350.

Baas, J. H., Best, J. L., Peakall, J., 2016. Predicting bedforms and primary current stratification in cohesive mixtures of mud and sand. J. Geol. Soc., 173: 12–45.

Bao, C., Chen, Y., Li, D., Wang, S., 2014. Provenances of the Mesozoic sediments in the Ordos Basin and implications for collision between the North China Craton (NCC) and the South China Craton (SCC). J. Asian Earth Sci. 96, 296–307.

Beate, L.S., Leren, J., Howell, H. E., Allard, W. M., 2010. Controls on stratigraphic architecture in contemporaneous delta systems from the Eocene Roda Sandstone, Tremp- Graus basin, northern Spain. Sediment. Geol. 229, 9–40.

Seilacher, A.1967. Bathymetry of trace fossils. Marine Geology 5, 413–428.

Bhattacharya, J.P., 2010. Deltas. In: James, N., Dalrymple, R. (Eds.), Facies Models. Geological Association of Canada (GAC), pp. 233–264.

Birgenheier, L.P., Berg, M.D.V., Plink-Bjo¨Rklund, P., Gall, R.D., Rosencrans, E., Rosenberg, M.J., Toms, L.C., Morris, J., 2020, Climate impact on fluvial-lake system evolution, Eocene Green River Formation, Uinta Basin, Utah, USA. Geol. Soc. Am. Bull. 132, 562–587. doi:10.1130/B31808.1.

Bhattacharyaa, J.P., Miall, A.D., Ferrona, C., Gabriela, J., Randazzoa, N., Kynastona, D., Jichac, B. R., Singerc, B. S., 2019. Time-stratigraphy in point sourced river deltas: Application to sediment budgets, shelf construction, and paleo-storm records. Earth Sci. Rev. DOI: 10.1016/j.earscirev.2019.102985.

Blatt, H., Middleton, G., Murray, R., 1980. Origin of sedimentary rocks, 2nd edn. Prentice–Hall, Englewood Cliffs, NJ.

Bohacs, K.M., Carroll A.R., Neal, J.E., Mankiewicz, P.J., 2000, Lake-basin type, source protentional, and hydrocarbon character: an integrated sequence-stratigraphic geochemical framework, in Gierlowski-Kordesch, E.H., and Kelts, K.R., eds., Lake Basins through Space and Time. AAPG Studies in Geology 46, 3–34.

Bohacs, K.M., Carroll A.R., And Neal, J.E., 2003, Lessons from large lake systems: thresholds, nonlinearity, and strange attractors, in Chan, M.A., and Archer, A.W., eds., Extreme Depositional Environments: Mega End Members in Geologic Time. Geol. Soc. Am. Spec. Pap., 370,75–90.

Boulesteix, K., Poyatos-Moré, M., Hodgson, D.M, Stephen S. F., Kevin, G. T., 2020. Fringe or background: Characterizing deep-water mudstones beyond the basin-floor fan sandstone pinchout. J. Sediment. Res. 90, 1678-1705.

Brizga, S.O., Finlayson, B.L. 1990. Channel avulsion and river metamorphosis: the case of the Thomson River, Victoria, Australia. Earth Surf. Process. Landf. 15, 391–404.

Bryant, M., Falk, P., Paola, C. 1995. Experimental study of avulsion frequency and rate of deposition. Geology 23, 365–368.

Buaotis, L. A and ,Mangano,　M. G.,,1993．Trace fossils from a Carboniferous turbiditic lake：Implications for the recognition of additional nonmarine ichnofacies．Ichnos2：237–258．

Budai, S ., Colombera, L. , Mountney, N. P., 2021.Quantitative characterization of the sedimentary architecture of Gilbert-type deltas. Sediment. Geol.1426, – https://doi.org/10.1016/j.sedgeo.2021.106022.

Burton, D., Woolf, K., Sullivan, B., 2014. Lacustrine depositional environments in the Green River Formation, Uinta Basin: Expression in outcrop and wireline logs. AAPG Bull., 98, 1699–171.

Carroll, A.R., Bohacs, K.M., 1999. Stratigraphic classification of ancient lakes: balancing tectonic and climatic controls. Geology. 27, 99–102.

Cartigny, M. J. B., Ventra, D., Postma, G.,Van Den Berg, J. H., 2014. Morphodynamics and sedimentary structures of bedforms under supercritical-flow conditions: new insights from flume experiments. Sedimentology 61, 712–748.

Chen, Q., Li, W., Gao,Y., Guo Y., Feng J., Zhang D., Cao H., Liang J., 2007. The deep-lake deposit in the Upper Triassic Yanchang Formation in Ordos Basin, China and its significance for oil-gas accumulation. Sci. China Ser. D. 50, 47–58.

Coleman, J. M., Gagliano, S. M. 1965. Sedimentary structure: Mississippi River deltaic plain. In: Middleton, G. V. ed., Primary sedimentary structures and their hydrodynamic interpretation. Spec. Publ.Soc. Econ. Palaeont. Miner., 12, 133–148.

Coleman, J.M., Prior, D.B., 1982. Deltaic environments of deposition. In: Scholle, P.A. and Spearing, D.R., Eds., Sandstone depositional environments. AAPG Memoir 31, 139–178.

Collinson, J., Mountney, N. 2019. Sedimentary structures, 4th edn. Dunedin Academic Press, Edinburgh, Scotland, 340 pp.

Colombera, L., Mountney, N.P., McCaffrey, W.D., 2012. A relational database for the digitization of fluvial architecture: concepts and example applications. Pet. Geosci. 18, 129-140.

Colombera, L., Mountney, N.P., McCaffrey, W. D. 2013. A quantitative approach to fluvial facies models: methods and example results. Sedimentology 60, 1526–1558.

Darby, B. J., Ritts, B. D., 2002. Mesozoic contractional deformation in the middle of the Asian tectonic collage: The intraplate western Ordos fold–thrust belt, China. Earth. Plan. Sci. Lett., 205, 13–24.

Davies, H. G. 1965. Convolute lamination and other structures from the Lower Coal Measures of Yorkshire. Sedimentology 5, 305–326.

Deng, X., Fu, J., Yao, J., Pang, J., Sun, B., 2011. Sedimentary facies of the Middle-Upper Triassic Yanchang Formation in the Ordos basin and breakthrough in petroleum exploration. J. Palaeogeogr. 13, 443–455 (In Chinese with English abstract).

Deng, X., Fu, J., Yao, J., Pang, J., Sun, B., 2011. Sedimentary facies of the Middle-Upper Triassic Yanchang Formation in the Ordos basin and breakthrough in petroleum exploration. J. Palaeogeogr. 13, 443–455 (In Chinese with English abstract).

Deng, X., Luo, A., Zhang, Z., Liu, X., 2013. Geochronological comparison on Indosinian tectonic events between Qinling orogeny and Ordos basin. Acta Sedimentol. Sin. 31, 939–953 (In Chinese with English abstract).

Dong, Y., Zhang, G., Neubauer, F., Liu, X., Genser, J., Hauzenberger, C., 2011. Tectonic evolution of the Qinling orogen, China: review and synthesis. J. Asian Earth Sci. 41, 213–237.

Eyles, N., Eyles, C.H., Miall, A.D., 1983. Lithofacies types and vertical profile models: an alternative approach to the description and environmental interpretation of glacial diamictite and diamictite sequences. Sedimentology 30, 393–410.

Feng, Y., Li, S., Lu, Y., 2013, Sequence stratigraphy and architectural variability in Late Eocene lacustrine strata of the Dongying Depression, Bohai Bay Basin, Eastern China. Sediment. Geol. 295, 1–26. doi:10.1016/j.sedgeo.2013.07.004.

Feng, Y., Jiang, S., Hu, S., Li, S., Lin, C., Xie, X., 2016, Sequence stratigraphy and importance of syndepositional structural slope-break for architecture of Paleogene syn- rift lacustrine strata, Bohai Bay Basin, E. China. Mar. Pet. Geol. 69, 183–204. doi:10.1016/j.marpetgeo.2015.10.013.

Fidolini, F., Ghinassi, M., 2016. Friction- and inertia-dominated effluents in a lacustrine, river-dominated deltaic succession (Pliocene Upper Valdarno Basin, Italy). J. Sediment. Res. 86, 1083–1101.

Fielding, C. R., 2010. Planform and facies variability in asymmetric deltas: Facies analysis and depositional architecture of the Turonian Ferron Sandstone in the Western Henry Mountains, south-central Utah, USA. J. Sediment. Res. 80: 455–479.

Fielding, C. R., Alexander, J., Allen, J., 2017. The role of discharge variability in the formation and preservation of alluvial sediment bodies. Sed. Geol., 365, 1–20.

Fielding, C. R., Trueman, J. D., Alexander, J., 2005. Sharp-based, flood-dominated mouth bar sands from the Burdekin river delta of northeastern Australia: extending the spectrum of mouth-bar facies, geometry, and stacking patterns. J. Sediment. Res.75, 55–66.

Fielding, C.R., 2006. Upper flow regime sheets, lenses and scour fills: extending the range of architectural elements for fluvial sediment bodies. Sediment. Geol.190, 227–240.

Fisk, H. N., Mcfarlan, J. E., Kolb, C. R. 1954. Sedimentary framework of the modern Mississippi delta. J. Sediment. Res. 24, 76–99.

Fongngern, R., Olariu, C., Steel, R., Mohrig, D., Kre´Zsek, C., Hess, T., 2018, Subsurface and outcrop characteristics of fluvial-dominated deep lacustrine clinoforms. Sedimentology 65,1447–1481, doi:10.1111/sed.12430.

Frazier, D. E., Osanik, A. 1961. Point-bar deposits, old river Locksite, Louisiana. Trans. Gulf Coast Assoc. Geol. Soc. 11, 127–137.

Friend, P. E 1965. Fluviatile sedimentary structures in the Wood Bay Series (Devonian) of Spitsbergen. Sedimentology 5, 39–68.

Fu, J., Wu, S., Wang, Zh, Liu, Y., 2015. Architecture model of shallow-water delta distributary channel in lake basin: A case study of the Yanchang Formation outcrops in the eastern margin of Ordos Basin. J. Central South Univ. (Sci. & Tech. Edn) 46, 4174–4182. (In Chinese with English abstract).

Fu, S., Liu, Z., Guo, Y. R., Ge, J. W., & Xu, X. M. (2019). Lacustrine paleoshoreline determination under established sequence stratigraphic framework and its controls on sand bodies and hydrocarbon accumulations. Marine and Petroleum Geology, 110, 497-517.

Fu, Q., Xu, Zh., Yao, J., Li, J., 2018. Geological environment of trace fossil assemblage in Yanchang Formation, Ordos Basin. J. TongJi Univ. 46, 695–699+686 (In Chinese with English abstract).

Gall, R.D., Birgenheier, L.P., Vanden Berg, M.D., 2017, Highly seasonal and perennial fluvial facies: implications for climatic control on the Douglas Creek and Parachute Creek members, Green River Formation, southeastern Uinta Basin, Utah, U.S.A. J. Sediment. Res. 2017, 87, 1019–1047. DOI: http://dx.doi.org/10.2110/jsr.2017.54.

Gao, Y., Jiang, X., James, L. B., Liu, Q., Zhang, J., 2019. Small- and large- scale soft-sediment deformations in a Triassic lacustrine delta caused by overloading and seismicity in the Ordos Basin, central China. Mar. Petrol. Geol. 103, 126–149.

Galloway, W.E., Hobday, D. K., 1996. Terrigenous clastic depositional systems: applications to fossil fuel and groundwater resources, 2nd edn. Springer Press, p288.

Gibling, M.R. 2006. Width and thickness of fluvial channel bodies and valley fills in the geological record: a literature compilation and classification. J. Sediment. Res. 76, 731–770.

Gong, C., Sztano, O., Steel, R.J., Xian, B., Galloway, W.E., Bada, G., 2019, Critical differences in sediment delivery and partitioning between marine and lacustrine basins: a comparison of marine and lacustrine aggradational to progradational clinothem pairs. Geol. Soc. Am. Bull. 131, 766–781. doi:10.1130/B32042.1.

Hart, B. S., Prior, D. B., Barrie, J. V., Currie, R. G., Luternauer, J.L., 1992. A river mouth submarine channel and failure complex, Fraser Delta, Canada. Sediment. Geol. 81, 73–87.

He, Z., 2002. The tectonic evolvement and petroleum in the Ordos Basin.Petroleum Industry Press, Beijing. 390 pp (in Chinese) .

Hutchinson, G. E., 1957. A treatise on limnology. In: Geography, physics and chemistry, vol.1. Wiley, New York.

Ingram, R. L. 1954. Terminology for the thickness of stratification and parting units in sedimentary rocks. Geol. Soc. Am. Bull. 85, 937–938.

Jiang, Z., Liu, H., 2010. Lacustrine palaeoshoreline and its controls on sandbodies and hydrocarbon. J. Palaeogeogr. 12, 589–598 (In Chinese with English abstract).

Jiang, Z., 2010. Sedimentology, 2nd edn. Petroleum Industry Publishing House, Beijing (In Chinese).

Jones, L. S., Schumm, S. A., 1999. Causes of avulsion: an overview. Special. Publs. int. Ass. Sediment. 28, 171–178.

Jorissen, E.L., Abels, H.A., Wesselingh, F.P., Lazarev, S., Aghayeva, V., Krijgsman, W., 2020, Amplitude, frequency and drivers of Caspian Sea lake-level variations during the Early Pleistocene and their impact on a protected wave-dominated coastline. Sedimentology 67, 649–676, doi:10.1111/sed.12658.

Ke, W. T., Shaw, J. B., Mahon, R. C., Cathcart, C. A., 2019. Distributary channel networks as moving boundaries: Causes and morphodynamic effects. JGR. Earth Surface, 124,1878–1898.

Keighley, D., Flint, S., Howell, J., Andersson, D., Collins, S., Moscariello, A., Stone, G., 2002, Surface and Subsurface Correlation of the Green River Formation in Central Nine Mile Canyon, SW Uinta Basin Carbon and Duchesne Counties, East-Central Utah. Utah Geological Survey, MP-02-01, 63 p.

Keighley, D., Flint, S., Howell, J., Mosariello, A., 2003. Sequence stratigraphy in lacustrine basins: a model for part of the Green River Fomation (Eocene), southwest Uinta basin, Utah, U. S. A. J. Sediment. Res. 73, 987–1006.

Keighley, D., Spinnangr, Ø., Howell, J., Flint, S., 2019, Interpretation of mouth-bar and related lacustrine and fluvial sand bodies from the middle Green River Formation (Eocene), southern Uinta Basin, Utah, in Starratt, S.W., and Rosen, M.R., eds., From Saline to Freshwater: The Diversity of Western Lakes in Space and Time: Geol. Soc. Am. Special Paper 536.

Kostaschuk, R.A., Luternauer, J.L., McKenna, G.T., Moslow, T.F., 1992. Sediment transport in a submarine channel system: Fraser River delta, Canada. J. Sediment. Petrol. 62: 273–282.

Lang, J., Le Heron, D. P., Van den Berg, J. H., Winsemann, J., 2020. Bedforms and sedimentary structures related to supercritical flows in glacigenic settings. Sedimentology. https://doi.org/10.1111/sed.12776.

Lemons, D. R., Chan, M. A., 1999. Facies architecture and sequence stratigraphy of fine-grained lacustrine deltas along the eastern margin of late Pleistocene Lake Bonneville, Northern Utah and Southern Idaho. AAPG Bull., 83, 635–665.

Li, S., Kusky, T.M., Wang, L., Lai, S., Liu, X., Dong, S., Zhao, G., 2007. Collision leading to multiple-stage large-scale extrusion in the Qinling orogen: insights from the Mianlue suture. Gondwana Res. 12, 121–143.

Li, W., Pang, J., Cao, H., Xiao, L., Wang, R., 2009. Depositional system and paleogeographic evolution of the late Triassic Yangchang stage in Ordos basin. J. Northwest Univ. Nat.Sci.Ed. 39, 501–506 (In Chinese with English abstract).

Liu, H., Pu, R., Wang, D., Zhao, Y., Zhang, J., Zhao, D., 2014. Progradational reflection from lacustrine Yanchang Formation in Ordos Basin, China. OGP 49, 985–996 (In Chinese with English abstract).

Liu, S., 1998. The coupling mechanism of basin and orogen in the western Ordos basin and adjacent regions of China. J. Asian Earth Sci. 16, 369–383.

Liu, Z., Shen, F., Zhu, X., Liao, J., Zhang, X., Meng, H. 2015. Progress of shallow-water delta research and a case study of continental lake basin. Oil & Gas Geol. 36, 576–604 (In Chinese with English abstract).

Martini, I., Ambrosetti, E., Sandrelli, F., 2017. The role of sediment supply in large-scale stratigraphic architecture of ancient Gilbert type deltas (Pliocene Siena-Radicofani Basin, Italy). Sediment. Geol. 350, 23–41.

Martini, I., Sandrelli, F., 2015. Facies analysis of a Pliocene river-dominated succession (Siena

Basin, Italy): implications for the formation and filling of terminal distributary channels: Sedimentology 62, 234–265.

Massari, F. 1996. Upper-flow-regime stratification types on steep-face, coarse-grained, Gilbert-type progradational wedges. J. Sed. Res. 66, 364–375.

Mathews, W. H., Shepard, F. P., 1962. Sedimentation of the Fraser River delta, British Columbia. AAPG Bull. 46, 1416–1438.

McCabe, P. J., 1984. Depositional environments of coal and coal-bearing strata. In: Rahmani, R.A., Flores, R.M. (Eds.), Sedimentology of Coal and Coal-Bearing Sequences. IAS, Special Publ. 7, p. 13–42.

McKee, E. D., Weir, G. W. 1953. Terminology for stratification and cross-stratification in sedimentary rocks. Geol. Soc. Am. Bull. 64, 381–390.

Mei, Z., Lin, J., 1991. Stratigraphic pattern and character of skeletal sandbodies in lacustrine deltas. Acta Sedimentol. Sin. 9, 1–11 (In Chinese with English abstract).

Miall, A. D., 1978, Lithofacies types and vertical profile models in braided stream deposits: a summary, in A. D. Miall, ed., Fluvial Sedimentology: Canadian Society of Petroleum Geologists Memoir 5, p. 597-604.

Miall, A. D., 1985. Architectural element analysis: a new method of facies analysis applied to fluvial deposits. Earth Sci. Rev. 22, 261–308.

Mills, P. C. 1983. Genesis and diagnostic value of soft sediment deformation structures- a review. Sediment. Geol. 35, 83–104.

Mohrig, D., Heller, P.L., Paola, C., Lyons, W.J., 2000. Interpreting avulsion process from ancient alluvial sequences: Guadalope-Matarranya system (northern Spain) and Wasatch Formation (western Colorado). GSA Bull. 112, 1787–1803.

Neill, C. F., Allison, M. A., 2005. Subaqueous deltaic formation on the Atchafalaya shelf, Louisiana. Mar. Geol. 214, 411–430.

Nemec, W., Steel, R. J., Gjelberg, J., Collinson, J. D., Prestholm, E., Oxnevad, I. E., 1988. Anatomy of collapsed and re-established delta front in lower cretaceous of eastern Spitsbergen: gravitational sliding and sedimentation processes. AAPG Bull. 72, 454–476.

Nutz , A., Ghienne, J. F., Schuster, M., Dietrich, P., Claude, R., Hay, M. B., Bouchette, F., Cousineau, P. A., 2015. Forced regressive deposits of a deglaciation sequence: Example from the Late Quaternary succession in the Lake Saint-Jean basin (Quebec, Canada). Sedimentology 62, 1573–1610.

Olariu, C., Bhattacharya, J. P., Leybourne, M. I., Boss, S. K., Stern, R. J., 2012. Interplay between river discharge and topography of the basin floor in a hyperpycnal lacustrine delta. Sedimentology 59, 704–728.

Olariu, C., Bhattacharya, J. P., Xu, X., Aiken, C. L. V., Zeng, X., McMechan, G.A., 2005. Integrated study of ancient delta front deposits, using outcrop, ground penetrating radar and three dimension photorealistic data: Cretaceous Panther Tongue sandstone, Utah, in Giosan, L., and Bhattacharya, J. P., eds., River Deltas: Concepts, Models, Examples: SEPM, Special Publ. 83, p. 155–178.

Olariu, C., Bhattacharya, J. P., 2006. Terminal distributary channels and delta front architecture of river-dominated delta systems. J. Sediment. Res.76, 212–233.

Olariu, C., Steel, R. J., Petter, A. L., 2010. Delta-front hyperpycnal bed geometry and implications for reservoir modeling: Cretaceous Panther tongue delta, book Cliffs, Utah. Am. Assoc. Petrol. Geol. Bull. 94, 819–845.

Olariu, C., Zhou, Ch., Steel, R., Zhang, Zh.,Yuan, X., Zhang, J., Chen, S., Cheng, D., Kim, W., 2021. Controls on the stratal architecture of lacustrine delta successions in low-accommodation conditions. Sedimentology, doi: 10.1111/sed.12838.

Ono, K., Plink-Björklund, P., Eggenhuisen, J.T., Cartigny, M. J. B., 2020. Froude supercritical flow processes and sedimentary structures: New insights from experiments with a wide range of grain sizes. Sedimentology, doi:10.1111/sed.12682.

Overeem, I., Kroonenberg, S.B., Veldkamp, A., Groenesteijn, K., Rusakov, G.V., Svitoch, A.A., 2003, Small-scale stratigraphy in a large ramp delta: recent and Holocene sedimentation in the Volga delta, Caspian Sea. Sediment. Geol. 159, 133–157. doi:10.1016/S00370738(02)00256-7.

Pang, J., Li, W., Chen, Q., 2010. Characteristics and forming mechanism of marker bed in Yanchang Formation of the ShanBei Area. J. Stratigr. 34, 173–178 (In Chinese with English abstract).

Paola, C., Wiele, S. M., Reinhart, M. A., 1989. Upper-regime parallel lamination as the result of turbulent sediment transport and low-amplitude bed forms. Sedimentology 36, 47–59.

Pusca, V. A., 2004, Wet/dry, terminal fan-dominated sequence architecture: a new, outcrop-based model for the lower Green River Formation, Utah. Ph.D. Res. Rep. University of Wyoming, 181 p.

Pettijohn, F. J. 1949. Sedimentary rocks, Harper & Bros., New York, p. 124–127.

Pettijohn, F .J., Potter, P. E. 1964. "Atlas and glossary of primary sedimentary structures."Springer-

Verlag, Berlin. 370pp.

Phillips, R. L., 2003, Depositional environments and processes in Upper Cretaceous nonmarine and marine sediments, Ocean Point dinosaur locality, North Slope, Alaska. Cretaceous Research 24, 499–523.

Plummer, P. S., Gostin, V. A., 1981. Shrinkage cracks: desiccation or synaeresis? J. Sediment. Petrol. 51, 1147–1156.

Postma, G., 1990. An analysis of the variation in delta architecture. Terra Nova 2, 124–130.

Qiu, X., Liu, C., Mao, G., Deng, Yu, Wang, F., Wang, J., 2014. Late Triassic tuff intervals in the Ordos Basin, Central China: their depositional, petrographic, geochemical characteristics and regional implications. J. Asian Earth Sci. 80, 148–160.

Qu, H., Yang, B., Gao, Sh., Zhao, J., Han, X., Chen, Sh., Hayat, K., 2020. Controls on hydrocarbon accumulation by facies and fluid potential in large-scale lacustrine petroliferous basins in compressional settings: A case study of the Mesozoic Ordos Basin, China. Mar. Pet. Geol.122(), 104668–. doi:10.1016/j.marpetgeo.2020.104668.

Reineck, H. E., Singh, I. B., 1986. Depositional Sedimentary Environments; With Reference to Terrigenous Clastics. Springer, Berlin. 439pp

Reineck, H. E., Wunderlich, E., 1968. Classification and origin of flaser and lenticular bedding. Sedimentology 11, 99–104.

Renaut, R.W., Gierlowski-Kordesch, E. H., 2010. Lakes. In: Facies Models (Ed. James, N.P.), St. John's, Newfoundland: Geological Association of Canada, 541–575.

Rossi, V. M., Steel, R. J., 2016. The role of tidal, wave and river currents in the evolution of mixed-energy deltas: example from the Lajas Formation (Argentina). Sedimentology 63, 824–864.

Rubi, R., Rohais, S., Bourquin, S., Moretti, I., Desaubliaux, G., 2018. Processes and typology in Gilbert-type delta bottomset deposits based on outcrop examples in the Corinth Rift. Mar. Petrol. Geol., 92, 193–212.

Schomacker, E. R., Kjemperud, A. V., Nystuen, J. P., Jahren, J. S., 2010. Recognition and significance of sharp-based mouth-bar deposits in the Eocene Green River Formation, Uinta Basin, Utah. Sedimentology 57, 1069–1087.

Seilacher, A.1967. Bathymetry of trace fossils. Marine Geology 5, 413–428.

Selley, R. C., 1965. Diagnostic characters of fluviatile sediments of the Torridonian Formation (PreCambrian) of North-West Scotland. J. Sediment. Petrol. 35, 366–80.

Shaw, J. B ., Mohrig, D., Whitman, S. K., 2013. The morphology and evolution of channels on the Wax Lake Delta, Louisiana, USA. J. Geophys. Res. Earth Surf. 118, 1562–1584.

Smith, N. D., 1972. Some sedimentological aspects of planar cross-stratification in a sandy braided river. J. Sediment. Petrol. 42, 624–634.

Smith, N. D., Cross, T. A., Dufficy, J. P., Clough, S. R., 1989. Anatomy of an avulsion. Sedimentology 36, 1–23.

Styan, W. B., Bustin, R. M., 1983. Sedimentology of Fraser River delta peat deposits: a modern analogue for some deltaic coals. Int. J. Coal Geol. 3, 101–43.

Syvitski, J., Saito, Y., 2007. Morphodynamics of deltas under the influence of humans. Glob. Planet.

Change. 57, 261–282.

Swenson, J. B., C. Paola, L. Pratson, V. R. Voller, and A. B. Murray., 2005. Fluvial and marine controls on combined subaerial and subaqueous delta progradation: Morphodynamic modeling of compound-clinoform development, J. Geophys. Res., 110, F02013, doi:10.1029/2004JF000265.

Talling, P. J., Masson, D. G., Sumner, E. J. Malgesini, G., 2012. Subaqueous sediment density flows: Depositional processes and deposit types. Sedimentology, 59, 1937–2003.

Tanner, L.H., Lucas, S.G., 2010. Deposition and deformation of fluvial-lacustrine sediments of the Upper Triassic-Lower Jurassic Whitmore Point Member, Moenave Formation, northern Arizona. Sediment. Geol. 223, 180–191.

Tara, S., Chakraborty, T., 2018. Deltaic coastline of the Siwalik (Neogene) foreland basin: evidences from the Gish River section, Darjeeling Himalaya. Geol. J. 53: 203–229.

Taylor, A.W., Ritts, B. D., 2004. Mesoscale heterogeneity of fluvial-lacustrine reservoir analogues: examples from the Eocene Green River and Colton Formations, Uinta Basin, Utah, USA. J. Petrol. Geol. 27, 3–26.

Terwindt, J. H. J., Breusers, H. N. C., 1972. Experiments on the origin of flaser, lenticular and sand-clay alternating bedding. Sedimentology 19, 85–98.

Tye, R. S., Coleman, J. M., 1989. Evolution of Atchafalaya lacustrine deltas, south-central Louisiana. Sediment. Geol. 65, 95–112.

Van der Kolk, D. A; Flaig, P. P., Stephen, H., 2015. Paleoenvironmental reconstruction of a late Cretaceous, muddy, river-dominated polar deltaic System: Schrader Bluff–Prince Creek Formation transition, Shivugak Bluffs, North Slope of Alaska, U.S.A. J. Sediment. Res. 85, 903–936.

Van Loon, A. J., Brodzikowski, K., 1987. Problems and progress in the research on soft sedimentation deformations. Sediment. Geol. 50, 167–194.

Ventra, D., Cartigny, M. J. B., Bijkerk, J. F., Acikalin, S., 2015. Supercritical-flow structures on a Late Carboniferous delta front: sedimentological and paleoclimatic significance. Geology 43, 731–734

Wang, J., Plink-Bjo ̈Rklund, P., 2020, Variable-discharge-river macroforms in the Sunnyside Delta interval of the Eocene Green River Formation, Uinta Basin, USA. Sedimentology 67,1914–1950. doi:10.1111/sed.12688.

Wang, Q., Li, W., Zhao, H., Wang, L., Qu, H., 2006. Characteristics and significance of lacustrine turbidites in the member 1 of Yanchang Formation, Upper Triassic in the southeastern Ordos Basin. China. J. Geo. 41, 54-63 (In Chinese with English abstract).

Wei, P., Pan, Sh., Wang, J., Lei, M., 2007. Study of the relationship between lithostratigraphic reservoirs and lakeshore line-Introduction on lakeshore line controlling oil/gas reservoirs in sag basin. Lithol. Reserv. 19, 27–31 (In Chinese with English abstract).

Williams, G. E., 1971. Flood deposits of the sandbed ephemeral streams of Central Australia. Sedimentology 17, 1–40.

Williams, P. B., Kemp, P. H., 1971. Initiation of ripples on flat sediment beds. J. Hydraul. Div. 97, 502–522.

Wright, L. D., 1977. Sediment transport and deposition at river mouths: a synthesis. Geol. Soc. Am.

Bull. 88, 857–868.

Wu, F., Li, W., Li ,Y., Xi, S., 2004. Delta sediments and evolution of the Yanchang Formation of Upper Triassic in Ordos Basin. J. Palaeogeogr. 6, 307–315 (In Chinese with English abstract).

Xie, X., 2016. Provenance and sediment dispersal of the Triassic Yanchang Formation, southwest Ordos Basin, China, and its implications. Sediment. Geol. 335, 1–16.

Xie, X., Heller, P. L., 2013. U-Pb detrital zircon geochronology and its implications: The early Late Triassic Yanchang Formation, south Ordos Basin, China. J. Asian. Earth. Sci. 64, 86–98.

Yang, H., 2010. Sedimentary features and hydrocarbon occurrence in the Chang 6-chang8 intervals of the Yanchang Formation, Ordos Basin. Postdoc. Res. Rep. Northwest Univ., 1–205 (In Chinese with English abstract).

Yang, H., Fu, Q., Fu, J., 2007. Sedimentary sequence and hydrocarbon accumulation in the Late Triassic, Ordos Basin, Geology Publishing House, Beijing, 1-163 (In Chinese).

Yang, H., Fu, Q., Qi, Y., Zhou, X., Gong, N., Huang, Sh., 2016. The paleontology phase zones and its geological significance on the late Triassic Yanchang stage Palaeolacustrine Ordos Basin. Acta Sedimentol. Sin. 34, 688-693 (In Chinese with English abstract).

Yang, K., Pang, J., Li, W., 2009. Determination method of lakeshore line in depressed-type lacustrine basin-taking the Yanchang Formation of Zhidan area as an example. J. Lanzhou Univ. Nat. Sci. Ed. 45, 13–17 (In Chinese with English abstract).

Yang, M., Liu, Ch., Zheng, M., Lan, Ch., Tang, X., 2007. Sequence framework of two different kinds of margins and their response to tectonic activity during the Middle–Late Triassic, Ordos

Basin. Sci. China Ser. D. 50, 203–216.

Yang, R., Jin, Z., Van Loon, A. J., Han, Z., Fan, A., 2017. Climatic and tectonic controls of lacustrine hyperpycnite origination in the Late Triassic Ordos Basin, central China: implications for unconventional petroleum development. AAPG Bull. 101, 97–117.

Yang, Y., Li, W., Ma, L., 2005. Tectonic and stratigraphic controls of hydrocarbon systems in the Ordos Basin: a multicycle cratonic basin in central China. Am. Assoc. Petrol. Geol. Bull. 89, 255–269.

Zavala, C., Ponce, J.J., Arcuri, M., Drittanti, D., Freije, H., Asensio, M., 2006. Ancient lacustrine hyperpycnites: a depositional model from a case study in the Rosayo Formation (Cretaceous) of west-central Argentina. J. Sediment. Res. 76, 41–59.

Zeng, Sh., 2017. Analysis of sedimentary architecture in chang 6 of Yanchang Formation, Upper Triassic, Ordos basin. MS Res. Rep.Yangtze Univ., 1–67 (In Chinese with English abstract).

Zhang, Ch., Liu, B., Shi, D., 2000. Physical simulation of formation process in distributary channels and debouch bars in delta. Earth Sci. Front. 7, 168–176 (In Chinese with English abstract).

Zhang, J., Olariu, C., Steel, R., And Kim, W., 2020, Climatically controlled lacustrine clinoforms: theory and modelling results. Basin Res. 32, 240–250. doi:10.1111/bre.12383.

Zhao, J., Liu, C., Wang, X., Zhang, C., 2009. Migration of depocenters and accumulation centers and its indication of subsidence centers in the Mesozoic Ordos Basin. Acta Geol. Sin. 83, 278–294.

Zhao, J., Mountney N. P., Liu, Ch., Qu, H., Lin J., 2015. Outcrop architecture of a fluvio-lacustrine succession: Upper Triassic Yanchang Formation, Ordos Basin, China. Mar. Pet. Geol. 68, 394–413

Zhao, X., He S., Chen, Zh., Liu, P., Wang, F. 2016. Charateristics and controlling factors of source rocks in Yanchang Formation sequent framework, Ordos Basin. Earth Sci. . 41: 1055-1066 (In Chinese with English abstract).

Zhu, X., Xu, W., 1990. Meso-Cenozoic Sedimentary Basins in China. Petroleum Industry Press, Beijing (In Chinese).

Zou, C., Zhang, X., Luo, P., Wang, L., Luo, Z., Liu, L., 2010. Shallow-lacustrine sand-rich deltaic depositional cycles and sequence stratigraphy of the Upper Triassic Yanchang Formation, Ordos Basin, China. Basin Res. 22, 108–125.